MONTHLY NOTICES

OF THE

ROYAL ASTRONOMICAL SOCIETY

Vol. 115 No. 5 1955

Published and Sold by the
ROYAL ASTRONOMICAL SOCIETY
BURLINGTON HOUSE
LONDON, W.1

Price Thirteen Shillings and Sixpence

NOTICE TO AUTHORS

1. *Communications.*—Papers must be communicated to the Society by a Fellow. They should be accompanied by a summary at the *beginning* of the paper conveying briefly the content of the paper, and drawing attention to important new information and to the main conclusions. The summary should be intelligible in itself, without reference to the paper, to a reader with some knowledge of the subject; it should not normally exceed 200 words in length. **Authors are requested to submit MSS. in duplicate. These should be typed using double spacing and leaving a margin of not less than one inch on the left-hand side. Corrections to the MSS. should be made in the text and not in the margin.** Unless a paper reaches the Secretaries more than seven days before a Council meeting it will not normally be considered at that meeting. By Council decision, MSS. of accepted papers are retained by the Society for one year after publication; unless their return is then requested by the author, they are destroyed.

2. *Presentation.*—Authors are allowed considerable latitude, but they are requested to follow the general style and arrangement of *Monthly Notices*. References to literature should be given in the standard form, including a date, for printing either as footnotes or in a numbered list at the end of the paper. Each reference should give the **name and initials** of the author cited, irrespective of the occurrence of the name in the text (some latitude being permissible, however, in the case of an author referring to his own work). The following examples indicate the style of reference appropriate for a paper and a book, respectively :—

A. Corlin, *Zs. f. Astrophys.*, **15**, 239, 1938.
H. Jeffreys, *Theory of Probability*, 2nd edn., section 5.45, p. 258, Oxford, 1948.

3. *Notation.*—For technical astronomical terms, authors should conform closely to the recommendations of Commission 3 of the International Astronomical Union (*Trans. I.A.U.*, Vol. VI, p. 345, 1938). Council has decided to adopt the I.A.U. 3-letter abbreviations for constellations where contraction is desirable (Vol. IV, p. 221, 1932). In general matters, authors should follow the recommendations in *Symbols, Signs and Abbreviations* London : Royal Society, 1951) except where these conflict with I.A.U. practice.

4. *Diagrams.*—**These should be designed to appear upright on the page, drawn about twice the size required in print and prepared for direct photographic reproduction except for the lettering, which should be inserted in pencil. Legends should be given in the manuscript indicating where in the text the figure should appear.** Blocks are retained by the Society for 10 years; unless the author requires them before the end of this period they are then destroyed.

5. *Tables.*—**These should be arranged so that they can be printed upright on the page.**

6. *Proofs.*—Costs of alteration exceeding 5 per cent of composition must be borne by the author. Fellows are warned that such costs have risen sharply in recent years, and it is in their own and the Society's interests to seek the maximum conciseness and simplification of symbols and equations consistent with clarity.

7. *Revised Manuscripts.*—When papers are submitted in revised form it is especially requested that they be accompanied by the original MSS.

Reading of Papers at Meetings

8. When submitting papers authors are requested to indicate whether they will be willing and able to read the paper at the next or some subsequent meeting, and approximately how long they would like to be allotted for speaking.

9. Postcards giving the programme of each meeting are issued some days before the meeting concerned. Fellows wishing to receive such cards whether for Ordinary Meetings or for the Geophysical Discussions or both should notify the Assistant Secretary.

MONTHLY NOTICES

OF THE

ROYAL ASTRONOMICAL SOCIETY

Vol. 115 No. 5

THE SPECTRUM OF NOVA SAGITTARII 1954 (HARO–HERRARO)

M. W. Feast

(Communicated by the Radcliffe Observer)

(Received 1955 July 25)

Summary

A general description is given of the spectrum of Nova Sagittarii 1954 (Haro–Herraro) from 1954 July 7 to August 20. Strong C I lines are present in the principal absorption spectrum which has a velocity of −729 km/sec. The hydrogen lines show several absorption components whose velocities are listed in Table II. The structures shown by the broad emission lines are discussed. A distance of 3 kps and an absolute magnitude at maximum of about $-7^{m}\cdot8$ are deduced from the equivalent widths of the interstellar Ca II lines.

Introduction and observations.—News was received at the Radcliffe Observatory on 1954 July 7 of the discovery on 1954 July 4 of a 7th magnitude nova ($17^{h}\ 50^{m}\cdot5\ -36^{\circ}\ 15'$ (1875)) in Sagittarius. Several spectrograms were obtained that night and the nova was observed from time to time till 1954 August 20. The nova had then become sufficiently faint that further spectroscopic work would have caused too much interference with other programmes. The spectrum of the nova underwent considerable changes during the period covered by the observations and the present paper is intended to give a summary of these changes.

The observations were all made with the 2-prism spectrograph at the Cassegrain focus of the 74-inch Radcliffe reflector. Between July 7 and August 5 the $f/3\cdot7$ camera (49 A/mm at Hγ) was used and after the latter date the $f/2$ camera (86 A/mm at Hγ). The spectrograms obtained are listed in Table I.

Generally Kodak 103aB plates were used and the focus was adjusted to the optimum value for the blue and violet spectral regions. Though in such cases the red region is not in the best possible focus, the loss in resolution is small and the plates are usable from Hα to Hζ (Hα is actually outside the normal working range of 103aB plates but its great strength in the nova ensures its appearance on the spectrograms).

Each spectrogram was measured for wave-lengths of absorption lines as well as widths and positions of structural features in the broad emission lines. It will be found simplest to discuss the absorption and emission spectra separately though in fact of course the two are closely related. It will also be convenient to use the nomenclature suggested by McLaughlin (**1, 2**) and to compare the present results with the hypothetical "typical" nova as described by McLaughlin. Though

rather rough magnitude estimates were generally made at the times of taking the spectrograms, it is not intended to discuss the light curve or its relation to the spectrum since accurate photoelectric measures of the nova are likely to become available in the near future (Dr A. B. Muller of the Leiden Southern Station, Johannesburg, informs me that he has obtained a good series of measures). In the present paper the time of development of various features is given so that when a light curve is published it should be relatively simple to relate it to the spectrum.

TABLE I

List of Radcliffe Spectra of Nova Sagittarii 1954

Date (U.T.)			Emulsion	Camera		Date (U.T.)			Emulsion	Camera	
1954											
July 7	17h	30	103aF	*f*/3·7		July 19	20h	51	103aO	*f*/3·7	
	17	37	,,	,,			21	36	103aF	,,	*
	17	41	,,	,,			22	09	,,	,,	*
	17	48	,,	,,			22	20	29	103aB	,,
	20	40	103aO	,,			26	21	53	,,	,,
	21	30	103aF	,,	*	Aug.	5	19	55	,,	,,
	21	55	,,	,,	*		8	20	40	,,	*f*/2
	23	55	,,	,,			10	20	26	,,	,,
9	21	00	103aB	,,			13	19	42	,,	,,
16	00	43	,,	,,			16	20	30	,,	,,
18	22	24	,,	,,			20	20	40	,,	,,

The spectrogram on July 16 was kindly obtained by Mr H. van Woerden.
The spectrograms on July 18 and August 10 were kindly obtained by Dr A. D. Thackeray.
*=spectrograph adjusted for best focus in red region.

The principal absorption spectrum.—When the nova was first observed on 1954 July 7 the spectrum showed rather weak emission but a strong set of absorption lines. This absorption spectrum persisted (with some modifications) for a month or more whilst the emission spectrum gradually increased in intensity.

On 1954 July 7 the main absorption spectrum matches moderately well a supergiant F type star except that all the lines are rather diffuse. This set of absorption lines is pretty clearly the principal spectrum and the lines in it were identified without difficulty. The compilation of Cecchini and Gratton (**3**) was very helpful in this respect. The stronger lines listed by Cecchini and Gratton in their Table IX are found in the principal absorption spectrum of the nova. The main contributors to the spectrum are H, Ti II, Fe II, Cr II, Sc II, Mg II, Sr II, Si II, Ca II, C I and O I. Whilst many of the lines are blends, about 14 (other than H lines) were selected as being free from any serious blending and were used for radial velocity determinations, though not all the lines were available for use on each spectrogram. Over the period from 1954 July 7 to August 5 the velocity was constant within the accuracy of the measures. The mean velocity was −729 km/sec. It should be noticed that the hydrogen lines of the principal spectrum were not used in deducing this velocity, for reasons given below.

An outstanding feature of the principal spectrum is the presence in considerable strength of the lines of C I. The lines λλ 4762, 4772–76, 5039–42, 5052 and 5380 are all strong. The absence of λ 4932 is probably due to the overlying Fe II 4924 emission. The lines appear to be of the same order of intensity as in the R Corona Borealis variables of types F–G which are held to have an anomalously high abundance of carbon in their atmospheres. The presence of C I absorption in nova spectra was first established in Nova Herculis (DQ) 1934 (**4**) and McLaughlin (**5**) has shown the lines to have been present in several earlier novae.

In view of this it has been suggested (for instance by Bidelman (**6**)) that novae are in some way related to carbon stars. However, it is not certain that strong C I absorption lines are always present in nova spectra and they were apparently missing from Nova RR Pictoris 1925.

Unfortunately none of the spectrograms is strong enough at 3883 A for the presence of CN to be detected (as it was in Nova Herculis). The band at 4216 is not detectable on the Radcliffe spectrograms but this is a less sensitive test for CN. The general similarity of the principal spectrum to that of the hot R Cr B variables suggested that weak C_2 bands might possibly be present in the nova spectrum. Whilst it is just possible that the bands at 5165 A and 4737 A are weakly present, no very definite conclusions can be drawn from the available spectrograms.

Fairly strong absorption lines of O I were observed in Nova Herculis (**4**) and several other novae (**5**) but not in Nova Pictoris. In the present nova the presence of O I absorption is not quite so clear as with the C I absorption. Probably the O I blend 6158 accounts for a line which would otherwise remain unidentified. O I 6455 is probably blended with Fe II 6456. The Ti II line 4368 interferes with the detection of O I 4368 but the line appears to be stronger in the nova than in π Sgr (cF2) so that a contribution from O I is indicated.

The principal absorption spectrum is observed from July 7 to August 5 apart from H which persists longer. A few other lines may also persist after August 5, but, due to the fading of the continuum and the lower dispersion used after this date, they are not very clearly seen. Whilst the velocity remains sensibly constant throughout, various changes are noted in the principal absorption spectrum. In particular the lines all gradually sharpen and there are also various changes in relative intensity. The most noticeable change is the rapid fading of Mg II 4481 and the increase in prominence of various lines of Ti II. Both these phenomena have been well observed in other novae and are probably connected with the dilution of the radiation in the shell as it moves away from the star. It does not appear that it would be very profitable to study the changes in detail on the present spectrograms due to the difficulties that would be encountered with the large number of blends present.

The hydrogen absorption components.—It now remains to discuss the various absorption components of the hydrogen lines. The various components that have been distinguished are denoted by roman numerals for convenience in discussion.

The hydrogen lines associated with the principal spectrum (I) are observed throughout the entire period July 7 to August 20. However, unlike the rest of the principal spectrum, the velocity of the H lines is not constant. At the start of the series on July 7 the velocity agrees fairly well with the rest of the principal spectrum (−729 km/sec) but the lines gradually increase their displacement towards the shorter wave-lengths, reaching −889 km/sec on July 22. The displacement then gradually decreases and is again close to −729 km/sec at the end of the series (August 20). In view of the constancy of the rest of the principal spectrum it appears unlikely that this is due to a real velocity change. The shift is more probably caused by an unresolved component (II) which has a greater negative velocity shift than I, and which gradually rises and then falls in intensity, being weak or absent on both the first and last spectrograms of the series.

Also present on July 7 is III with a velocity of −1700 km/sec. On July 7 I is the strongest absorption but III gradually increases in strength and is stronger than I on July 18. III becomes rather broad and between July 7 and July 19 shows a progressive shift towards shorter wave-lengths, reaching −1895 km/sec. This is

apparently the effect of blending of components of varying relative intensities since on July 22 the broad line is seen separated into two components, at −1775 km/sec and −2053 km/sec. The former is considered as a continuation of III whilst the latter is a new component IV. By August 5 both III and IV are weak and, with the continual fading of the continuum and the change to a lower dispersion camera, they are not seen again after this date. On August 5 a new component V is seen for the first time with a displacement of −1164 km/sec. It is possible that V was actually present at an earlier date but blended with I. By August 8 this component has increased in intensity but is not subsequently seen, due presumably to both true fading and to weakening of the continuum.

Whilst it appears that I can be assigned to the principal spectrum and II, III and IV are in all probability part of the diffuse enhanced spectrum, which is known to be frequently multiple, the place of V in McLaughlin's scheme is not quite so clear. V is probably another component of the diffuse enhanced spectrum though its assignment to an Orion absorption phase is not impossible.

As noted earlier the principal spectrum (I) is quite rich in lines and a considerable number of elements have been identified in it. On the other hand, apart from the strongest lines of Fe II which are present in absorption III no lines other than those of H have been identified with certainty in any but the principal spectrum. It should, however, be borne in mind that such lines could easily be masked by lines of the principal spectrum. The absorption lines of N III (4097, 4103) are frequently seen in the later stages of nova development. Whilst displaced N III has sometimes been suspected in the present nova, the continuum near 4100 A is weak at the time when these lines would be expected to be strong.

The velocity measurements in the nova are summarized in Table II.

The emission spectrum.—In this section a summary is given of the lines identified in the emission spectrum and their changes in relative intensity and structure. As with the absorption spectrum the emission lines are sufficiently close to the "typical" nova for it only to be necessary to point out the principal features of the spectrum.

Below are listed the main lines identified at one stage or another of the nova development :

H : α, β, γ, δ, ϵ, ζ
He I : 5876, 4471
C II : 4267
N II : 5942–52, 5667–86, 5530–44, 5045, 5005–4994, 4774–4803, 4447, contribution to 4640.
N III : 4097, 4103
[N II] : 5755
O I : 6158
O II : 4415, contribution to 4640
[O I] : 6364, 6300, 5577
[O III] : 5007, 4959, 4363
Na I : 5890, 5896
Ca II : 3986 (blended with Hϵ) 3933
Fe II : 6456, 6248, 5317, 5276, 5235, 5197, 5169, 5018, 4924, 4583, 4233, 4174

The following lines are of doubtful identification :

6004 : A fairly strong line through the series of spectrograms. It has also been found in some other novae. Its identification is discussed by Larsson-Leander (7) who found the line to be present in Nova DK Lacertae. The identification

with N I 5999, 6008 is considered by him to be unsatisfactory in view of the absence of the other N I lines. This view is confirmed by the observations of the present nova.

5814 : A diffuse band. The variations in the intensity of this line suggest that it is part of the Orion spectrum (see below). It is possibly C IV 5802–12 which is found in Wolf–Rayet stars and has been suggested (**8**) as a possible identification for a line in the Orion spectrum of Nova Herculis. The identification should, however, be considered rather doubtful.

A broad emission from 4030 to 4063 : Contributions from O II and N II are possible.

TABLE II

Velocity Measurements in Nova Sagittarii 1954

Absorption I	−729 km/sec
II	(<I)
III	−1700 km/sec
IV	−2053 km/sec
V	−1164 km/sec

Interstellar Ca II velocity −6 km/sec

A broad band stretching from 4565 to 4497 gives the impression, especially on the last spectrogram of the series, as consisting of two overlapping emissions with centres at approximately 4515 and 4539. These may be 4510–4514 N III and 4541 He II. (4686 He II is probably present.) Fe II 4508–4549 may also contribute.

In the main essentials at least the development of the emission spectrum follows that shown in the "synthetic spectra" of a "typical" nova as constructed by McLaughlin (**2**). The first spectrum obtained is probably a little earlier than McLaughlin's "spectrum" for $1^{m}{\cdot}0$ below maximum and the last is between his "spectra" for $3^{m}{\cdot}8$ and $4^{m}{\cdot}6$ below maximum.

The actual drop in magnitude during the period covered by the observations appears, however, to have been greater than is indicated by these figures.

The chief changes found may be listed as follows :—

(1) The gradual fading of Fe II and Ca II and the increase of [O I] [O III] [N II] He I, and C II.

(2) The moderately rapid rise to maximum about August 5 of diffuse lines of N II. This is the Orion spectrum.

(3) The rapid development of the wide 4640 Orion emission about this time and its persistence throughout the rest of the series.

(4) The presence of wide H and Fe II lines of the diffuse enhanced spectrum which overlie the principal emission spectrum lines from early in the series but which fade out with the fading of the diffuse enhanced absorption.

McLaughlin (**9**) recognizes various rather definite stages in nova development characterized by the change in relative intensities of various lines. An attempt has been made to estimate these stages in the present case. They are:—

(1) The [O I] flash July 18
(2) The [N II] flash July 26 or slightly earlier
(3) The Helium flash July 26
(4) C II 4267/Fe II 4233 = 1 about August 13
(5) First trace of 5007 [O III] August 13
(5) [O III] 5007/Fe II 4924 = 1·0 between August 13 and 16

Later stages are not covered by the present series of spectrograms.

On the first spectrograms of the nova the emission spectrum is weak, even the hydrogen lines being relatively inconspicuous. Hγ and δ have the appearance

of broad hazy bands extending from the principal absorption line (I) (at −729 km/sec) to about +1050 km/sec with broad maxima at +630 km/sec and −200 km/sec and a minimum at +100 km/sec. The relative intensities of these features seem to change along the Balmer series. The maximum at −200 km/sec strengthens from Hδ and γ to Hβ and α; in fact, Hβ and α appear to show this maximum alone as a moderately sharp line displaced −200 km/sec. It seems unlikely that Fe II 4351 can markedly affect the appearance of Hγ since other Fe II lines are very weak at this stage. The interpretation of these lines is not quite clear as the well-known profile consisting of the H lines of the principal spectrum on which are superimposed the wider and weaker lines of the diffuse enhanced emission spectrum does not develop properly till between July 9 and 15.

By July 15 the emission lines have become strong and thereafter the interpretation is relatively simple. The diffuse enhanced emission never becomes very strong and the main features, apart from the Orion phase shown mainly by N II, are the wide but fairly sharply defined lines of the principal spectrum. The H lines of the principal spectrum, as seen about July 15, show two broad maxima at about +415 km/sec and −420 km/sec, the shortward peak being the stronger. A minimum is seen between the two peaks.

The main development in these bands from July 15 onwards is the gradual fading of the shortward peak and its further displacement towards the short wavelength edge of the line (to about −620 km/sec) together with the strengthening and sharpening of the longward peak, till from August 8 onwards the hydrogen lines have the appearance of broad uniform bands with a strong line superposed at +415 km/sec.

Since the majority of the lines observed are in the visual region of the spectrum where the dispersion is rather small, especially with the *f*/2 camera, it is not possible to discuss the structures of these lines in any detail. And in any case a detailed discussion could only be attempted after accurate spectrophotometry. However, it may be said that all the lines (apart from the diffuse lines of the Orion spectrum) tend to show structures similar to the hydrogen lines and to develop peaks approximately 800 km/sec apart. Nevertheless all the lines do not have the same structure, as is well illustrated by the lines 4267 C II and 4471 He I. These lines increase rapidly in intensity towards the end of the series and are strong on the last spectrogram obtained (August 20). Since these lines are in the blue region their structure is more easily studied than is the case with the majority of the lines. These lines appear as broad uniform bands with fairly sharp peaks near each edge (at +423 and −570 km/sec). The peaks with positive velocity displacement agree in position with the prominent peaks shown by the H lines but in 4267 and 4471 this peak is considerably weaker than the peak of negative velocity displacement, the latter being present, if at all, only very weakly in the H lines.

The interstellar Ca II H and K lines.—Strong sharp interstellar Ca II H is seen throughout the series of spectrograms. Ca II K is only seen near the beginning of the series, as later the fading of both the nova Ca II K broad emission and the continuum leave no background in this region of the spectrum. The persistence of broad Hε emission ensures a background on which Ca II H absorption may be seen. A mean velocity of −6 km/sec has been derived for these lines from the various spectrograms. The constancy of this velocity as well as the general appearance of the lines leaves little doubt that not only are they interstellar in origin but also that they are not affected by blending with nova features.

The position of the nova is sufficiently close to the direction of the galactic centre for the galactic rotation effect to be negligible. Thus a distance for the nova cannot be derived from the radial velocity of the interstellar lines. An attempt has therefore been made to estimate the distance of the nova from their intensities. Microphotometer tracings of the H and K region were obtained from two of the most suitable $f/3{\cdot}7$ spectrograms and equivalent widths were derived. Spot sensitometer marks were used to calibrate the photographic plates. The mean of the two plates is:—

Equivalent width Ca II H 0·7 A
Equivalent width Ca II K 1·1 A

The ratio of the equivalent widths is therefore K/H = 1·6. This ratio is in good agreement with the observations of Sanford and Wilson (**10**) who find that with increasing equivalent widths the ratio approaches 1·56, being practically equal to this value for H > 0·4 A.

Using the relationship between the intensity of the K line and distance, recently derived by Beals and Oke (**11**), a nova distance of about 3000 ps is deduced. If a general space absorption of $0^{m}{\cdot}8$/kps is assumed the distance modulus is $M - m = 14^{m}{\cdot}8$, so that if the nova reached $7^{m}{\cdot}0$ at maximum (it may perhaps have become even brighter) the absolute magnitude at maximum was $-7^{m}{\cdot}8$. In view of the considerable uncertainties involved in this type of calculation the value is in very satisfactory agreement with the absolute magnitude of other novae. McLaughlin (**12**) deduced a mean absolute magnitude of $-7^{m}{\cdot}0 \pm 0{\cdot}2$ for novae but since he used, amongst other data, the absolute magnitudes of novae in both the Magellanic Clouds and the Andromeda nebula which are now known to be in error by about 1^{m} in view of the new distance scale (**13**), his mean required changing to about $-7^{m}{\cdot}5$.

Acknowledgments.—I should like to express my thanks to Professor F. J. M. Stratton and Dr A. D. Thackeray for the very helpful discussions I have had with them on the subject of this paper. My thanks are also due to Dr Thackeray and Mr van Woerden who kindly obtained some of the spectrograms.

Radcliffe Observatory,
Pretoria:
1955 *July* 19.

References

(1) D. B. McLaughlin, *Michigan Publications*, **8**, No. 12, 1943.
(2) D. B. McLaughlin, *Pop. Ast.*, **52**, 109, 1944.
(3) G. Cecchini and L. Gratton, *Le Stelle Nuove*, Milano, 1942.
(4) F. J. M. Stratton and A. Beer, *M.N.*, **95**, 432, 1935.
(5) D. B. McLaughlin, *Ap. J.*, **84**, 104, 1936.
(6) W. P. Bidelman, *Trans. I.A.U.*, **8**, 852, 1952.
(7) G. Larsson-Leander, *Stockholms Obs. Annaler*, **18**, No. 4, 1954.
(8) D. B. McLaughlin, *Michigan Publications*, **6**, No. 12, 1937.
(9) D. B. McLaughlin, *Ap. J.*, **95**, 428, 1942.
(10) R. F. Sanford and O. C. Wilson, *Ap. J.*, **90**, 235, 1939.
(11) C. S. Beals and J. B. Oke, *M.N.*, **113**, 530, 1953.
(12) D. B. McLaughlin, *Pop. Ast.*, **50**, 233, 1942.
(13) W. Baade and A. D. Thackeray, *Trans. I.A.U.*, **8**, 397, 1952. A. D. Thackeray and A. J. Wesselink, *Nature*, **171**, 693, 1953.

AN OCCULTATION OF ANTARES OBSERVED AT THE UNION OBSERVATORY

David S. Evans

(Communicated by H.M. Astronomer at the Cape)

(Received 1955 January 28)*

Summary

The reappearance of Antares on 1953 March 8 was observed by Union Observatory and Leiden Southern Station personnel using the Rockefeller Twin Photographic Telescope of the Leiden Station, Union Observatory, Johannesburg. A photoelectric trace of both components was obtained. The angular diameter of the principal star is approximately 0".039. An auditory record was also obtained on magnetic tape in the form of a continuous note, frequency-modulated according to the output of the photocell.

Personnel.—The work described in this paper was done at the request of the author, and the analysis of the observation and preparation of this report were undertaken at the request of the Union Astronomer. The work was organized by Dr W. S. Finsen; Dr Th. Walraven was responsible for the photometer and associated amplifiers; Mr J. Hers for the frequency-modulation recorder; Mr P. C. Seligman for the Hathaway recorder; Mr J. Churms acted as time-keeper.

Equipment.—The telescope used was the Rockefeller Twin Photographic telescope of 16 inches aperture, and focal length 2·25 metres. The guiding telescope was of 6 inches aperture with a micrometer capable of being offset by about one degree. The focal plane diaphragm was of $\frac{1}{2}$ mm diameter, and behind it was placed a simple lens of 1 inch focal length. The photocell was an R.C.A. 931 A operated at 90 volts per stage with 90 volts on the collector stage. A filter, Schott BG 5, which, apart from infra-red transmission, has a maximum transmission of about 14 per cent at about 4300 A was employed, for the following reasons: first, to reduce the secondary spectrum and to permit the use of a small diaphragm (the peak transmission of the filter corresponds closely with the wave-length for which the object-glass of the telescope was corrected); second, in preliminary experiments it was found that with no filter and full aperture the light from Antares produced overshooting of the recording galvanometer. In these circumstances the initial deflection was not maintained, but fell rapidly over a period of several seconds, finally settling down to a value about half as great as the initial one. Application of a d.c. voltage to the amplifier produced no such effect. When the filter was introduced, the effect was much reduced, but there was still a change in deflection with time after every strong change in light, in the reverse direction from that initially seen (i.e. an undershoot instead of an overshoot), somewhat slower, and of a much smaller magnitude.

The explanation of this behaviour has not been found: it was considered by the Union Observatory team to be due to excessive light from Antares, and, for the given photocell, and in the given circumstances, there may be validity

* Received in original form 1954 August 8.

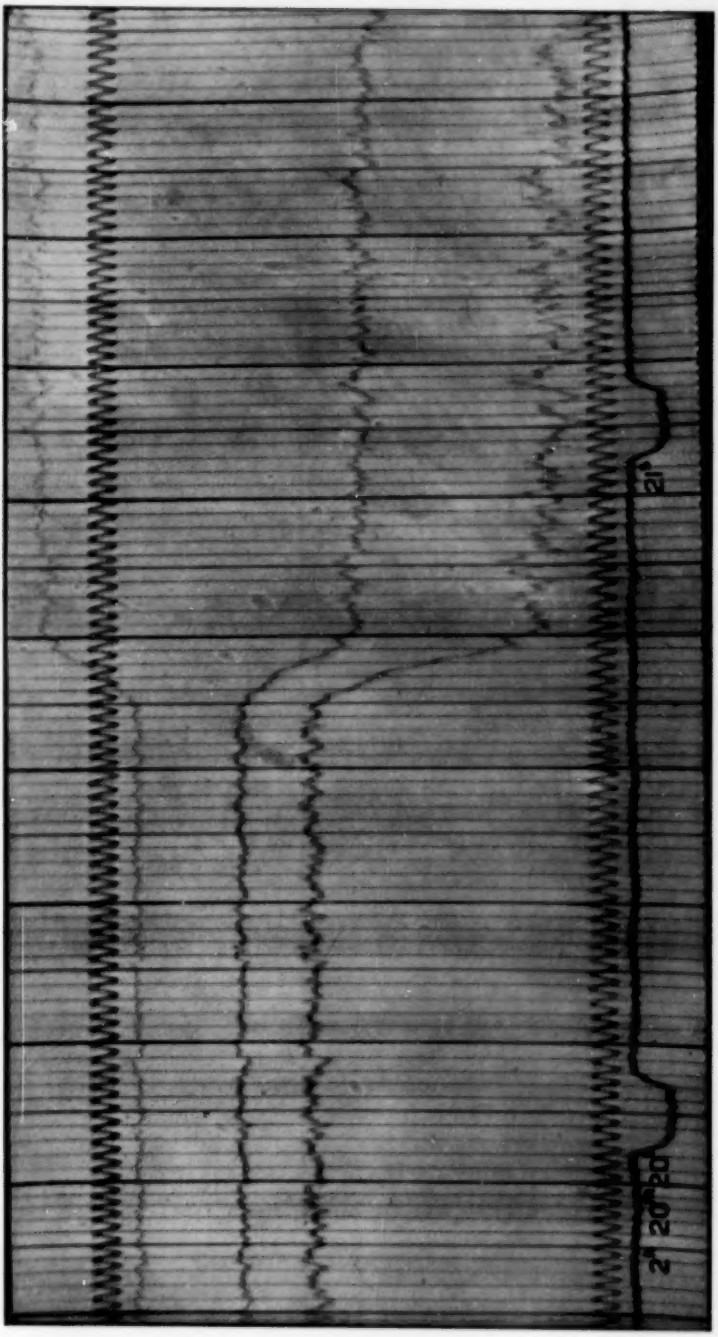

Reappearance of Antares A. The trace shows (i) records by three galvanometers (I, II, III) of the star light; (ii) 50 c/s from quartz clock (top and bottom); (iii) one-second pips with times marked. Time increases from left to right.

in this explanation. On the other hand, exactly parallel tests with much higher fluxes have been made on the occasion of other observations of Antares occultations without showing any behaviour of this kind. All that has ever been observed when the cells have been deliberately over-tried on very bright stars has been the normal progressive type of fatigue, in which there has been a loss of response of a few hundredths of a magnitude per minute, and only slow recovery. The incident flux for the full light of Antares can readily be computed from Whitford's formula (**1**) as $1{\cdot}7 \times 10^{-8}$ lumens for photoelectric light. The photocell current, with the filter in, was 0·1 microamperes. Even allowing for a reduction of as much as 5 magnitudes by the filter, if the values for the unobscured light of Antares are brought into comparison with data for the performance of 931 A photocells (**2**), it can be seen that even extremely slight, very slow, fatigue is only just possible, while saturation phenomena should only have occurred with fluxes tens of thousands of times greater.

What concerns us now is the validity of the observation. It is considered that, although the necessity for correcting the remaining instrumental drift introduces an element of personal judgment, an approximate value of the diameter of Antares can be derived from it.

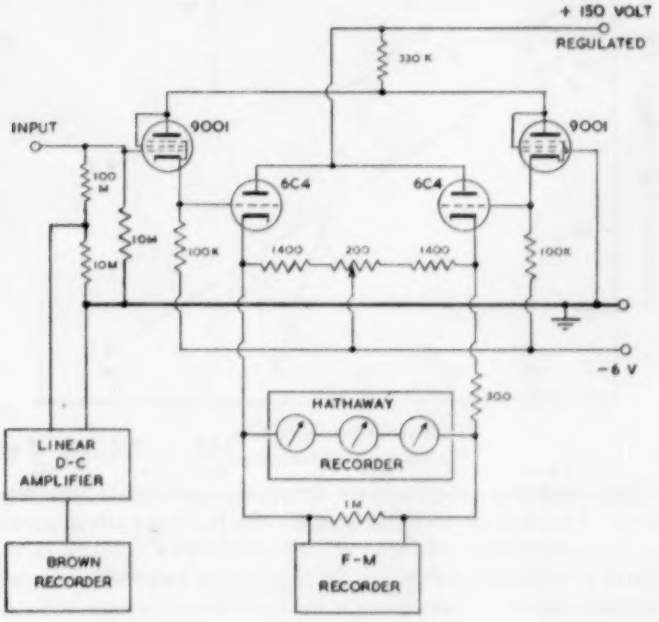

FIG. 1.

To return to the equipment: the output from the photocell could be fed to three recording devices. The first of these was a Brown recorder, the feed being brought through a 100 megohm series resistor to the 10 megohm input of the amplifier of this instrument. The second was a Hathaway recorder. The output of the photocell was fed to it through a d.c. amplifier, and the output of this at low impedance fed to three galvanometers of the Hathaway connected in

series and providing a load of about 150 ohms. Two of these galvanometers deflected in one direction, the third in the opposite direction. They had sensitivities of the order of 10 microamp/mm, and with damping resistors their response was flat to 150 c/s (Fig. 1). The galvanometer block was removed from the recorder case and was mounted separately to avoid motor vibration. Low-speed galvanometers were used to record one-second pips and alternating current at 50 c/s from the quartz crystal clock. The frequency of the latter is accurate to better than one part in 10^7 and at the time of the occultation the clock correction was +0·007 seconds. The recording speed in the Hathaway recorder was 5 inches per second: the internal time-marker was run from the 50 c/s mains merely in order to provide lines for ease of measurement later.

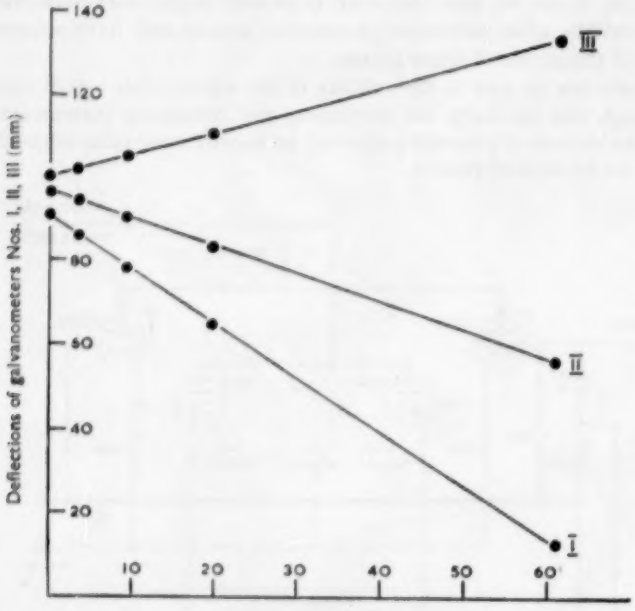

FIG 2.—*Calibration tests.*

The third recording device was the frequency-modulation recorder devised by Mr Hers. This was connected in parallel with the three galvanometers of the Hathaway recorder. The principle of this instrument consists in frequency modulation of a low-frequency carrier, the modulation frequency being a function of the photocell output. The record is made on magnetic tape and it has been found that when the tape is played back through a suitable demodulator to the Hathaway recorder, the result does not differ materially from that obtained directly. It is hoped to publish details of the method elsewhere. Its principal advantages appear to be: tape economy (for the tape can be left running for thirty minutes and can be re-used); wide frequency response; reduced liability to accident as compared with many types of recorder; and provision of an audible monitor, convenient during the event itself, as well as during preliminary adjustments and for demonstration purposes.

The equipment was calibrated by comparing the responses of the galvanometers with those of the Brown recorder (assumed linear) to the same source. The source was Antares itself immediately after the occultation, reduced by various filters. The filters were (in addition to the Schott BG 5): empty aperture, Schott NG 3, Schott NG 4, and Schott NG 5. The simultaneous records on the galvanometers and on the Brown recorder for these settings, repeated several times, enable the overall linearity of the equipment to be tested. Using the deflections attained after instrumental drift has ceased, one finds the linearity of the three records given by the three galvanometers to be very good (Fig. 2), and no correction is necessary.

The observation.—On nights previous to the occultation the micrometer was carefully set on the guiding star CPD -26° 5642, with Antares centred in the diaphragm. This adjustment was checked shortly before disappearance and again immediately after reappearance, when Antares was found to be accurately centred in the diaphragm. The photometric seeing at the time of the observation was much better than average and decidedly better than on previous nights.

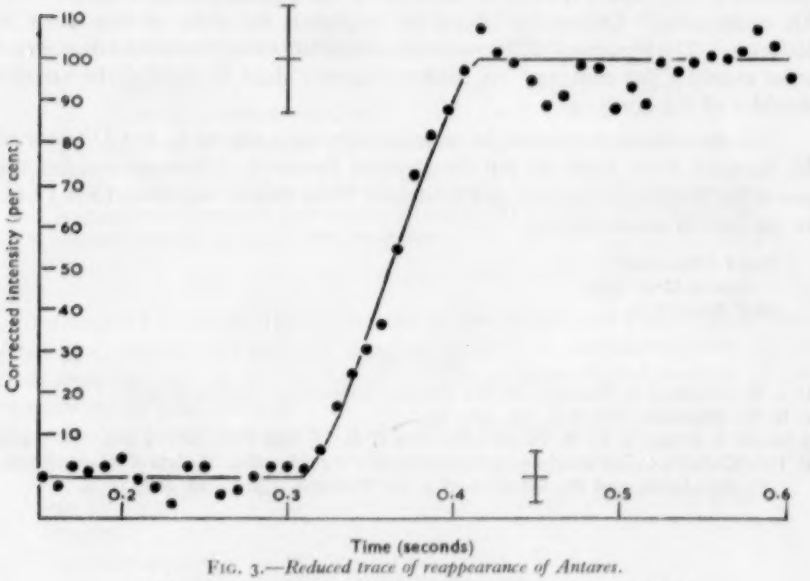

FIG. 3.—*Reduced trace of reappearance of Antares.*
The lengths of the vertical lines show the maximum displacement due to seeing at those levels.

This is borne out by comparison of the traces obtained for the occultation with those obtained at rehearsals, the latter showing far greater fluctuations. As a check, the diaphragm was placed at such a distance from the bright limb of the Moon that the intensity of the sky light approximated to that of Antares itself. The photocurrent fluctuations were then much less than in the case of Antares, showing that atmospheric conditions are the principal cause of the fluctuations recorded.

The companion reappeared at $2^h\ 20^m\ 11^s{\cdot}93$ U.T. and the centre of the principal star $8^s{\cdot}78$ later. This last-named figure has already been used in combination with other observations to derive a separation of $3''{\cdot}16$ and a P.A. of $274°\ 38'$ for the pair (**3**). The trace of the principal star as recorded on the three galvanometers is shown in Plate 6. The reappearance took slightly over $\frac{1}{10}$ second, so that there is no distortion produced by lag in the galvanometers. On galvanometer II, which was used for the reduction, the deflection for Antares B was 2·6 mm, and for A, 26 mm. Two or three trial reductions from measures of the traces of galvanometers Nos. II and III have been made. They indicate that the chief source of uncertainty in drawing the final curve lies in the allowance to be made for drift immediately after the reappearance of the principal component. The extent of this uncertainty in the estimated diameter is three or four units in the third place of decimals. The measures shown in Fig. 3, which are reduced to percentage deflections, represent what is considered to be the best choice for the value of the drift. The rate of advance of the lunar limb normal to itself at the point of emergence was taken to be $0''{\cdot}360$ per second. The continuous curve drawn in is that for the advance of a straight edge across a uniform disk of diameter $0''{\cdot}039$, which is taken as the value of the angular diameter indicated by this observation. Diffraction effects are negligible for disks of this order of diameter. The numerical differences introduced by taking this effect into account never exceed 1 per cent, and are confined to very short sections at the toe and shoulder of the curve (**4**).

The observation team wish to acknowledge their thanks to the Director of the Bernard Price Institute for Geophysical Research, Johannesburg, for the loan of the Hathaway recorder, and to Messrs Thos. Barlow and Sons (S.A.) Ltd, for the loan of accumulators.

Royal Observatory,
Cape of Good Hope:
1955 *January* 21.

References

(1) A. E. Whitford, in Strong's *Modern Physical Laboratory Practice*, p. 396.
(2) R. W. Engstrom, *J.O.S.A.*, **37**, 420, 1947.
(3) David S. Evans, J. C. R. Heydenrych and J. D. N. van Wyk, *M.N.*, **113**, 781, 1953.
(4) This elementary, but laborious, computation is best made using the data of Jahnke-Emde, *Funktiontafeln*, and the formulae of J. D. Williams, *Ap. J.*, **89**, 467, 1939.

SURFACE PHOTOMETRY OF THE MAGELLANIC CLOUDS

A. R. Hogg

(Communicated by the Commonwealth Astronomer)

(Received 1955 May 3*)

Summary

Two-colour photoelectric observations have been made at a number of points in the Magellanic Clouds and results reduced to the (B, V) system of Johnson and Morgan. Isophotes have been drawn for B magnitudes and sectional diagrams for the variation of colour B–V across the brighter regions of the Clouds.

The observational results give, for certain limited regions of the Clouds, the following figures :—

	S.M.C.	L.M.C.
Area sq. degrees (measured)	10·8	27·5
B magnitude	+2·6	+1·4
B–V colour	+0·1–+0·6	+0·33
Central brightness mag. sec^{-2}	21·4	21·4

The integrated brightnesses given are obviously lower limits to the actual figures.

The colour of the Small Cloud is found to be systematically bluer in the brighter central regions than nearer the edge. The Large Cloud shows no regular variation of colour over its surface.

Introduction.—Integrated magnitudes of the Magellanic Clouds have been given by G. van Herck (**1**), by H. Shapley (**2**), by J. S. Paraskevopoulos (**3**), by E. Hubble (**4**), and by G. de Vaucouleurs in an unpublished revision of the Shapley–Ames catalogue (**5**).

The magnitudes on photographic scales are as follows :—

		S.M.C.	L.M.C.
van Herck		$+2^m·8$	$+1^m·2$
Shapley		+2–3	–
Paraskevopoulos	(*a*)	+1·8	–
	(*b*)	+2·3	–
Hubble		+1·5	+0·5
de Vaucouleurs		+0·6	−0·6

and show a scatter reflecting the difficulties surrounding the measurement of such objects.

The results given by van Herck were obtained by extra-focal photometry and are probably the most satisfactory of those so far published. The figure given by Shapley was derived from star counts, whilst the results attributed to Paraskevopoulos were obtained by comparison of in-focus images of the Clouds with

* Received in original form 1955 January 19.

extra-focal images of bright stars. With a lens of 1 in. focal length Paraskevopoulos' result was $1^m{\cdot}8$ whilst with a lens of $\frac{1}{2}$ in. focal length the result was $2^m{\cdot}3$. The figures mentioned by Hubble are described by him as "estimates based upon published descriptions".

The present investigation aimed at defining isophotes in the Cloud regions by scanning with a photoelectric cell to determine a magnitude at least for the central regions of the Clouds. Partly because of the small acceptance cone of the photometer and the large angular dimensions of the object, this method becomes very tedious if applied to the detailed examination of the peripheral regions of the Clouds; and this has not been aimed at in the present series of results.

Observational.—The observations were made at the Cassegrain focus of a 20-inch reflector. Stray light from the sky was excluded by means of an iris diaphragm mounted on an extension of the draw tube. A diaphragm in the focal plane defined an area of sky approximately 3·4 minutes of arc in diameter and admitted light via a Fabry lens to the cathode of an EMI photomultiplier (Type 5060). The photocurrent was amplified and fed to a Brown recording potentiometer. Filters employed were b = 3 mm BG 18 and y = 2 mm GG 5. Apparently dark regions of the sky adjoining the Clouds were used as control areas and measures were made of the magnitude difference between the control areas and regions of the Clouds. The control regions chosen were as follows :—

for the S.M.C.	$\alpha(1950) = 02^h\ 00^m$	$\delta(1950) = -75°$
L.M.C.	$05\ 20$	-73
	$05\ 30$	-73
	$05\ 40$	73

In the case of the L.M.C. the mean of the three areas was used as a control.

These control areas were also compared with the star F of the Harvard F1 region (**6**), the magnitude of which had been found by comparison with a number of stars (particularly 40 Leonis, which is very nearly the same colour as F) for which magnitudes have been given by Johnson and Morgan (**7**) (UBV system). Magnitude–colour relations were so obtained to convert the "natural" system of filters and cell to the UBV scale. This gave for F a result on the B scale of $7^m{\cdot}91$ and a colour of $+0^m{\cdot}33$ on the B–V scale. The magnitude of the control areas by comparison with F amounted to :—

S.M.C. control area	$12^m{\cdot}58$ per sq. minute
L.M.C. control area (mean of 3 positions)	$12^m{\cdot}67$ per sq. minute

from measures on five and eight nights respectively. These magnitudes are on the B scale quoted above.

Magnitude measures and isophotes.—Measures with the blue filter (*b*) were made at 113 points in the S.M.C. on 8 nights (total 397 observations) and at 84 points in the L.M.C. on 7 nights (total 302 observations). In setting the telescope for these measures care was taken to exclude any obvious bright stars from the field. The limit of such stars was probably 12^m–13^m. The measures were partly traces at constant α with varying δ and partly traces at constant δ with varying α. Results were arranged in order of δ and by interpolations appropriate curves were drawn to define isophotes (Fig. 1). The central regions of the Small Cloud give average total readings (sky + Cloud) $0^m{\cdot}8$ brighter per unit area than the control area, i.e. they are 2·09 times the brightness of the

control area which, as mentioned above, is $12^m.58/min^2$. The brightness due to the Cloud alone (assuming that the control area truly represents the background) is 1·09 times that of the control area, i.e. $12^m.58 - 0^m.09 = 12^m.5/min^2 = 21^m.4/sec^2$ (S.M.C.). The corresponding figure for the Large Cloud is $12^m.67 - 0^m.19 = 12^m.5/min^2 = 21^m.4/sec^2$ (L.M.C.). These figures are on the B scale.

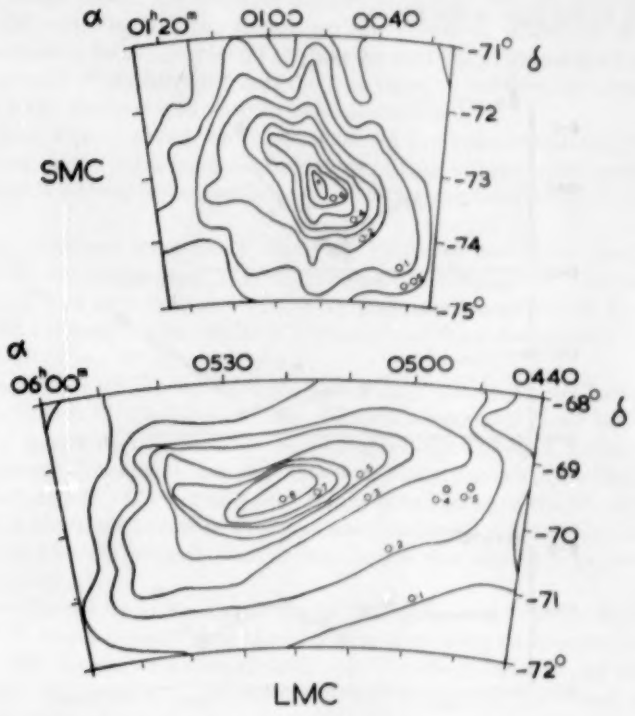

FIG. 1.—*Isophotes in the Magellanic Clouds (B system). The contours refer to the magnitude difference between the control regions and the total light received from object + sky.*

This result shows the measured parts of the central regions of the two Clouds to have about the same surface brightness, although the bright central portion of the Small Cloud covers much less area than that of the Large. The isophotes give some indication of the westward extension of the Small Cloud often referred to as the "wing".

Integrated magnitudes.—Integrated magnitudes were obtained by measurements with a planimeter of the areas included by the isophotes in Fig. 1. Partly because of the extended area of the object some difficulty was experienced in locating the $0^m.0$ isophote. Accordingly the following arbitrary limits of measurement were adopted :—

S.M.C. (1950) $\alpha = 00^h25^m - 01^h25^m$; $\delta = -71° - -75° = 18$ sq. deg.
L.M.C. (1950) $\alpha = 04^h40^m - 06^h00^m$; $\delta = -68° - -72° = 27\frac{1}{2}$ sq. deg.

In the case of the Small Cloud the limits seem to include most of the obviously brighter portions of the object, but with the Large Cloud the adopted limits excluded some obviously bright but irregular areas on the northern edge. The magnitudes given by this process, viz.

$$\text{S.M.C.} = +2^{m}\cdot6$$
$$\text{L.M.C.} = +1^{m}\cdot4$$

are therefore to be regarded as lower limits to the total brightness of the Clouds especially in the case of the Large.

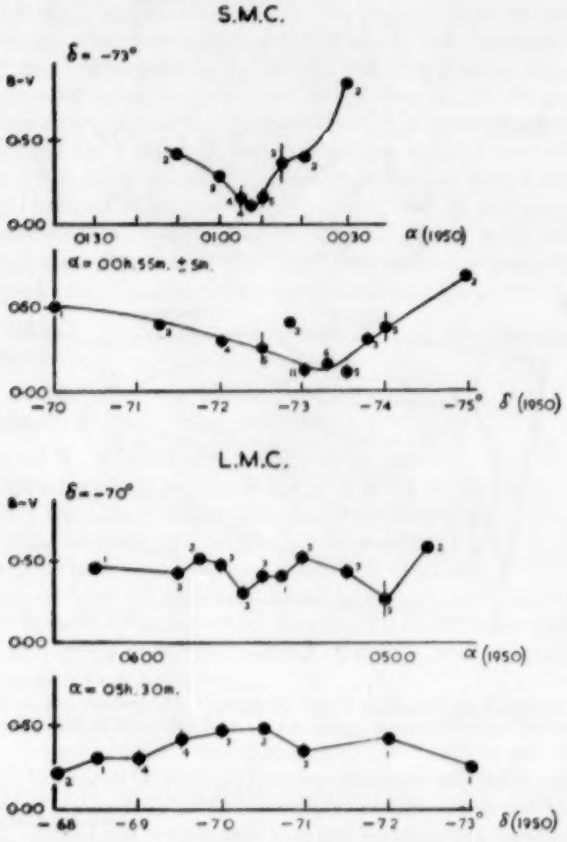

FIG. 2.—*Colours in the Magellanic Clouds (B-V system). The figures alongside the points indicate the number of observations and the vertical lines through the points denote standard deviations for those cases where more than two observations are available.*

The regions measured are notably less than the recognized dimensions of the Clouds, e.g. H. Shapley (**8**), gives angular diameters of 8° and 12° for the Small and Large Clouds respectively and the latter figure has been increased to 20° by G. de Vaucouleurs (**9**). Furthermore the measured integrated brightness will also be affected if the adopted control area does not represent the true sky background, i.e. the sum of (*a*) the amount of light from terrestrial sources, (*b*) the

amount of light coming from stars between the observer and the Cloud and (*c*) the amount of unobscured light coming from behind the Cloud. This is obviously a difficult quantity to measure with certainty and is not necessarily represented by readings taken around the edges of the Cloud. Some readings were obtained which indicated the presence of regions which were some one or two hundredths of a magnitude fainter than the control areas although in the case of the Large Cloud the mean of several peripheral regions showed zero magnitude difference against the control on the V system whilst the B result showed this mean to be brighter by $0^m{\cdot}01$ than the control. If the adopted control areas were actually $0^m{\cdot}02$ brighter than the true background then the integrated magnitudes given above would need to be decreased by $0^m{\cdot}1$.

Whilst there was no reason to suspect that the present photoelectric results were greatly in error (the integrated magnitudes being in reasonable agreement with van Herck's figures) it seemed desirable to undertake certain check observations.

Therefore measures were made, after the isophotes had been drawn, by observations on sections through the brighter parts of each Cloud. In the case of the Small Cloud new measures (O) at 13 points were made with the same apparatus and compared with results (C) interpolated from the diagram. This gave a mean $O-C=-0^m{\cdot}00\pm0{\cdot}02$ (s.d.).

A new photometer (EMI cell Type 5659, filter combination 1 mm Chance OBI glass + 2 mm Schott GG15 glass) with a different photometer head having an aperture of 3′ was used to obtain similar check readings on both Clouds.

For the Small Cloud O – C for 18 points was $+0{\cdot}01\pm0{\cdot}02$ and for the Large Cloud for 10 points $O-C=+0{\cdot}04\pm0{\cdot}03$. The grand mean of the O – C for 41 check points is therefore a little in excess of one hundredth of a magnitude. In view of the small-scale irregularities in the Clouds this can be regarded as a satisfactory result.

Colours.—The colour of the Small Cloud was determined mainly from two N–S and E–W traces centred near the brightest area using 70 observations on five nights. The figures were brought to the (B–V) scale of Johnson and Morgan by comparison of 13 stars. The results clearly show that the Small Cloud exhibits a definite gradient of colour, being bluer towards the centre than at the edges. The same effect is also shown in Table I, where the mean colour is determined for regions of varying brightness. The standard deviations and general drift of the means show that this is not a chance result.

Colour variations across a galaxy (the M31 nebula) have been detected by Stebbins and Whitford (**10**), and also by Fricke (**11**), but in this case the colour increases towards the centre and also exhibits a marked intensification in a dark area (see Fricke, Fig. 17). The colour of the Small Cloud at the centre is notably bluer than the results for other irregular nebulae quoted by Holmberg (**12**). Qualitatively a discrepancy of this sort could arise from an unsuitable choice of background region. In the present case it is found that, in the unlikely event of the true background being fainter than the corrected background by as much as $0^m{\cdot}02$ in the yellow, the colour should be $0^m{\cdot}05$ bluer than indicated ; a correction which does not improve the discrepancy.

The distribution of colour in the Small Cloud is difficult to account for by absorption due to dust intermingled with the stars in any regular fashion. The distribution suggests that the hotter stars are concentrated towards the centre

of the Cloud. The overall colour of the Small Cloud does not support the idea of a Type II population, which according to Baade (**13**), would be much redder. This fails to confirm a preliminary result obtained by Gascoigne and Kron (**14**); a result which is now being withdrawn by the authors (private communication).

TABLE I

Colours B–V of the Magellanic Clouds compared with surface brightness in magnitudes brighter than control areas

Surface brightness	*B–V*	*n*
	S.M.C.	
m	m m	
0·10	+0·57 ± 0·05 (s.d.)	17
·20	·50 ·10	12
·31	·38 ·04	12
·39	·22 ·05	7
·52	·17 ·06	9
·76	·13 ·03	9
	L.M.C.	
0·09	+0·30 ± 0·02	23
·20	·38 ·04	33
·29	·36 ·02	29
·39	·36 ·02	23
·51	·25 ·05	18
·60	·27 ·05	9
·70	·42 ·04	11
·87	·30 ·07	9

The colour results for the Large Cloud are arranged according to surface brightness in Table I, which summarizes 155 observations on 7 nights at 45 points. Traces across the Cloud at $\alpha = 05^h\ 40^m$ and $\delta = -70°$ are shown in Fig. 2. This figure also displays the number of observations used for each point and when this exceeds two, the standard deviation is indicated by lines. Although the trace in declination suggests a slight reddening at $-70°{\cdot}5$ the standard deviations are such as to make it unlikely that the result is real. There is also no systematic change of colour with the surface brightness (Table I) and it seems appropriate to represent the results by a grand mean giving a colour of $+0^m{\cdot}33$ for the Large Cloud; even though one area at $\alpha(1950) = 5^h40^m$ and $\delta(1950) = 69°{\cdot}5$ was found, where $B–V = +0^m{\cdot}12$. The average colour transferred to a photoelectrically defined International Colour Scale (**7**) is $+0^m{\cdot}19$, which is rather bluer than the result given by Holmberg for the resolvable irregular nebulae ($+0^m{\cdot}3$).

Conclusion.—The foregoing results clearly indicate a distinction between both Magellanic Clouds and other irregular nebulae for which colours have been found. Whilst it is not impossible that despite the relatively high galactic latitudes of the Clouds ($-32°$ for the Large and $-45°$ for the Small) some galactic absorption occurs, it would not qualitatively affect the conclusions that the Small Cloud is bluer than a Type II population and that the Large Cloud is also bluer than the usual resolvable irregular nebula. The colour of the central portion of the Large

Cloud is somewhat, and that of the central portion of the Small Cloud is considerably bluer than the colour of other irregular nebulae. Further, the systematic variation of colour across the Small Cloud contrasts with the practical uniformity of colour over the Large.

The assistance of Mrs A. de Vaucouleurs in measuring and reducing the records is gratefully acknowledged.

Commonwealth Observatory,
Canberra, A.C.T.:
1955 *April* 27.

References

(1) G. van Herck, *B.A.N.*, **6**, 61, 1930.
(2) H. Shapley, *Harv. Circ.*, No. 260.
(3) J. S. Paraskevopoulos, *Harv. Bull.*, No. 840.
(4) E. Hubble, *Ap. J.*, **64**, 321, 1926 = *M.W.C.* 324.
(5) H. Shapley and E. Ames, *Harv. Ann.*, **88**, 41, 1950.
(6) E. C. Pickering, *Harv. Ann.*, **71**, 304, 1917.
(7) H. Johnson and W. Morgan, *Ap. J.*, **117**, 313, 1953.
(8) H. Shapley, *Pub. Obs. Michigan*, *X*, 79, 1950.
(9) G. de Vaucouleurs, *Obs.*, **74**, 23, 1953.
(10) J. Stebbins and A. Whitford, *M.N.*, **110**, 416, 1950.
(11) E. Fricke, *Zs. f. Astrophysik*, **34**, 137, 1954.
(12) E. Holmberg, *Lund. Medd.*, Series II, No. 128.
(13) W. Baade, *Pub. Obs. Michigan*, *X*, 10, 1950.
(14) S. C. B. Gascoigne and G. E. Kron, *P.A.S.P.*, **65**, 52, 1953.

THE PERIOD–LUMINOSITY RELATION IN POPULATION II

V. C. Reddish

(Communicated by Professor W. M. H. Greaves)

(Received 1955 April 5)

Summary

Correlations between the periods, luminosities and radii of Population II variables with periods between one and a hundred days are investigated. It is shown that the recently suggested division of the period–luminosity relation into three discrete lines (1) probably cannot be justified on the basis of existing data.

A further analysis of the published observations on twelve variables (1, 2) leads to the conclusion that two of the variables differ considerably in composition, though not in mass, from the remainder, and have therefore probably evolved along different lines.

The results of accurate observations of the colours and magnitudes of thirteen Population II variables have recently been published by H. C. Arp (1). The variables have periods in the range one to a hundred days. In an analysis of the data, Arp suggests that the period–luminosity relation consists of three discrete lines, each differing from its neighbour by a factor of two in period, and representing different modes of pulsation.

In this paper the analysis of the observations is extended, and considered in conjunction with pulsation and stellar structure theory. It is shown that there is probably no justification, on the basis of existing data, for supposing that these variables pulsate in different modes. It appears that two of the variables (those with the shortest periods) differ considerably in composition, though not in mass, from the remainder. The remaining variables specify a unique period–luminosity relation.

The period–luminosity relation* is reproduced in Fig. 1 on an M_{bol} scale, together with Arp's lines. The data is given in Table I. The mean M_{pg} are those given by Arp (1). Mean spectral types are from observations by Joy (2). Luminosity class and effective temperature from the Table in Hynek's *Astrophysics* (3); bolometric corrections by Kuiper (4).

Arp noted that in four of the variables successive cycles differed but alternate ones reproduced. He suggested that the true period was therefore the time for two cycles. The effect of doubling the previously used periods is shown on Fig. 1 by dashed arrows.

The period of pulsation of a variable is related to its mass and radius by the relation

$$P(M/R^3)^{1/2} = 0{\cdot}041 \qquad (1)$$

where the period is in days and the mass and radius in solar units, the constant being that derived by Epstein (5).

* Only the twelve stars for which spectral types are known are plotted, since only for these can reasonably accurate bolometric corrections be made (see next footnote).

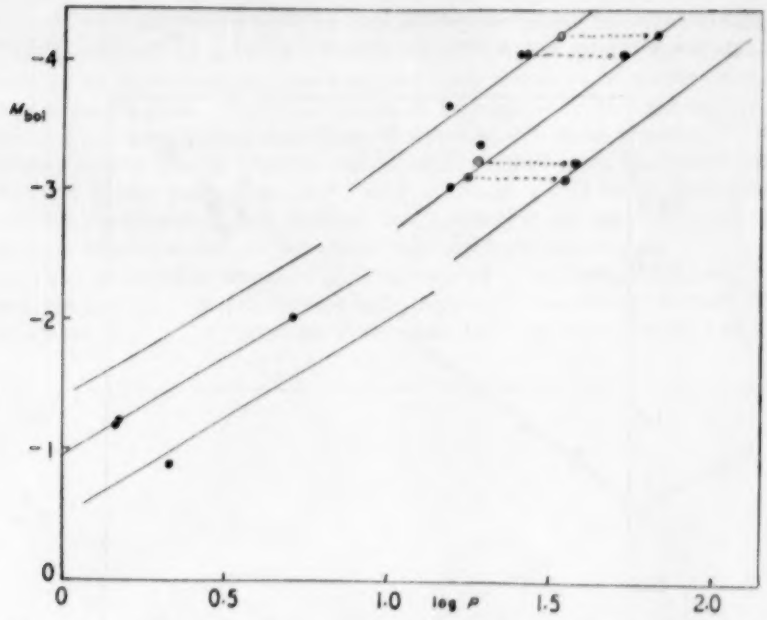

FIG. 1.—*The period–luminosity diagram according to Arp. The circled dots are those for which Arp doubled the period, as shown by arrows and crosses.*

TABLE I

Sources of the data are given in the text

Cluster	Variable	log P	Mean M_{pg}	Mean Sp.	Lum. Class	log T_e	$B.C.$	M_{bol}	log R
M3	154	1·184	−3·40	F9	II–Ib	3·72	0·26	−3·66	1·73
M5	42	1·410	−3·77	F8·5	Ib	3·72	0·29	−4·06	1·81
	84	1·423	−3·72	G0	Ib	3·70	0·35	−4·07	1·85
M13	1	0·164	−0·98	A7	II–III	3·91	0·24	−1·22	0·86
	6	0·325	−0·82	F3·5	II	3·825	0·07	−0·89	0·97
	2	0·708	−1·89	F6·5	II	3·765	0·14	−2·03	1·32
M10	3	0·896	−2·06	?					
	2	1·273	−2·99	F8·5	II–Ib	3·725	0·25	−3·24	1·64
M15	1	0·158	−1·01	A9	II–III	3·89	0·17	−1·18	0·90
M2	1	1·192	−2·75	G0	II	3·71	0·28	−3·03	1·63
	5	1·244	−2·90	F8	II	3·74	0·21	−3·11	1·58
	6	1·286	−3·11	F9	II	3·725	0·25	−3·36	1·66
	11	1·527	−3·91	F9	Ib	3·71	0·31	−4·22	1·86

From the point of view of the structure related to pulsation, a radius–period diagram is therefore more fundamental than a period–luminosity relation. Such a diagram is given on Fig. 2 from the data in Table I.* The radius increases

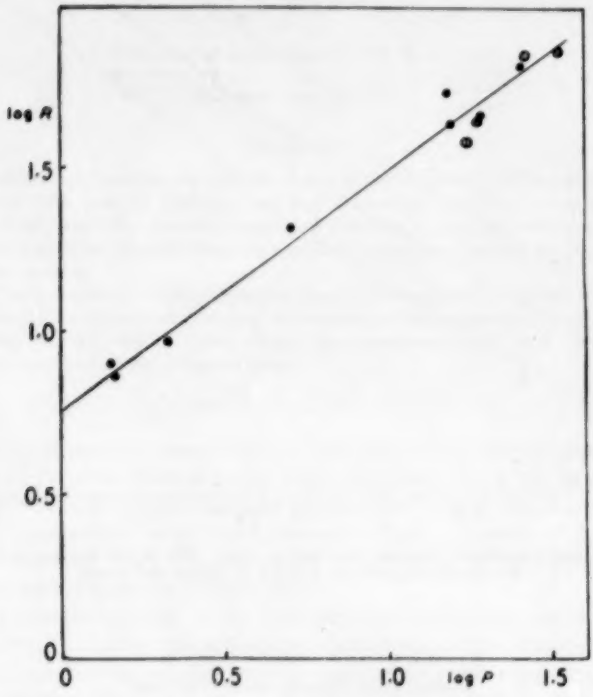

FIG. 2.—*Radius–period diagram. The circled dots are those for which Arp used double the period.*

continuously with period. It therefore follows from equation (1) that *there is no discontinuity of mass along the sequence.*

Fig. 2 gives the relation

$$\log R = 0{\cdot}74 \log P + 0{\cdot}75. \tag{2}$$

Equation (1) may be written

$$\log R = 0{\cdot}67 \log P + 0{\cdot}33 \log M + 0{\cdot}925. \tag{3}$$

Equations (2) and (3) lead to the relation

$$\log M = 0{\cdot}21 \log P - 0{\cdot}54. \tag{4}$$

* The radii have been obtained using surface temperatures derived from the spectral types. If the colours are used to give surface temperatures, the resulting relation similar to equation (4) predicts masses as small as $0{\cdot}01 M_{\odot}$ for the brightest variables. Considerations of age and evolution show that this is ridiculous. The colours result in too high surface temperatures, the error increasing with luminosity. The use of spectral types gives much more agreeable results. It is *not* suggested that the measured colours are in error; the possibility of such a difficulty occurring was pointed out by Arp; it is a result of insufficient knowledge of colour–temperature relations.

For $\log P = 0$, $P = 1$ day, this gives $M = 0{\cdot}3$, and for $\log P = 1{\cdot}5$, $P = 30$ days, $M = 0{\cdot}6$. These values are only about, or less than, half those to be expected according to recent estimates of the masses of the brighter Population II stars (**6**). This discrepancy (if in fact it is) could result from the spectral types being too early by 0·1 to 0·2 spectral classes or (and more probably) from over-estimating the luminosity class. Since the masses of Population II stars are considerably less at a given magnitude than those of Population I, their densities at a given luminosity and spectral type are less; thus those stars given luminosity class II in Table I may perhaps be Ib.* Such a change would lower the calculated effective temperatures and increase the bolometric corrections; both these changes would increase the calculated radii and hence the masses.

Theories of stellar structure give relations involving mass, luminosity, radius and composition. A radius–luminosity diagram is therefore of interest, and is shown on Fig. 3. All but two of the stars fall close to a straight line. The

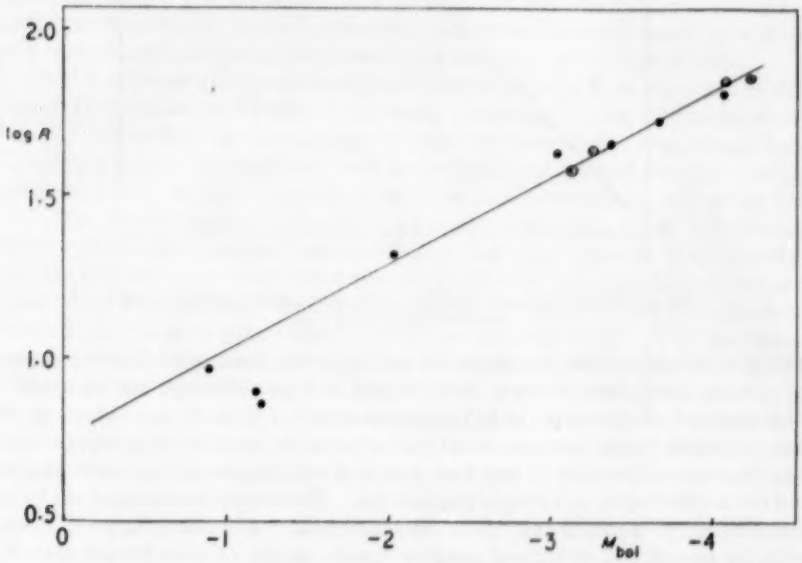

FIG. 3.—*Radius–luminosity diagram. The circled dots are those for which Arp used double the period.*

radius and luminosity vary continuously along the remaining sequence of stars. Since the mass also varies continuously *there is no discontinuity in composition along this sequence.* However, since the masses and radii of the two stars lying off this sequence are continuous with those on it, *they must differ from the remainder in luminosity and hence in composition.* For a given radius and period, they are *brighter by about three-quarters of a magnitude than the sequence formed by the other ten stars.* They deviate from the line by six and eight times the standard deviation of the remaining points: such large displacements are unlikely to be due to chance.

* Popper (**7**) classified some of the brighter stars in M3 and M13 as Ib.

It is now instructive to re-examine the period–luminosity diagram, given in Fig. 4 (the points are the same as on Fig. 1). The two stars which do not

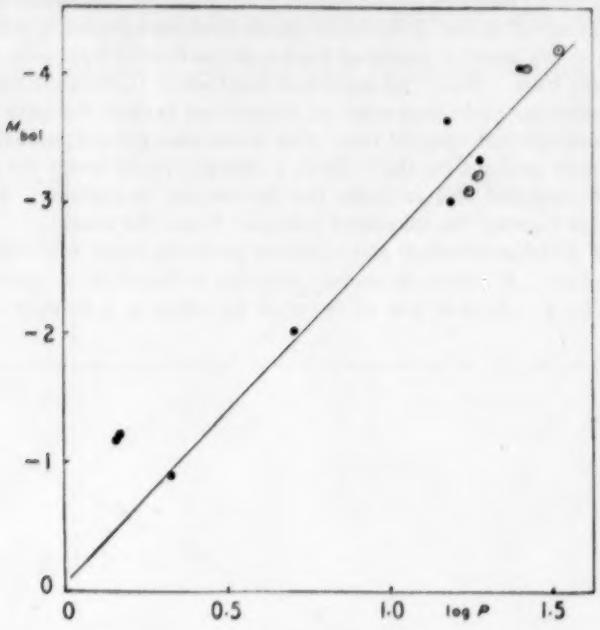

FIG. 4.—*Period–luminosity diagram. The circled dots are those for which Arp used double the period.*

form part of the continuous sequence on Fig. 3 are the two of shortest period. Neglecting these two points a straight line is drawn through the remainder. The standard deviation of the ten points about the line is $0^m{\cdot}22$. Much of the error probably results from the calculation of mean luminosities from the observed magnitudes, uncertainty of the zero point of the magnitudes in each cluster, and the conversion to bolometric magnitudes. The dispersion is about the value that should be expected (1). The distribution of the errors is in good accord with the law of distribution of random errors, as can be seen from Table II; this supports the view that the ten points define a single linear relation,

$$M_{bol} = -0{\cdot}07 - 2{\cdot}67 \log P. \qquad (5)$$

TABLE II

Deviations of the ten points from the straight line on Fig. 4, compared to those to be expected from a normal error distribution

x = deviation in magnitudes	Observed number with deviation $\geqslant x$	Expected number with deviation $\geqslant x$
0·4	1	1
0·25	3	3
0·20	6	4
0·15	6	5
0·10	7	7
0·05	10	8
0·00	10	10

The two stars of shortest period are again about three-quarters of a magnitude brighter than the sequence defined by the remaining stars.

It is evident from Fig. 3 that these two stars differ from the remainder not, as Arp assumed, in period as a result of a different mode of pulsation, but in luminosity as a result of a difference in composition. The distribution of the remaining ten points gives no justification for a division into different modes of pulsation. The differences of successive cycles, and similarity of alternate ones, which were noted in four of the variables, may result from interaction between the fundamental and other frequencies rather than from high excitation of the second harmonic.

The opacity in such high luminosity, low density stars will be due to electron-scattering (unless the abundance of heavy elements in their envelopes is very high). The luminosity then depends on the composition in proportion to $\mu^4/(1+X)$ where μ is the molecular weight in the envelope and X the hydrogen abundance. For a factor of two in luminosity this implies a difference of about 15 per cent in molecular weight and a difference of between 10 per cent and 30 per cent in hydrogen abundance. Thus the two stars of shortest period probably have about 20 per cent less hydrogen in their envelopes than the remaining ten stars.

Such a difference in the composition of the envelopes may be supposed to have existed throughout the lifetime of the stars, or to have developed comparatively recently. The first alternative suggests that the luminosity L has always been higher by a factor of at least two,* and since age is proportional, for a given stage in the evolution, to M/L where M is the mass, the age would be only about half that of the remaining stars. However, if a group of stars forms with considerably different composition and at a time different from the majority, it is extremely unlikely that they would evolve at such a rate that at some particular later time those which had reached a certain stage in their evolution would have the same masses as the remaining stars which had also reached that stage. It is much more probable that the two stars have only recently strayed from the path of evolution followed by the rest, and that the change in the composition of their envelopes has occurred fairly quickly. That such a splitting of the evolutionary paths may occur has been predicted by the writer (**8**), but of course the existence of two stray stars cannot be considered as strong evidence of this; they merely point to the need for more observations.

On his final period–luminosity diagram, Arp included six variables in ω Centauri for which the values of m_{pg} were known. Since the mean spectra are not known, it is not possible to include them in Fig. 4. It appears likely, however, that four of them will fall close to the straight line, while the other two may be close to the pair which are three-quarters of a magnitude brighter than the line.

Department of Astronomy,
University of Edinburgh:
1955 *April* 4.

* This figure may not be correct if there are differences in heavy element abundances, since in the earlier life of the stars opacity may be due partly to photoelectric absorption; but arguments similar to that which follows will still hold.

References

(1) H. C. Arp, *A. J.*, **60**, 1, 1955.
(2) A. H. Joy, *Ap. J.*, **110**, 105, 1949.
(3) J. A. Hynek, *Astrophysics*, p. 20, McGraw-Hill, 1951.
(4) G. P. Kuiper, *Ap. J.*, **88**, 429, 1938.
(5) I. Epstein, *Ap. J.*, **112**, 6, 1950.
(6) V. C. Reddish, *M.N.*, **115**, 32, 1955.
(7) D. M. Popper, *Ap. J.*, **105**, 204, 1947.
(8) V. C. Reddish, *The Observatory*, **74**, 68, 1954.

POLARIZATION MEASUREMENTS ON THREE INTENSE RADIO SOURCES

R. Hanbury Brown, H. P. Palmer and A. R. Thompson

(Communicated by A. C. B. Lovell)

(Received 1955 May 2)

Summary

The radiation from three intense extra-terrestrial radio sources, in Cygnus, Cassiopeia and Taurus, has been tested for polarization at a wave-length of 1·9 m. The results show that, in the flux from the sources in Cygnus and Cassiopeia, there is no plane polarized component greater than 1 per cent and no circularly polarized component greater than 4 per cent. In the case of the source in Taurus (the Crab Nebula) the corresponding limits are 2½ per cent and 4 per cent respectively.

1. *Introduction.*—At the present time the Sun is the only extra-terrestrial radio source which is known to emit polarized radiation. It is well established that, under certain conditions, a significant fraction of the solar radio flux is circularly polarized. The radiation from the discrete sources of galactic and extra-galactic radio emission (radio stars) is generally taken to be unpolarized, although there is little evidence to support this assumption. The only published experiments appear to be those of Ryle and Smith (**1**) who examined the intense sources in Cygnus (19N4A)* and Cassiopeia (23N5A)* with an interference polarimeter. They concluded that, at a frequency of 80 Mc/s, the flux from these two sources is unpolarized and they set an upper limit of about 5 per cent to the intensity of any polarized component.

The present paper reports some measurements which were intended to check, and if possible improve, the existing limits set by Ryle and Smith, and also to extend the observations to the intense source in Taurus (05N2A)*. This source has been identified with the Crab Nebula, and the recent report (**3**) that the light from this nebula is polarized suggested that the radio flux should also be tested for polarization.

2. *The Equipment.*—An outline of the equipment is shown in Fig. 1. The two aerials X and Y were arranged to form an interferometer with a baseline of about 200 metres. This distance was chosen so that, at a wavelength of 1·9 m, the interferometer had a resolving power of about half a degree and was therefore capable of separating the discrete sources from the general background radiation. The two aerials were circular paraboloids with diameters of 30 ft and 25 ft. A reflector with double curvature, such as a paraboloid, is not ideal for polarization tests; nevertheless the present aerials were selected because of their unusual construction, which allowed each paraboloid to be rotated about its axis of symmetry without altering its direction. This particular property made it possible to reduce the systematic errors in the measurements.

* The numbers given against these sources refer to the "Catalogue of Reliably Known Discrete Sources of Cosmic Radio Waves" prepared by a committee of I.A.U. (see reference (**2**)).

The 30 ft paraboloid (X) was equipped with two identical primary feeds at right angles, each feed consisting of a dipole and reflector. The 25 ft paraboloid (Y) was equipped in the same way for the detection of plane polarization (Fig. 1(*a*)); but, for the detection of circular polarization (Fig. 1(*b*)), a single dipole and reflector were substituted. In the arrangement shown in Fig. 1(*a*) the two dipoles in each aerial were connected by short cables of equal length to a coaxial changeover switch (S_1,S_2) which in turn was connected to a preamplifier feeding a long cable to a central receiver. The two switches were remotely controlled from the receiver in

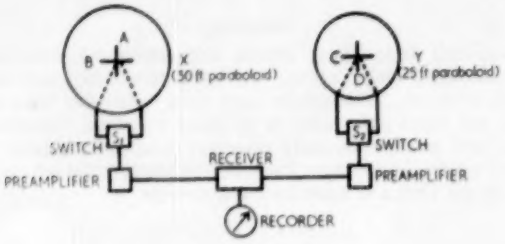

(*a*)

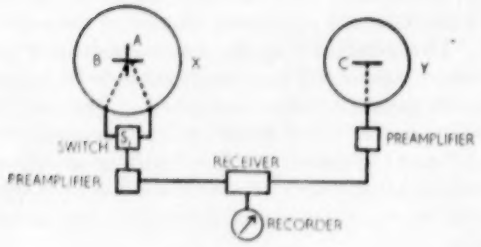

(*b*)

FIG. 1.—*Outline of apparatus for measuring polarization, (a) for plane polarization, (b) for circular polarization.*

such a way that either of the dipoles in each aerial could be selected at will. In the second arrangement, shown in Fig. 1(*b*), only one coaxial switch was employed.

The central receiver was tuned to 158·2 Mc/s and had a pre-detector bandwidth of 400 kc/s and an output time-constant of 5 seconds. It operated on the "rotating-lobe" principle and has been described elsewhere (**4**); in effect it multiplied the two signals together and displayed their product on a pen recorder.

3. *Method of observation.* (*a*) *The measurement of plane polarization.*—For the measurement of plane polarization the apparatus was connected as shown in Fig. 1(*a*). The two aerials were fixed in azimuth (due south), and were tilted in elevation so that the axes of the paraboloids were directed to the declination of the source. The paraboloids were then rotated about their axes so that the primary feeds were in the relative positions shown in Fig. 2(*a*). With the aerials in this position the amplitude of the interference pattern produced by the source was observed during its transit through the aerial beams, the observations being made alternately with the dipoles AD and BC.

In order to minimize any errors in the relative amplitude of the patterns observed, the receiver was switched between the two aerial combinations (AD,BC) every five minutes during the period of observation (Fig. 3). This switching procedure eliminated the effects of any slow changes in the receiver gain, such as might be expected from day to day. It was found convenient to increase the frequency of the interference pattern, by means of a rotating phase-shifter (**4**), so that at least ten complete cycles occurred in each switching interval, thus enabling the amplitude of the pattern to be measured with satisfactory accuracy.

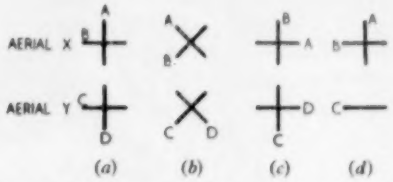

FIG. 2.—*Relative positions of the primary feeds in the two aerials as viewed from the source.*

The first observations were made on the most intense of the sources, namely that in Cassiopeia. After a sufficient number of satisfactory transits had been observed with the aerials in the relative positions shown in Fig. 2(*a*), the two paraboloids were rotated through 45° (Fig. 2(*b*)) and the measurements were repeated. Finally a third set of observations were made with the paraboloids rotated through 90° (Fig. 2(*c*)).

The sources in Cygnus and Taurus were observed in the same way, except that the measurements were confined to two positions of the aerials 45° apart (Figs. 2(*a*) and 2(*b*)).

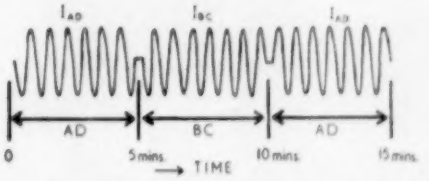

FIG. 3.—*A simplified diagram of an interference pattern.*

(*b*) *The measurement of circular polarization.*—For the measurement of circular polarization the apparatus was connected as in Fig. 1(*b*) and the paraboloids were adjusted so that the primary feeds occupied the relative positions shown in Fig. 2(*d*). The amplitudes of the interference patterns produced by each source were then observed using alternately the parallel dipoles BC and the orthogonal dipoles AC; as in previous tests the receiver was switched between these two combinations every five minutes.

4. *Plane polarization-analysis and results.* (*a*) *Method of analysis.*—If the radiation incident on the aerial system of the apparatus shown in Fig. 1(*a*) is randomly polarized or circularly polarized, then the amplitude of the interference patterns (I_{AD}, I_{BC}) observed with the orthogonal pairs of dipoles (AD or BC) will be equal and independent of the rotation of the paraboloids about their axes. But,

if a significant component of plane polarization is present, then there will be a difference in the amplitudes of the patterns given by

$$\frac{I_{AD}-I_{BC}}{I_{AD}+I_{BC}} = m_p \cos(2\theta) \qquad (1)$$

where m_p (assumed to be $\ll 1$) is the fraction of the incident flux which is plane polarized, and θ is the angle between the plane of polarization and that of the dipoles A and D.

The records of each source were analysed to give values of I_{AD} and I_{BC} for each angular position of the aerial system. The upper limit to the value of the polarization (m_p) was then estimated by means of equation (1). It was assumed in making this estimate that the plane of polarization might have any value, but that it remained constant throughout the period covered by the observations. This assumption is discussed later in Section 6.

It was assumed in equation (1) that the gain of each aerial is independent of which of the two primary feeds is in use. Since the beam formed by each paraboloid is elliptical, this assumption is only valid for directions close to the axis. Thus, in principle, observations of the amplitudes I_{AD}, I_{BC} should be restricted to the instant when the source transits the centres of the aerial beams. In the present experiment this difficulty was overcome by recording the mean values of I_{AD}, I_{BC} in alternate five minute intervals for about half an hour before and after the transit of the source. The amplitudes I_{AD}, I_{BC} corresponding to the time of transit were then obtained from smooth curves drawn through these observed values.

It was also necessary to ensure that there was no systematic difference in the gain of the two aerials with the two orthogonal sets of primary feeds. A difference in gain is to be expected if there is any lack of symmetry in the paraboloids or if the primary feeds are not identical. The necessary check was provided by the observations made on the source in Cassiopeia. It was found that for all three positions of the aerials (Figs. 2(*a*), 2(*b*) and 2(*c*)) there was no detectable difference between the amplitudes of the patterns observed with the dipoles AD and BC. It followed from this result that any difference between the gains of the aerials with the two combinations of primary feeds could be neglected.

TABLE I

Results of plane polarization measurements

Source	Percentage of flux which is plane polarized ($m_p \times 100$)
Cassiopeia (23N5A)	<1 per cent
Cygnus (19N4A)	<1 per cent
Taurus (05N2A)	$<2\frac{1}{2}$ per cent

(*b*) *Results.*—The results of the tests for plane polarization are shown in Table I. They are based on six transits of the sources in Cassiopeia and Taurus, and five transits of the source in Cygnus. All the observations were made within a period of four weeks in December 1954 and January 1955. The observations on Cassiopeia were divided between the three aerial positions shown in Figs. 2(*a*), (*b*) and (*c*), while those on Cygnus and Taurus were taken with the two aerial positions shown in Figs. 2(*a*) and (*b*).

No evidence of plane polarization was found for any of the three sources. In all cases the difference in the amplitudes of the two patterns ($I_{AD} - I_{AC}$) was not significantly greater than the uncertainty introduced by random noise. Thus the limits given in Table I were determined entirely by the signal to noise ratio, and to improve them substantially would require the use of larger aerials.

5. *Circular polarization-analysis and results.* (*a*) *Method of analysis.*—If the radiation incident on the aerial system (Fig.1(*d*)) is randomly polarized, then an interference pattern will be observed with the parallel dipoles BC but not with the orthogonal dipoles AC. However, if there is a component with circular polarization, then a pattern will be observed with both combination of feeds. Thus if I_{AC}, I_{BC} are the amplitudes of these two patterns then

$$\frac{I_{AC}}{I_{BC}} \simeq m_c \qquad (2)$$

where m_c is the fraction (assumed to be $\ll 1$) of the total incident flux which is circularly polarized.

The records of the three sources were analysed in the same way as those obtained in the previous tests. The resulting values of I_{AC} and I_{BC}, corresponding to the time when the source was in the centre of the aerial beams, were then used to estimate the upper limit to any circular polarization by means of equation (2).

It must, of course, be noted that a plane-polarized component can also give rise to an interference pattern with orthogonal dipoles. However, this possibility could be neglected in the present analysis, since the presence of plane polarization had already been ruled out by the previous tests.

TABLE II

Results of circular polarization measurements

Source	Percentage of flux which is circularly polarized ($m_c \times 100$)
Cassiopeia (23N5A)	<4 per cent
Cygnus (19N4A)	<4 per cent
Taurus (05N2A)	<4 per cent

(*b*) *Results.*—No significant evidence of circular polarization was found for any of the three sources. The results of the tests are shown in Table II. They are based on two transits of Cassiopeia, three transits of Cygnus and four transits of Taurus. All the observations were made between 1955 January 12 and 17.

The upper limits given in Table II were set, not by the signal-to-noise ratio, but by imperfections in the aerial system. In practice it is difficult to ensure that the response of each aerial is zero to waves polarized at right angles to the plane of the feed; in consequence a large component of unpolarized flux produces a small, but observable, interference pattern even when the dipoles in the two aerials are orthogonal. The presence of this spurious pattern sets a limit to the minimum fraction (m_c) of circular polarization which can be measured. An estimate of the errors in the aerial system, together with a comparison of the records obtained on the three sources, showed that the minimum value of m_c which could be detected reliably was about 4 per cent, and hence this limit has been given in Table II.

6. *Discussion.*—The results presented above show that any component of plane polarization from the sources in Cygnus and Cassiopeia must be less than 1 per cent of their flux at 1·9 m. They also show that any component of circular

polarization must be small (<4 per cent) and therefore confirm the conclusion reached by Ryle and Smith (**1**).

No evidence of polarization, plane or circular, was found in the radiation from the source in Taurus (the Crab Nebula). Thus the suggestion that the radio flux from this object, like the light, might be polarized is not confirmed at 1·9 m. If, as has been suggested by several authors, the radio emission from the Crab Nebula is due to fast electrons in a magnetic field, then it seems rather unlikely that a substantial percentage of polarization would be observed at this wavelength. Thus, in the presence of the necessary magnetic field ($\sim 10^{-2} - 10^{-4}$ gauss), the plane of a polarized wave would be rotated many times in the nebula; however, it must be noted that this rotation is proportional to the square of the wavelength, and it is therefore important to test for polarization at considerably shorter wavelengths.

In conclusion one peculiar difficulty of the present type of measurement is of interest. Throughout this paper it has been assumed that the position angle (θ) of the plane of polarization remains constant from day to day. However it has been shown elsewhere (**5**), (**6**) that, in the presence of the Earth's magnetic field, the polarization of an extra-terrestrial radio wave is modified by the ionosphere. A very rough estimate (**5**) shows that, at a frequency of 100 Mc/s, a plane-polarized wave may be rotated through as many as 3 complete revolutions. Since this rotation depends upon the total electron content of the ionosphere, the apparent plane of the wave may vary significantly from day to day and even from hour to hour. Not only does this phenomenon complicate the problem of measuring the plane of a wave, but it may also reduce the chance of detecting polarization with the technique described here. A detailed analysis of the present results has therefore been made on the assumption that the plane of a polarized component remained constant throughout a single observation but that it was completely random from day to day. The results show that the chance that the limits given in Table I were exceeded is increased by a negligible amount, and that therefore the conclusions reached above are not significantly altered by the effects of the ionosphere.

The authors wish to thank Professor A. C. B. Lovell for his interest in the investigation. One of the authors (A. R. T.) is indebted to the Department of Scientific and Industrial Research for a maintenance grant.

University of Manchester,
Jodrell Bank Experimental Station,
Lower Withington,
Macclesfield,
Cheshire:
1955 *April* 29.

(**1**) Ryle, M. and Smith, F. G., *Nature*, **162**, 462, 1948.
(**2**) Pawsey, J. L., *Ap. J.*, **121**, 1, 1955.
(**3**) Dombrovski, V. A., *Dok. Akad. Nauk.*, **94**, 1021, 1954.
(**4**) Hanbury Brown, R., Palmer, H. P. and Thompson, A. R., *Phil. Mag.*, **46**, 857, 1955.
(**5**) Hanbury Brown, R. and Twiss, R. Q., *Phil. Mag.*, **45**, 663, 1954.
(**6**) Murray, W. A. S. and Hargreaves, J. K., *Nature*, **173**, 944, 1954.

CENTRE-LIMB VARIATIONS IN THE EQUIVALENT WIDTHS OF SOME INFRA-RED FRAUNHOFER LINES

B. E. J. Pagel

(Received 1955 June 13)

Summary

Using tracings recorded on Mount Wilson with the McMath–Hulbert Observatory duplicate infra-red spectrometer, the equivalent widths of nine Fe I lines in the neighbourhood of λ 15 500 with excitation potentials close to 5·60 volts have been measured at angles of emergence from the solar surface corresponding to $\mu = 1{\cdot}0$, 0·8, 0·6, 0·5, 0·4, 0·3 and 0·2. The results were compared with those which would be predicted on the basis of three photospheric models recently put forward by Aller and Pierce, de Jager, and Michard. The line profiles were calculated in detail for each model with the aid of modern techniques of high-speed computation, using the EDSAC at the University Mathematical Laboratory, Cambridge. The centre-limb variations in equivalent width calculated from the models differ mainly as a result of differences in the first and second derivatives of the source function close to the surface. The behaviour of the stronger lines observed is best reproduced from the temperature distribution of de Jager, while that of the weaker lines (except close to the limb) is more consistent with those of Aller and Pierce, and Michard. Finally, the observations were used for an inductive determination of the temperature distribution; this distribution was then corrected to give agreement with the observational data. The final model thus obtained agrees closely in the deeper layers ($\tau_0 \geqslant 0{\cdot}06$) with Michard's model. In the outer layers, the temperature gradient is considerably steeper, as in de Jager's model, but the additional feature of a temperature inversion appears very close to the surface ($\tau_0 = 0{\cdot}015$). It is suggested that a model of this type may be consistent with observations of the intensity of the continuum at the extreme limb, as well as with the observed behaviour of Fraunhofer lines.

---

1. *Introduction.*—The determination of the detailed structure of the solar photosphere is of great interest in connection with two separate problems—the examination of the physical character of the outer regions of the Sun, and the quantitative chemical analysis of the solar atmosphere from measurements of Fraunhofer line intensities. Much work has been carried out with the object of determining the distributions of temperature, total gas pressure, and electron pressure with optical depth in the photosphere, and the models that have been put forward may in general be divided into three classes according to the manner in which the temperature distribution is derived. One class consists of theoretical models in which the temperature distribution is governed by the theory of radiative equilibrium (Chandrasekhar, 1950), with or without modifications introduced to take into account the occurrence of convective instability at optical depths $\tau_0 > 1{\cdot}0$ and the "blanketing effect" of radiation scattered or reradiated

in Fraunhofer lines near the surface. A second class consists of the limb-darkening models, in which the source function (and hence the temperature) is derived empirically from the observed limb-darkening curves at various wave-lengths, combined with the relative energy–wave-length distribution at the centre of the disk, by means of trial solutions of the integral equation of limb-darkening (Chalonge and Kourganoff, 1946; Pierce and Aller, 1951; Peyturaux, 1952). In the third class, finally, we have the empirical models in which the temperature distribution is derived from the behaviour of line profiles or equivalent widths across the disk (Voigt, 1950; de Jager, 1952; Houtgast, 1952). All models assume the value of the solar constant as a boundary condition, and the distributions of pressure and electron pressure are usually derived from the temperature distributions; for this purpose, local thermodynamic and hydrostatic equilibrium are assumed, together with a chemical composition consistent with the observed spectrum (Strömgren, 1940).

A detailed survey of the present state of studies of the photosphere is given by Minnaert (1953). The derivation of a theoretical model is complicated by three factors: the difficulty in calculating the Chandrasekhar mean of the continuous absorption coefficient (Chandrasekhar and Münch, 1946; Aller and Pierce, 1952), the remaining uncertainty in the precise effect of the onset of convective instability, and the inadequate convergence of the iterations employed in calculating the blanketing effect. Hence, at present, it is necessary to find the true temperature distribution empirically. Observations of continuous limb-darkening at different wave-lengths, interpreted through expansions of the source function in exponential integrals as suggested by Kourganoff (1949), apparently lead to very satisfactory results for the layers with monochromatic optical depths $\tau_\lambda > 0{\cdot}2$, but the source function nearer the surface is uncertain owing to the difficulty in obtaining limb-darkening measurements closer to the limb than $\mu = 0{\cdot}2$, where μ is the cosine of the angle of emergence. The study of line intensities offers supplementary information of great value, since the residual intensities at the different points of a line profile are determined by the variation of the source function over the entire range of depths visible from outside: in particular, the sharp increase towards the surface in the selective absorption coefficients of neutral metal lines leads to a high weighting of the outer layers ($\tau_\lambda \leqslant 0{\cdot}2$) in the calculation of the central intensities and equivalent widths of these lines. By observing their variation across the disk, it is possible to eliminate some of the uncertainties in the amount of the selective absorption coefficient and in its precise broadening mechanism that would complicate the interpretation of a line profile measured only at the centre of the disk. If, as now seems likely, the mechanisms of non-coherent scattering and pure absorption predominate in the formation of Fraunhofer lines (Houtgast, 1942; Spitzer, 1944; Unsöld, 1948; Houtgast, 1952), the source function in any layer is directly related to the temperature through Planck's radiation formula, though corrections must be applied in the cases where scattering predominates. The temperature distribution with continuous optical depth τ_λ may then be deduced if the relation between τ_λ and the selective optical depth τ_l is known for each portion of a line profile; the most convenient method of obtaining such a relation is to calculate the continuous and selective absorption coefficients as functions of τ_λ in a previously given model that is known to be approximately correct. If the ratio η of the two absorption coefficients is critically dependent on the assumed

temperature, this procedure must be repeated several times before the final model can be obtained; if not, η may be assumed to be the same in the final model as in the initial one.

The results of recent investigations of the infra-red solar spectrum with high resolution, using photoconductive detectors, have been described by Goldberg (1950). The variation across the disk in the profiles of the Si I lines near λ 16 000 has been investigated at the McMath–Hulbert Observatory by R. M. Page (1951), and the variations in the equivalent widths of the CO lines at λ 23 000 and at λ 46 000 have been studied by G. Newkirk using tracings obtained with the Snow Telescope (Goldberg and Müller, 1953). A full list of solar lines in the wave-length range $1{\cdot}4\mu$–$2{\cdot}5\mu$, together with their identifications and equivalent widths, has been published by Mohler, Pierce, McMath, and Goldberg (1953). The tracings obtained with the McMath–Hulbert Observatory duplicate infra-red spectrometer (Mohler, Pierce, McMath, and Goldberg, 1950) now have a resolving power of the order of 60 000 (R. R. McMath, private communication), and are very suitable for equivalent width measurements, although accurate studies of line profiles must still be confined to the wings of stronger lines (E. W. $>$250 mA). In the present paper, the observed centre-limb variations in some infra-red equivalent widths are analysed in terms of three empirical photospheric models recently put forward, and a new model, consistent with the observational material, is derived.

2. *Observational results.*—The plan in this investigation has been to collect a series of data on a number of lines formed under similar conditions of wave-length, excitation potential, and ionization potential in order that the trends may not be obscured by a number of independently varying parameters. The wave-length range λ 15 530–λ 15 670 is ideal for this purpose, as it contains several Fe I lines with excitation potentials in the neighbourhood of 5·60 eV and with equivalent widths ranging from 12 mA to 350 mA, so that their behaviour across the disk may be studied as a function of line intensity only; small differences in the degree of collision and Stark damping have a negligible effect on equivalent width in this range of line intensity. Telluric lines are almost completely absent in this wave-length range.

Through the courtesy of Professor R. R. McMath and of Professor I. S. Bowen, it was possible for the writer to obtain a long series of tracings of this wave-length region (Fig. 1) at seven different points of the solar disk, corresponding to $\mu = 1{\cdot}0, 0{\cdot}8, 0{\cdot}6, 0{\cdot}5, 0{\cdot}4, 0{\cdot}3, 0{\cdot}2$, taken between 1952 December and 1953 February with the McMath–Hulbert Observatory duplicate infra-red spectrometer; the tracings were recorded by Mr W. Livingston. The spectra were taken under excellent atmospheric conditions with a slit width of 0·25 A (or 0·11 cm^{-1}; resolving power 60 000) and the effective resolving power, though difficult to measure precisely, certainly does not fall far short of this. The calibration curve of the recording system is substantially linear apart from a depression of the zero (Mohler, Pierce, McMath, and Goldberg, 1950); this depression was compensated during the tracings by permitting an auxiliary beam of light of a suitable constant intensity to reach the photoconductive cell. The deflection of the records is thus directly proportional to the intensity of incident radiation; an inspection of the instrumental profile recorded with light from a mercury discharge tube indicates that a negligible amount of radiation is scattered outside the range of the normal profile (which will leave equivalent widths unaffected). The

TABLE I

Observational results

λ	E.P.	Degree of blend	W (Mohler *et al.*)	W, r_c'						
				$\mu=1.0$	$\mu=0.8$	$\mu=0.6$	$\mu=0.5$	$\mu=0.4$	$\mu=0.3$	$\mu=0.2$
15531·80	5·64	A	99	119±3 (10) 0·846	125±2 (3) 0·840	130±4 (4) 0·838	131±3 (5) 0·835	137±3 (4) 0·834	141±4 (5) 0·832	132±3 (4) 0·833
15534·31	5·64	A	107	132±2 (10) 0·815	134±5 (3) 0·813	138±4 (4) 0·812	141±1 (5) 0·810	146±1 (4) 0·810	150±4 (5) 0·812	145±4 (4) 0·812
15537·71	5·79	B	71	71±1 (5) 0·908	72±1 (2) 0·908	81±1 (2) 0·896	80±3 (4) 0·890	88±3 (4) 0·885	88±4 (5) 0·881	90±2 (4) 0·878
15542·15	5·64	B	93	111±3 (3) 0·840	115±2 (3) 0·836	119±3 (4) 0·834	125±3 (4) 0·829	126±7 (2) 0·830	129±5 (5) 0·826	133±6 (4) 0·820
15565·38	5·61 5·42	C	12	12·4±0·3 (10) 0·977	13·8±0·1 (2) 0·977	14·3±1·0 (3) 0·969	15·9±1·0 (4) 0·974	16·6±1·0 (4) 0·971	19·4±0·7 (5) 0·966	20·3±1·0 (3) 0·962
15566·88	5·62	A	26	36·7±0·2 (9) 0·944	38·1±0·5 (3) 0·945	41·0±2·0 (4) 0·936	42·1±1·3 (4) 0·932	43·4±1·0 (3) 0·930	45·3±1·7 (5) 0·928	50·3±0·5 (3) 0·926
15593·71	5·03	C	32	31·6±1·0 (9) 0·952	32·3±0·2 (3) 0·951	34·0±0·5 (4) 0·948	37·0±1·0 (3) 0·944	40·4±2·3 (3) 0·940	40·4±2·0 (5) 0·938	43·7±1·0 (3) 0·935
15621·68	5·54	A	256	342±3 (11) 0·676	346±8 (3) 0·681	345±7 (3) 0·690	347±10 (3) 0·686	350±5 (4) 0·698	355±6 (4) 0·720	329±9 (3) 0·717
15662·05	5·60	A	185	222±3 (11) 0·749	223±5 (3) 0·750	228±4 (3) 0·752	227±3 (5) 0·758	230±2 (4) 0·757	230±3 (5) 0·759	208±7 (5) 0·766

wave-lengths and identifications of the lines were taken from the published list (Mohler, Pierce, McMath, and Goldberg, 1953) and the dispersion on the tracings is very uniform; its value is 0·620 ± 0·002 cm/A (0·161 A/mm), and the equivalent widths were found by measuring each area ten times with a planimeter. The rate of scanning employed was 4·0 A/min.

The results of the measurements are given in Table I, where the equivalent widths in mA, W, are recorded together with the r.m.s. errors, the number of tracings on which each result is based (in parentheses), and the apparent central residual intensities r_c' (uncorrected for instrumental broadening). The first four columns of Table I are taken from the table given by Mohler, Pierce, McMath, and Goldberg (1953). The equivalent widths obtained by the writer at the centre of the disk are appreciably larger (~20 per cent) than those published by the Michigan group of workers. The percentage discrepancy increases systematically with line strength, and is probably due partly to changes in resolving power and partly to the manner in which the line wings have been taken into account in the present series of measurements. The height of the continuum on our tracings is about 20 cm at the centre of the solar disk, so that the discrepancy is too large to be accounted for by an error in the position of the zero; furthermore, such an error would result in the same percentage discrepancy for all lines. It is interesting to note that the discrepancy tends to be much smaller in the case of the more blended "B" and "C" lines; the reason for this is not clear, but it seems to point to differences in the treatment of the unblended line wings. Such differences will not affect the degree of variation across the disk in a line of given strength.

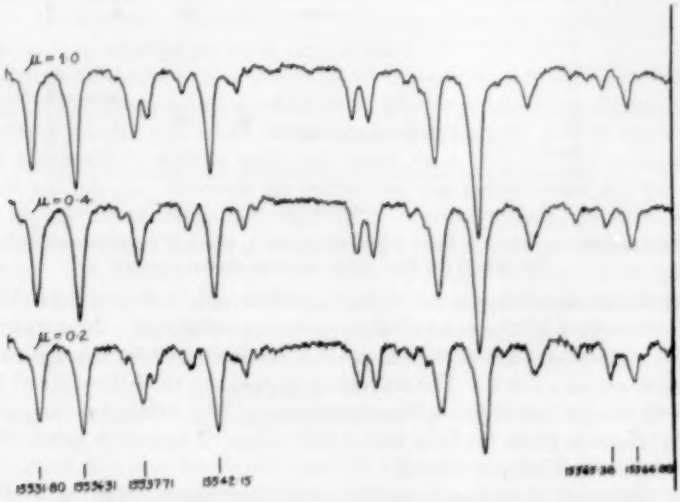

FIG. 1.—*Tracings of Fraunhofer spectrum at λ 15530, taken with the McMath–Hulbert Observatory duplicate infra-red spectrograph.*

An inspection of Fig. 1 shows that a certain allowance must be made for blending in the profiles of nearly all the lines, though the blending is not severe in most cases. When only one half of a line is blended, the Michigan workers suggest the reconstruction of the blended half by symmetry. However, such

a procedure would introduce serious errors if applied to faint lines such as these, as it is not easy to draw the central "axis" of a line with sufficient accuracy; furthermore, any asymmetry in the effective instrumental profile would introduce a systematic error. Since the degree of blending is always so slight that the residual intensity of either line wing would exceed 0·90 in the absence of the other line, it is sufficiently accurate to neglect "saturation" effects and write

$$r = r_1 r_2,$$

where r is the resultant true residual intensity due to two separate line wings which would have residual intensities r_1, r_2 in the absence of blending; this formula is strictly valid in the case of blending between a solar and a telluric line (Mohler, Pierce, McMath and Goldberg, 1953). Its adequacy in this context is confirmed by the calculations of Section 4, since the residual intensity $r = 0{\cdot}90$ (corresponding to $W \simeq 30$ mA) turns out to be on the linear portion of the curve of growth for $\mu \geqslant 0{\cdot}2$.

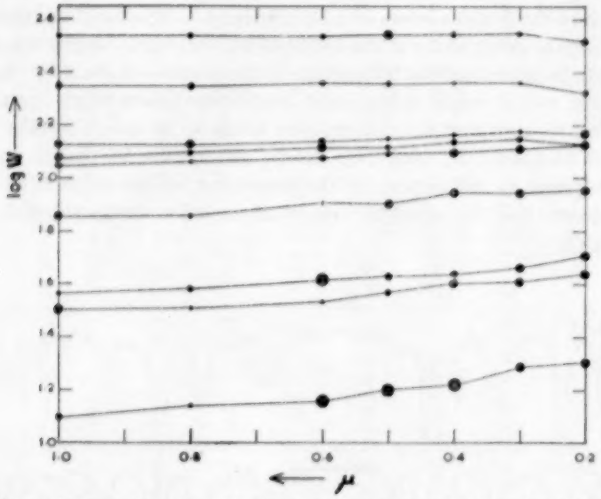

FIG. 2.—*Observational results: log W is plotted against μ, where W is equivalent width in mA. The sizes of the black circles represent the r.m.s. errors.*

The observational results are shown logarithmically in Fig. 2, the r.m.s. errors being represented by the sizes of the representative circles. It is clear that all the lines increase in intensity out to $\mu = 0{\cdot}3$, while all but the strongest continue to increase out to $\mu = 0{\cdot}2$. The mutual consistency in the behaviour of different lines with similar intensities is very satisfactory; Fig. 2 may be compared with a similar diagram given for lines with a wide range of excitation potentials in the visible region by Houtgast (1952).

3. *Calculation of equivalent widths in a given model.*—Owing to the high excitation potentials of the Fe I lines studied here, it is appropriate to assume that the re-emission is governed by local thermodynamic equilibrium or "pure absorption" (Unsöld, 1948; Pagel, 1954). The equation of transfer may then be expressed in the form

$$\mu \frac{dI_l(\tau_\lambda, \Delta\lambda, \mu)}{d\tau_\lambda} = \{1 + \eta(\tau_\lambda, \Delta\lambda)\}\{I_l(\tau_\lambda, \Delta\lambda, \mu) - B_\lambda(\tau_\lambda)\}, \qquad (1)$$

where $I_l(\tau_\lambda, \Delta\lambda, \mu)$ is the intensity of radiation at a given point of a line profile distant $\Delta\lambda$ A from the line centre in a layer with monochromatic optical depth τ_λ, and $B_\lambda(\tau_\lambda)$ is the Planck emission function for wave-length λ corresponding to the temperature $T(\tau_\lambda)$. To determine the line profile in a given model, it is necessary to calculate the functions $B_\lambda(\tau_\lambda), \eta(\tau_\lambda, \Delta\lambda)$ for several different values of $\Delta\lambda$, and then to integrate equation (1) subject to the boundary condition

$$\frac{dI_l}{d\tau_\lambda} \to 0 \quad \text{as} \quad \tau_\lambda \to \infty. \tag{2}$$

For a given μ, such an integration leads to the surface intensities $I_l(0, \Delta\lambda, \mu)$ for the line and $I_\lambda(0, \mu)$ for the adjacent continuum; the equivalent width is deduced by integrating the degree of absorption

$$R(\Delta\lambda, \mu) = 1 - r(\Delta\lambda, \mu) = \frac{I_\lambda(0, \mu) - I_l(0, \Delta\lambda, \mu)}{I_\lambda(0, \mu)} \tag{3}$$

over the line profile.

Over a limited range of optical depth, it is possible to represent the functions B, $\eta(\Delta\lambda)$ by simple algebraic functions of τ_λ, and this method of "schematic models" has been applied by Houtgast (1952) to the analysis of line profile variations in terms of a number of different photospheric models. In this investigation, however, the observational material consists of equivalent widths, the values of which depend on the behaviour of B, η over a wide range of optical depths. It is therefore preferable to use numerical procedures exclusively, employing high-speed automatic techniques to deal with the large amount of computing involved. The integrations of the transfer equation were carried out using the EDSAC at the University Mathematical Laboratory, Cambridge, tables of τ_λ, B_λ, and $\eta(\Delta\lambda)$ being prepared in advance by hand computation.

The data published by the authors of the various models were first reduced to standard form by computing tables of τ_λ (for λ 15 500), Θ, $\log P$, and $\log P_e$ corresponding to the published temperature distributions and to a standard chemical composition with a hydrogen-metal ratio $A = 10^4$ and a negligible proportion of helium. Reasons for preferring this composition are given by Michard (1953); its precision is not crucial here, as the electron pressure is very nearly cancelled out in the calculation of η for neutral metals, while the lines observed are not intense enough for their equivalent widths to be affected appreciably by changes of the order of 50 per cent in the collision and Stark damping constants (cf. Section 4). The source function B was then calculated at each tabulated interval from Planck's formula, which leads to

$$B_{15500}(\Theta) = \frac{1{\cdot}3327 \times 10^{13}}{10^{0{\cdot}8018\Theta} - 1} \text{ erg/cm}^2\text{/sec/cm/sterad}. \tag{4}$$

The calculation of η may be divided into the following steps:—

(*a*) The continuous mass-absorption coefficient κ_λ was found from the equation

$$\kappa_\lambda = \frac{1}{m_H} \{P_e a_\lambda(H^-) + a_\lambda(H)\}, \tag{5}$$

where m_H is the mass of the hydrogen atom, $a_\lambda(H^-)$ is the total cross-section of H^- per neutral H atom at unit electron pressure, and $a_\lambda(H)$ is the atomic cross-section for absorption by neutral H (Chandrasekhar and Münch, 1946). The

values of $a_\lambda(H^-)$ were obtained by interpolating for λ 15 500 and for the relevant values of Θ in the tables of Chandrasekhar and Breen (1946); $a_\lambda(H)$ was calculated from the formula

$$a_\lambda(H) = 6{\cdot}211 \times 10^{-16}\Theta^{-1}10^{-13{\cdot}05\Theta} \tag{6}$$

deduced from the standard formula (Unsöld, 1938). The correction for stimulated re-emission was not included in these calculations, as it applies equally to the continuous and selective absorptions. The ionization of hydrogen does not affect the opacity appreciably in the relevant photospheric layers.

(*b*) The fraction of Fe atoms in the neutral state was calculated from the Saha equation, assuming an ionization potential of 7·90 volts (Moore, 1952). The relevant partition functions in the solar atmosphere have been tabulated by Claas (1951).

(*c*) The relative number of atoms in the lower state of a line with excitation potential 5·60 volts was calculated from the Boltzmann equation. Since the statistical weight of the lower state varies from one line to another, and since the f values for the relevant transitions are in any case unknown, the ratio n_s/g_s of the occupation number to the statistical weight was calculated as a function of τ_λ rather than n_s itself. The effect of possible deviations from the Boltzmann and Saha equations is discussed later (Section 6).

(*d*) The Doppler width $\Delta\lambda_D$ was calculated from

$$\Delta\lambda_D = \frac{\lambda}{c}\sqrt{\left(\frac{2RT}{M} + \xi_t^2\right)}, \tag{7}$$

where R is the gas constant, M the atomic weight of Fe, and ξ_t the r.m.s. component of small-scale isotropic turbulent velocity along the line of sight. We assume $\xi_t = 1{\cdot}7 \times 10^5$ cm/sec.

(*e*) In order to obtain the profile of the selective absorption coefficient with due regard to damping, it is necessary to obtain the broadening parameter

$$a = \frac{\Gamma}{4\pi\Delta\nu_D} = \frac{\lambda^2}{4\pi c}\frac{\Gamma}{\Delta\lambda_D}, \tag{8}$$

where Γ is the total damping constant, due to natural, collision, and Stark damping, and $\Delta\nu_D$ is the analogue in frequency units of $\Delta\lambda_D$. Formulae for Γ_{coll} and Γ_{Stark}, as deduced from the Lorentz–Weisskopf theory of line broadening, are given by Aller (1953), and these are used here with the modification that the van der Waals interaction constant C is replaced by the difference $C_1 - C_2$ between the C's of the upper and lower states (Unsöld and Weidemann, 1955). It has also been assumed that the a's for all the lines may be calculated with sufficient accuracy from the formulae deduced for the transition $e^5D_1 - t^5D_0^0$ at λ 15 542·15. The calculations of Γ_{coll} and Γ_{Stark}, details of which are given elsewhere (Pagel, 1954), lead to the formulae

$$\log a_{coll} = \log P + 0{\cdot}7\log\Theta - \log\Delta\lambda_D - 6{\cdot}80, \tag{9}$$

$$\log a_{Stark} = \log P_e + \tfrac{2}{3}\log\Theta - \log\Delta\lambda_D - 3{\cdot}30. \tag{10}$$

Natural damping contributes at the most a few per cent to the total value of a and it has been neglected. The Stark interaction constant $C_1 - C_2$ has, in the absence of more specific data, been assumed equal in order of magnitude to the value deduced by Aller (1953) from the experimental data published by Panter and Foster (1937) for the line λ 5162·28 (which has the largest Stark effect observed in the visible region).

(*f*) The atomic cross-section for selective absorption at an interval

$$\Delta\lambda = u\Delta\lambda_D$$

from the line centre has been calculated as a function of a, u by D. L. Harris (1948). From Harris' tables one may deduce the ratio α/α_0, where α is the relevant atomic cross-section for absorption and α_0 is the "fictitious absorption coefficient", given by

$$\alpha_0 = \frac{\pi^{1/2}e^2}{mc} f \frac{1}{\Delta\nu_D} = 1{\cdot}20\ 10^{-12} \frac{f}{\Delta\lambda_D}\ \text{cm}^2 \qquad (11)$$

at λ 15 500 if $\Delta\lambda_D$ is measured in A. The value of α/α_0 was found at each tabulated optical depth for the following values of $\Delta\lambda$: 0·00, 0·05, 0·10, 0·15, 0·20, 0·25, and 0·30 A. In the case of two models calculated without damping (Section 4), the value $\Delta\lambda = 0{\cdot}30$ was omitted. The variation of $\Delta\lambda_D$ with depth is so gradual that α_0 may be treated as constant.

(*g*) If the f values for the relevant atomic transitions were known, it would now be possible to calculate $\eta(\Delta\lambda)$ as a function of optical depth for each $\Delta\lambda$. However, neither theoretical nor experimental f values are available for Fe I in this wavelength region and we have therefore calculated relative absorption coefficients

$$n = \frac{10^8\eta}{Ng_e\alpha_0}, \qquad (12)$$

where N is the number of Fe atoms per gram of photospheric material. The integrations were carried out for a series of assumptions as to the ratio η/n, ascending by powers of 2 from $\eta = (1/16)n$ to $\eta = 4n$. In this way, curves of growth were developed for each μ in the various models.

To carry out the integration, the equation of transfer was rewritten in its finite-difference form

$$k = \Delta I = \frac{1+\eta}{\mu}(I - B)\Delta\tau, \qquad (13)$$

where the suffixes of equation (1) have been dropped, and use was made of the Runge–Kutta subroutine in the EDSAC library (Wilkes, Wheeler, and Gill, 1951)*. In the Runge–Kutta process, an approximate increment k in the dependent variable I corresponding to the whole interval $\Delta\tau$ in the independent variable is calculated from equation (13) four times, using values of I, B, η calculated once for the initial point, twice for the mid-point, and once for the end-point of the interval. The final value of ΔI is a weighted mean of the four k's (Scarborough, 1950)

$$\Delta I = \tfrac{1}{6}(k_1 + 2k_2 + 2k_3 + k_4), \qquad (14)$$

and the accuracy of the process corresponds to that of Simpson's rule, though the version in the EDSAC library is slightly improved. In accordance with the boundary condition (2), the starting value $I(\tau_1)$ is equal to $B(\tau_1)$ if τ_1 is sufficiently large; $\tau_1 = 4$ gives sufficient accuracy in the continuum, and smaller values may be used if large values of η occur, as is shown below.

To carry out the computations, the tabulated values of τ, with the corresponding values of B and $n(\Delta\lambda)$ were punched on a data tape; the values of B, n corresponding to a series of pre-assigned integration intervals in τ were then

* The writer is greatly indebted to Professor D. R. Hartree for pointing out the advantages of using this subroutine as against attempting to evaluate the integral of the transfer equation directly.

found in the EDSAC by Lagrangian interpolation using Neville's process (W. E. Milne, 1949). The results of the interpolations were used as the initial data in the integrations, η being obtained from n by multiplication by a suitable power of 2. The values of μ—1·0, 0·8, 0·6, 0·5, 0·4, 0·3, 0·2, 0·1—were successively supplied to the machine on a separate data tape, and in this way a "limb-darkening relation" for one $\Delta\lambda$ was built up in about 20 minutes of machine time. The line profiles were obtained by repeating the procedure with the n's corresponding to a new $\Delta\lambda$, and curves of growth were developed by repeating the procedure but doubling the ratio η/n. The equivalent widths were obtained from the line profiles by means of Weddle's rule.

The accuracy of computations of this kind is ultimately limited by the accuracy with which the constants $B(\tau)$, $n(\tau, \Delta\lambda)$ are calculated. These constants are known at best to an accuracy of 1 per cent (bearing in mind the compensation of errors in the damping when the profiles are integrated to obtain the equivalent widths); we therefore aim at a similar accuracy in the computed equivalent widths. This requires an accuracy of a few parts per thousand in the computed intensities $I_l(0, \Delta\lambda, \mu)$. Errors in programming, machine errors, and round-off errors were eliminated by standard methods. Truncation errors, inherent in the numerical procedure, may arise from the following causes:

1. The starting value $I = B$ was taken at a finite optical depth τ_1 instead of at $\tau = \infty$ as implied by the boundary condition (2).

2. The values of B, n for the half-intervals were found, and the integrations carried out, by third-order numerical procedures.

The effect of these approximations may be found by considering the solution of the transfer equation for the case $\mu = 1{\cdot}0$, $\eta = 0$. We have

$$I(0) = I(\tau_1)e^{-\tau_1} + \int_0^{\tau_1} B(\tau)e^{-\tau}d\tau. \tag{15}$$

$$I(\tau_1) = e^{\tau_1}\int_{\tau_1}^{\infty} B(\tau)e^{-\tau}d\tau. \tag{16}$$

For sufficiently large values of τ, we may write

$$B(\tau) = a + b\tau; \tag{17}$$

e.g., in de Jager's Model VII (de Jager, 1952), equation (17) holds for $\tau_1 > 3{\cdot}5$ with $a = 4{\cdot}91 \times 10^{13}$ erg/cm²/sec/cm/sterad., $b = 0{\cdot}17 \times 10^{13}$ erg/cm²/sec/cm/sterad. Hence, from equations (16), (17),

$$I(\tau_1) - B(\tau_1) = b$$

and the error in $I(0)$ due to the approximation $I(\tau_1) = B(\tau_1)$ is, from equation (15),

$$\delta I(0) = be^{-\tau_1}.$$

The relative error is thus

$$\frac{\delta I(0)}{I(0)} = \frac{0{\cdot}17e^{-\tau_1}}{4{\cdot}1} \simeq 10^{-3},$$

if $\tau_1 = 4{\cdot}0$. In the general case, this condition is replaced by

$$\int_0^{\tau_1}(1+\eta)\frac{d\tau}{\mu} = 4{\cdot}0. \tag{18}$$

The starting point of the integration was chosen by the programme itself in accordance with equation (18).

The second approximation inherent in the numerical procedure is harmless if the intervals of integration are chosen to be sufficiently small. In addition, any error in I that is present at optical depth τ_1 is attenuated according to equation (15) by a factor $\exp\{-\int_0^{\tau_1}(1+\eta)d\tau/\mu\}$ by the time that the surface is reached. Hence the highest accuracy is needed in the layers closest to the surface. Ideally, the lengths of the intervals should be reduced to compensate increases in $1/\mu$ and η, but to do this would make the programme too complicated to be of practical utility. Thus the intervals near the surface were chosen to be very small ($\Delta\tau = 0{\cdot}01$), while larger intervals were permissible at greater depths ($\Delta\tau = 0{\cdot}5$). The whole range $4{\cdot}0 > \tau > 0{\cdot}0$ was divided into 25 intervals at convenient points and the accuracy checked by repeating some of the integrations with different intervals of the same order of magnitude. The difference in I_l was found to be at the most 0·1 per cent for $\mu = 0{\cdot}2$.

4. *Results of the computations for three recent models and comparison with the observational data.*—The procedure described in Section 3 was applied to photospheric models corresponding to the temperature distributions put forward by Aller and Pierce (1952), de Jager (1952), and Michard (1953).

Aller and Pierce use the continuous limb-darkening data at various wavelengths to deduce the distribution of temperature with the Chandrasekhar mean optical depth $\bar{\tau}$ and give tables of $\log P$, $\log P_e$, and $\bar{\kappa}$ (the Chandrasekhar mean absorption coefficient) corresponding to a series of different chemical compositions. Their model was reduced to standard form by interpolating in their tables to obtain the values of $\log P$, $\log P_e$, $\bar{\kappa}$ corresponding to a composition with $\log A = 4{\cdot}0$ and no helium; the values of τ_λ (for λ 15 500) were found from the relation

$$\tau_\lambda(\bar{\tau}) = \int_0^{\bar{\tau}} \frac{\kappa_\lambda(\bar{t})}{\bar{\kappa}(\bar{t})}\, d\bar{t}, \qquad (19)$$

the monochromatic continuous opacity κ_λ being found from the tables of Chandrasekhar and Breen (1946). In the outermost layers ($\bar{\tau} < 0{\cdot}1$), the temperatures were lowered in accordance with the results of blanketing-effect calculations by Labs (1951)*. Some uncertainty exists in the exact relation between τ_λ and $\bar{\tau}$, owing to the discrepancy between the values of $\bar{\kappa}$ originally calculated and the values required to obtain the correct value of the solar effective temperature; Aller and Pierce remedied this discrepancy by multiplying the values of $\bar{\kappa}$ by a constant factor of 1·35. This uncertainty affects the calculated intensity of the continuum (cf. Fig. 3), but should have no serious influence on line strengths. The constants for the Aller–Pierce model are given in Table II; the n values were calculated without allowing for damping ($a = 0$).

de Jager (1952) uses the variations in the profiles of the hydrogen lines across the disk to deduce the temperature distribution as a function of the optical depth τ_0 corresponding to λ 5000 and gives the values of $\log P$, $\log P_e$ for an atmosphere with 20 per cent helium. The corresponding values of τ_λ were deduced from a table given by Neven and de Jager (1951) and the values of $\log P$, $\log P_e$ for our standard composition were computed by the iteration procedure described by Aller and Pierce (1952). The n values were calculated twice—with and without damping—and the two sets of equivalent width calculations give an indication of the importance of this effect. The results are given in Tables III, IV.

* The writer is indebted to Dr L. H. Aller for suggesting this procedure.

TABLE II

Constants in Aller-Pierce model

$\bar{\tau}$	τ_λ	Θ	log P	log P_e	$B_\lambda(\tau_\lambda)$	n (without damping) $\Delta\lambda =$			
						0·00	0·05	0·10	0·20
0·00	0·000	1·176			$1·752 \times 10^{13}$				
0·01	0·002	1·080	3·81	−0·04	2·112	16·40	13·11	6·85	0·506
0·02	0·005	1·072	4·06	0·00	2·148	16·32	13·09	6·83	0·503
0·04	0·010	1·054	4·20	0·08	2·233	14·78	11·91	6·26	0·484
0·08	0·022	1·020	4·39	0·32	2·403	9·52	9·86	5·20	0·400
0·15	0·043	0·979	4·55	0·54	2·629	9·52	7·70	4·10	0·333
0·20	0·059	0·956	4·62	0·65	2·766	8·26	6·66	3·56	0·286
0·30	0·092	0·923	4·71	0·80	2·978	6·80	5·50	2·97	0·253
0·50	0·164	0·877	4·81	1·08	3·307	5·06	4·13	2·25	0·197
0·75	0·241	0·841	4·88	1·28	3·544	4·13	3·40	1·87	0·170
0·90	0·324	0·825	4·91	1·44	3·732	3·56	2·92	1·61	0·147
1·20	0·455	0·797	4·94	1·64	3·988	2·90	2·38	1·32	0·130
1·40	0·543	0·781	4·97	1·76	4·145	2·56	2·10	1·17	0·113
1·80	0·734	0·754	5·01	1·97	4·426	2·02	1·66	0·93	0·093
2·50	1·125	0·718	5·03	2·24	4·840	1·42	1·18	0·67	0·070
	1·629	0·684	5·04	2·47	5·265	0·96	0·80	0·46	0·050
	2·286	0·652	5·05	2·71	5·722	0·67	0·56	0·32	0·037
	3·660	0·605	5·06	3·05	6·493	0·37	0·31	0·18	0·023

TABLE III

Constants in de Jager model (1): *n without damping*

τ_0	τ_λ	Θ	log P	log P_e	$B_\lambda(\tau_\lambda)$	n (without damping) $\Delta\lambda =$			
						0·00	0·10	0·15	0·25
0·01	0·00	1·180			$1·700 \times 10^{13}$				
0·03	0·01	1·098	4·08	−0·06	2·028	16·40	6·86	2·30	0·07
0·06	0·02	1·043	4·32	0·22	2·284	15·40	6·54	2·24	0·07
0·08	0·03	1·020	4·43	0·36	2·398	13·87	5·89	2·02	0·07
0·10	0·04	1·003	4·50	0·45	2·488	12·90	5·49	1·88	0·06
0·15	0·065	0·972	4·62	0·61	2·664	12·89	5·56	1·95	0·07
0·20	0·09	0·941	4·69	0·75	2·854	10·20	4·40	1·54	0·05
0·30	0·15	0·883	4·79	1·04	3·254	9·43	4·19	1·53	0·06
0·40	0·21	0·843	4·84	1·29	3·570	6·55	2·94	1·10	0·05
0·50	0·275	0·829	4·88	1·39	3·689	5·07	2·38	0·87	0·04
0·80	0·48	0·803	4·95	1·60	3·923	4·31	1·97	0·74	0·03
1·00	0·62	0·785	4·98	1·74	4·097	3·43	1·57	0·59	0·03
1·20	0·77	0·769	5·00	1·86	4·258	2·88	1·34	0·51	0·02
1·60	1·08	0·739	5·03	2·09	4·584	2·21	1·04	0·40	0·02
2·00	1·41	0·718	5·06	2·25	4·831	1·61	0·87	0·34	0·02
2·50	1·85	0·700	5·07	2·39	5·055	1·46	0·70	0·27	0·01
3·00	2·34	0·690	5·09	2·48	5·184	1·36	0·57	0·26	0·01
5·00	4·30	0·658	5·13	2·73	5·632	0·93	0·46	0·19	0·01

In his table (Model VII), de Jager does not give the value of the surface temperature T_0 (corresponding to $\tau_0 = 0{\cdot}00$). Our computations have therefore been carried out with two assumptions as to the value of T_0 : $T_0 = 4270°$ (corresponding to $\tau_0 = 0{\cdot}01$, $\tau_\lambda = 0{\cdot}003$) and $T_0 = 4000°$ (close to the value deduced by de Jager from his observations, but not finally adopted by him owing to the higher temperature indicated by observations of the continuum at the extreme limb).

TABLE IV

Constants in de Jager model (2): *n with damping*

$\lambda = 10^8\eta / N g_c \alpha_0$

$\tau_{1\cdot 85}$	$B_{1\cdot 85}(\tau)$	$\Delta\lambda =$ 0·00	$\Delta\lambda =$ 0·05	$\Delta\lambda =$ 0·10	$\Delta\lambda =$ 0·15	$\Delta\lambda =$ 0·20	$\Delta\lambda =$ 0·25	$\Delta\lambda =$ 0·30
0·00	$1{\cdot}700 \times 10^{12}$	...	...	...	...	...	...	...
0·01	2·028	16·58	13·42	7·06	2·46	0·602	0·133	0·042
0·02	2·284	14·58	11·91	6·42	2·35	0·636	0·171	0·067
0·03	2·398	12·75	10·47	5·73	2·16	0·609	0·180	0·076
0·04	2·488	11·25	9·25	5·11	1·96	0·583	0·175	0·078
0·065	2·664	10·14	8·39	4·73	1·89	0·599	0·197	0·090
0·09	2·854	7·92	6·58	3·77	1·56	0·522	0·183	0·090
0·15	3·254	5·33	4·49	2·66	1·17	0·429	0·165	0·084
0·21	3·570	3·76	3·20	1·95	0·857	0·314	0·121	0·062
0·275	3·689	3·50	2·99	1·86	0·873	0·347	0·143	0·077
0·34	3·777	3·18	2·73	1·72	0·851	0·370	0·167	0·092
0·48	3·923	2·71	2·35	1·52	0·786	0·364	0·172	0·098
0·62	4·097	2·25	1·97	1·32	0·715	0·344	0·176	0·104
0·77	4·258	1·89	1·66	1·14	0·654	0·343	0·182	0·109
0·93	4·416	1·57	1·40	0·984	0·597	0·336	0·187	0·115
1·08	4·584	1·32	1·16	0·843	0·537	0·328	0·191	0·121
1·41	4·831	1·006	0·886	0·642	0·442	0·300	0·197	0·127
1·85	5·055	0·793	0·696	0·503	0·357	0·264	0·186	0·134
2·34	5·184	0·689	0·604	0·433	0·317	0·242	0·182	0·135
4·30	5·632	0·376	0·366	0·260	0·207	0·164	0·135	0·105

Michard (1953) deduces the temperature distribution as a function of τ_0 from the observational data on continuous limb-darkening at various wave-lengths, but corrects it in the outer layers to give the observed excitation temperatures of Fe I and Ti I. His value of T_0 is 4270°. The values of τ_λ corresponding to each τ_0 were again deduced from the table of Neven and de Jager (1951) and the values of $\log P$, $\log P_e$ were taken over directly from Michard's table for the adopted chemical composition. The constants corresponding to Michard's model are shown in Table V, damping being taken into account.

Figs. 3, 4 show the absolute and relative limb-darkening curves in the continuum calculated from the three models. The observational data given for comparison were deduced by combining the value $I_\lambda(0, 1)$ for the intensity at the centre of the disk given by Minnaert (1953) with the limb-darkening coefficients measured by Pierce and Aller (1951). The agreement is satisfactory, bearing in mind the uncertainties in the solar constant and in the precise values of τ_λ (particularly in the model of Aller and Pierce).

TABLE V

Constants in Michard model

τ_0	τ_λ	Θ	$\log P$	$\log P_e$	$B_\lambda(\tau_\lambda)$	n (with damping) $\Delta\lambda =$ 0·00	0·10	0·15	0·25
0·00	0·000	1·180			$1{\cdot}700\times10^{13}$				
0·02	0·007	1·117	4·11	−0·05	1·947	19·15	8·15	2·83	0·152
0·05	0·017	1·060	4·37	+0·23	2·198	15·13	6·69	2·44	0·176
0·10	0·040	1·007	4·54	0·46	2·466	11·67	5·30	2·02	0·180
0·15	0·065	0·971	4·64	0·62	2·669	9·54	4·45	1·76	0·179
0·25	0·115	0·918	4·77	0·89	3·004	6·73	3·28	1·41	0·186
0·50	0·270	0·851	4·89	1·28	3·504	4·14	2·15	1·00	0·167
1·00	0·62	0·782	4·99	1·765	4·126	2·20	1·30	0·70	0·174
2·00	1·40	0·710	5·06	2·33	4·929	0·95	0·61	0·44	0·204
3·00	2·29	0·662	5·09	2·75	5·576	0·41	0·34	0·30	0·199
4·00	3·28	0·624	5·10	3·09	6·168	0·26	0·22	0·20	0·156

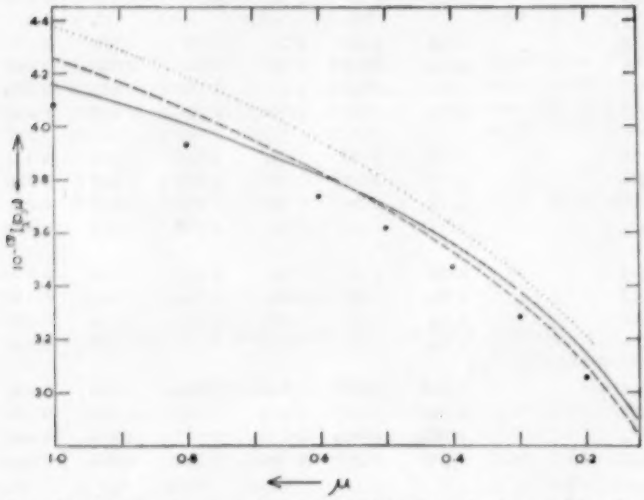

FIG. 3.—*Intensity of the continuum at λ 15 500 calculated from the three models. Dotted line : Aller–Pierce. Full line : de Jager. Broken line : Michard. Black circles : observed values.*

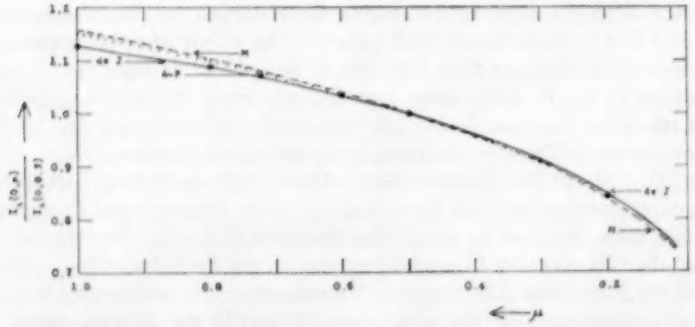

FIG. 4.—*Relative limb-darkening curves calculated from the three models, taking $I_\lambda(0, 0{\cdot}5)$ as unity. Dotted line : Aller–Pierce. Full line : de Jager. Broken line : Michard. Black circles : observed values.*

Table VI gives the line profiles and equivalent widths calculated from de Jager's Model VII (with damping; $T_0 = 4000°$). The results obtained from the other models are omitted for the sake of brevity.

In order to compare the computed centre-limb variations in equivalent width with the observational results of Table I, the computed curves of growth were interpolated for values of η/n chosen to make the computed and observed equivalent widths coincide, in general, at $\mu = 0{\cdot}5$. This interpolation was carried out in practice by taking weighted means, for each μ, of the equivalent widths calculated for two successive values of η/n, the weighting factors being chosen to give the coincidence at $\mu = 0{\cdot}5$. The results are shown graphically in Fig. 5.

TABLE VI

Line Profiles in de Jager model ($T_0 = 4000°$)

Each entry gives the value of $(1-r)$ corresponding to the given $\Delta\lambda, \mu$

(*a*) $\eta = (1/16)n$

$\Delta\lambda$ \ μ	1·0	0·8	0·6	0·5	0·4	0·3	0·2	0·1
0·00	0·0491	0·0544	0·0613	0·0659	0·0715	0·0787	0·0886	0·0994
0·05	0·0414	0·0459	0·0518	0·0556	0·0603	0·0665	0·0751	0·0850
0·10	0·0248	0·0273	0·0307	0·0328	0·0355	0·0391	0·0443	0·0511
0·15	0·0110	0·0120	0·0132	0·0139	0·0149	0·0162	0·0181	0·0208
0·20	0·0041	0·0043	0·0048	0·0048	0·0049	0·0052	0·0056	0·0062
0·25	0·0018	0·0018	0·0018	0·0018	0·0018	0·0017	0·0018	0·0018
0·30	0·0011	0·0011	0·0010	0·0010	0·0010	0·0008	0·0009	0·0008
W	10·83	11·93	13·35	14·25	15·38	16·86	18·98	21·49
$\frac{W}{1-r_{0\cdot00}}$	220	220	218	217	215	214	214	217
$\frac{W}{1-r_{0\cdot10}}$	438	437	435	435	433	431	428	420

(*b*) $\eta = (1/8)n$

$\Delta\lambda$ \ μ	1·0	0·8	0·6	0·5	0·4	0·3	0·2	0·1
0·00	0·0920	0·1011	0·1126	0·1199	0·1288	0·1399	0·1540	0·1663
0·05	0·0784	0·0863	0·0962	0·1027	0·1105	0·1204	0·1335	0·1460
0·10	0·0479	0·0526	0·0587	0·0626	0·0675	0·0739	0·0829	0·0939
0·15	0·0216	0·0235	0·0258	0·0273	0·0292	0·0316	0·0354	0·0407
0·20	0·0083	0·0088	0·0093	0·0096	0·0099	0·0104	0·0112	0·0125
0·25	0·0036	0·0037	0·0035	0·0036	0·0037	0·0034	0·0035	0·0036
0·30	0·0019	0·0022	0·0018	0·0020	0·0017	0·0017	0·0016	0·0016
W	20·69	22·67	25·07	26·68	28·62	31·04	34·41	38·00
$\frac{W}{1-r_{0\cdot00}}$	225	224	223	223	223	222	224	229
$\frac{W}{1-r_{0\cdot10}}$	432	431	427	426	425	421	416	405

TABLE VI (*cont.*)

(*c*) $\eta=(1/4)n$

$\Delta\lambda$ \ μ	1·0	0·8	0·6	0·5	0·4	0·3	0·2	0·1
0·00	0·1624	0·1751	0·1904	0·1997	0·2106	0·2225	0·2350	0·2380
0·05	0·1405	0·1522	0·1666	0·1752	0·1852	0·1993	0·2104	0·2153
0·10	0·0897	0·0976	0·1072	0·1133	0·1210	0·1302	0·1424	0·1527
0·15	0·0420	0·0462	0·0497	0·0526	0·0556	0·0602	0·0659	0·0739
0·20	0·0167	0·0176	0·0187	0·0190	0·0199	0·0213	0·0218	0·0242
0·25	0·0073	0·0075	0·0070	0·0073	0·0076	0·0069	0·0070	0·0072
0·30	0·0038	0·0043	0·0036	0·0039	0·0034	0·0033	0·0032	0·0031
W	37·91	41·11	44·58	46·92	49·58	53·08	56·54	59·22
$\frac{W}{1-r_{0\cdot00}}$	234	235	235	235	236	238	241	249
$\frac{W}{1-r_{0\cdot10}}$	422	421	416	413	411	407	397	388

(*d*) $\eta=(1/2)n$

$\Delta\lambda$ \ μ	1·0	0·8	0·6	0·5	0·4	0·3	0·2	0·1
0·00	0·2573	0·2716	0·2871	0·2955	0·3040	0·3117	0·3158	0·3082
0·05	0·2295	0·2425	0·2588	0·2677	0·2769	0·2861	0·2926	0·2869
0·10	0·1557	0·1669	0·1803	0·1883	0·1974	0·2083	0·2194	0·2218
0·15	0·0782	0·0838	0·0905	0·0947	0·1002	0·1067	0·1160	0·1243
0·20	0·0318	0·0334	0·0352	0·0365	0·0374	0·0395	0·0415	0·0453
0·25	0·0139	0·0141	0·0137	0·0140	0·0142	0·0135	0·0137	0·0141
0·30	0·0072	0·0073	0·0072	0·0073	0·0073	0·0072	0·0072	0·0073
W	64·15	67·95	72·46	75·13	78·08	81·15	84·34	85·00
$\frac{W}{1-r_{0\cdot00}}$	250	251	252	255	257	261	267	276
$\frac{W}{1-r_{0\cdot10}}$	413	407	401	399	396	389	385	384

TABLE VI (*cont.*)

(*e*) $\eta = n$

$\Delta\lambda$ \ μ	1·0	0·8	0·6	0·5	0·4	0·3	0·2	0·1
0·00	0·3618	0·3722	0·3815	0·3854	0·3881	0·3886	0·3855	0·3779
0·05	0·3319	0·3445	0·3556	0·3608	0·3650	0·3671	0·3652	0·3550
0·10	0·2468	0·2592	0·2728	0·2803	0·2881	0·2953	0·2993	0·2910
0·15	0·1359	0·1441	0·1539	0·1598	0·1667	0·1754	0·1852	0·1880
0·20	0·0588	0·0619	0·0644	0·0663	0·0700	0·0720	0·0757	0·0804
0·25	0·0262	0·0265	0·0262	0·0264	0·0265	0·0260	0·0264	0·0270
0·30	0·0145	0·0147	0·0145	0·0146	0·0146	0·0144	0·0145	0·0147
W	98·8	102·8	107·0	109·2	111·6	113·6	115·3	114·1
$\frac{W}{1-r_{0\cdot00}}$	273	275	281	284	287	292	299	302
$\frac{W}{1-r_{0\cdot10}}$	400	396	392	390	387	385	386	392

(*f*) $\eta = 2n$

$\Delta\lambda$ \ μ	1·0	0·8	0·6	0·5	0·4	0·3	0·2	0·1
0·00	0·4507	0·4544	0·4558	0·4555	0·4541	0·4516	0·4493	0·4200
0·05	0·4272	0·4325	0·4357	0·4361	0·4353	0·4330	0·4288	0·4107
0·10	0·3474	0·3569	0·3657	0·3695	0·3722	0·3727	0·3692	0·3582
0·15	0·2173	0·2269	0·2377	0·2441	0·2510	0·2582	0·2631	0·2555
0·20	0·1037	0·1101	0·1118	0·1145	0·1179	0·1223	0·1286	0·1310
0·25	0·0481	0·0486	0·0484	0·0485	0·0484	0·0483	0·0492	0·0496
0·30	0·0275	0·0275	0·0265	0·0259	0·0253	0·0254	0·0239	0·0233
W	138·3	141·5	144·2	145·6	146·8	147·8	148·2	142·9
$\frac{W}{1-r_{0\cdot00}}$	307	312	316	319	323	327	331	340
$\frac{W}{1-r_{0\cdot10}}$	399	396	395	394	394	396	402	398

TABLE VI (*cont.*)

(*g*) $\eta = 4n$

$\Delta\lambda$ \ μ	1·0	0·8	0·6	0·5	0·4	0·3	0·2	0·1
0·00	0·5156	0·5152	0·5134	0·5122	0·5118	0·5100	0·5060	
0·05	0·4980	0·4981	0·4965	0·4951	0·4935	0·4934	0·4903	
0·10	0·4358	0·4396	0·4411	0·4407	0·4392	0·4362	0·4317	
0·15	0·3113	0·3199	0·3285	0·3327	0·3362	0·3377	0·3349	0·3216
0·20	0·1681	0·1731	0·1787	0·1824	0·1867	0·1920	0·1972	0·1917
0·25	0·0839	0·0845	0·0844	0·0845	0·0845	0·0852	0·0866	0·0851
0·30	0·0501	0·0497	0·0485	0·0474	0·0463	0·0452	0·0453	0·0428
W	178·4	180·3	181·7	182·3	182·7	183·1	182·2	(176)
$\frac{W}{1-r_{0\cdot00}}$	346	350	354	356	357	359	360	
$\frac{W}{1-r_{0\cdot10}}$	409	410	411	413	416	419	420	

An inspection of Fig. 5 shows the following principal features:—

(*a*) All models predict the observed variation of the fainter lines ($W<40$ mA) within the observational error, except close to the limb ($\mu<0\cdot3$), where the Aller–Pierce temperature distribution does not predict a strong enough increase. Since the n values (apart from damping) are nearly the same in all three models, we conclude that the differences are due to the different gradients of the source function $B_\lambda(\tau_\lambda)$ in the region $\tau_\lambda<0\cdot3$. The reduction in intensity due to a given amount of selective absorption at a given μ is determined by the gradient of $B_\lambda(\tau_\lambda)$ in the relevant optical depth range (cf. equation (21)); the gradient with μ is therefore related more directly with the curvature of $B_\lambda(\tau_\lambda)$ than with the gradient itself. The influence of damping is shown by a comparison of the two curves corresponding to de Jager's model; near the centre of the disc, the effect is approximately equal to the influence of the transition from the Aller–Pierce model (without damping) to the Michard model (with damping), so that we may regard the difference between the two curves in this range as being predominantly due to the fact that damping was taken into account in the latter; near the limb, the difference between the line intensities calculated from these two models is considerably greater than the damping effect, so that here the lower temperatures in the neighbourhood of the surface envisaged by Michard and de Jager seem to be confirmed by the observations.

(*b*) For a line of intermediate strength ($W\simeq40$ mA; Fig. 5(ii)), the curve based on Michard's model reproduces the trend of the observations with remarkable precision out to $\mu=0\cdot3$. The variation deduced from the Aller–Pierce model is not sufficiently sharp (though it would be improved if damping were taken into account), while the increase deduced from de Jager's model is somewhat too rapid. In accordance with the effect of the curvature in the source function previously mentioned, the high gradient with μ deduced from de Jager's model may be associated with the "knee" in his temperature curve at $\tau_\lambda=0\cdot22$ (cf. Fig. 8).

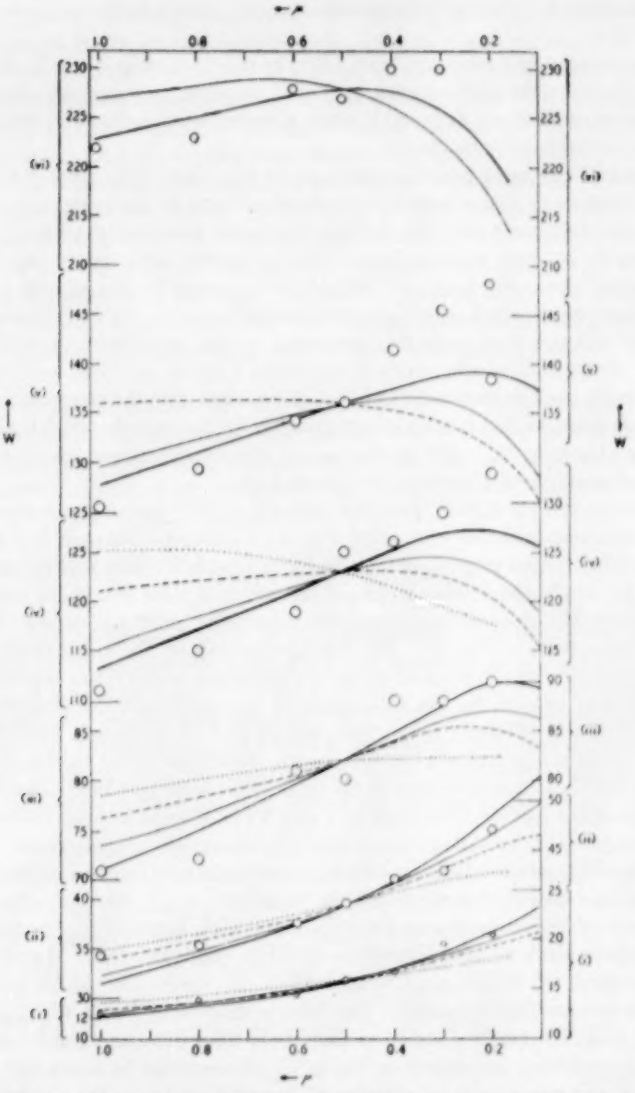

FIG. 5.—*Observed and computed centre-limb variations in equivalent widths. Open circles : observed values for* (*i*) λ 15565·38 ; (*ii*) *mean of* λ 15593·71, λ 15566·88 ; (*iii*) λ 15537·71 ; (*iv*) λ 15542·15 ; (*v*) *mean of* λ 15531·80, λ 15534·31 ; (*vi*) λ 15662·05. *Dotted line : Aller–Pierce* (*without damping*) *for* (*i*) $\eta = 0{\cdot}089n$; (*ii*) $\eta = 0{\cdot}238n$; (*iii*) $\eta = 0{\cdot}775n$; (*iv*) $\eta = 2{\cdot}02n$. *Broken line : Michard* (*with damping*) *for* (*i*) $\eta = 0{\cdot}063n$; (*ii*) $\eta = 0{\cdot}178n$; (*iii*) $\eta = 0{\cdot}540n$; (*iv*) $\eta = 1{\cdot}20n$; (*v*) $\eta = 1{\cdot}57n$. *Light full line : de Jager* (*i*) *without damping, for* $\eta = 0{\cdot}075n$; (*ii*) *without damping, for* $\eta = 0{\cdot}194n$; (*iii*) *without damping, for* $\eta = 0{\cdot}585n$; (*iv*) *with damping, for* $\eta = 1{\cdot}35n$ ($T_0 = 4270°$) ; (*v*) *with damping, for* $\eta = 1{\cdot}80n$ ($T_0 = 4270°$) ; (*vi*) *with damping, for* $\eta = 12n$ ($T_0 = 4270°$). *Heavy full line : de Jager* (*with damping*) *for* (*i*) $\eta = 0{\cdot}075n$; (*ii*) $\eta = 0{\cdot}194n$; (*iii*) $\eta = 0{\cdot}585n$; (*iv*) $\eta = 1{\cdot}30n$ ($T_0 = 4000°$) ; (*v*) $\eta = 1{\cdot}67n$ ($T_0 = 4000°$) ; (*vi*) $\eta = 9{\cdot}6n$ ($T_0 = 4000°$).

The smooth temperature curves obtained by Michard and Aller and Pierce seem to be in much better agreement with the observations in this equivalent-width range.

(*c*) For somewhat stronger lines ($W \simeq 80$ mA; cf. Fig. 5(iii)), de Jager's model reproduces the observations very well (bearing in mind the considerable observational errors for λ 15537·71), while the gradients deduced from the other models are considerably too low.

(*d*) For still stronger lines ($W \simeq 100$ mA; cf. Fig. 5(iv), (v)), none of the models considered seems to give as much strengthening towards the limb as is observed, although the representation by de Jager's model (especially with $T_0 = 4000°$) is considerably superior to the others. The agreement between de Jager's model and the observations for λ 15542·15 would be improved by the adoption of a still lower surface temperature, e.g. $T_0 = 3800°$ as suggested by Böhm–Vitense (1954), but further computations show that one result of this would be an increase in the predicted intensities of the lines λ 15531·80, λ 15534·31 from $\mu = 0{\cdot}3$ to 0·2 (cf. Fig. 5(v)); such an increase would be inconsistent with the observed behaviour of these two lines, so that it is no longer possible to improve the overall agreement merely by changing T_0. We prefer to use the observational material for the inductive derivation of a new model (Section 5).

(*e*) The two strongest lines observed (200 mA $< W <$ 350 mA) both show almost precisely the same variation with μ (cf. Fig. 2; λ 15662·05 is shown in Fig. 5(vi)), which is tolerably well reproduced by de Jager's model. The sudden drop from $\mu = 0{\cdot}3$ to $\mu = 0{\cdot}2$ is a somewhat awkward feature to explain, but there can be little doubt of its reality since all four lines with equivalent widths in excess of 120 mA show the same feature (Fig. 2). Its significance will be discussed below.

We conclude that the present series of equivalent width observations may be adequately represented, for the most part, by a temperature distribution corresponding to that of Michard for $\tau_\lambda > 0{\cdot}2$ and to that of de Jager's Model VII for $\tau_\lambda < 0{\cdot}2$. Certain adjustments will be required very close to the surface ($\tau_\lambda < 0{\cdot}05$) to account for the behaviour close to the limb of the strongest lines observed.

A study of the line profiles given in Table VI is of some interest in connection with the suggestion by Allen (1949) that the observed increase from centre to limb in the widths of faint lines may be due to some form of anisotropic turbulence. Doubt has been cast on this suggestion by Houtgast (1952), who finds that Allen's observations of line broadening are consistent with isotropic turbulence if the detailed mechanism of line formation is taken into account. In Table VI, values are given of $W/(1 - r_{0{\cdot}90})$, where W is the equivalent width in mA and $r_{0{\cdot}90}$ the central residual intensity. For lines with $\eta = n$ in Table VI, $r_{0{\cdot}90}$ changes very little from $\mu = 1{\cdot}0$ to $\mu = 0{\cdot}3$, so that these lines are comparable with those considered by Allen; according to Table VI, the increase in line width is about 10 per cent, compared with 30 per cent as found by Allen in the neighbourhood of λ 4300. To compare the behaviour of the line wings in the two wave-length regions, we use two approximate relations given by Unsöld (1948):

$$\frac{I_\lambda(0,\mu)}{I_\lambda(0,1)} = \frac{B_\lambda(\tau_\lambda = \mu)}{B_\lambda(\tau_\lambda = 1)} \tag{20}$$

and

$$\frac{R(\mu)}{R(1)} = \frac{\left(\dfrac{d \ln B_\lambda}{d\tau_\lambda}\right)_{\tau_\lambda = \mu}}{\left(\dfrac{d \ln B_\lambda}{d\tau_\lambda}\right)_{\tau_\lambda = 1}} \frac{\Delta\tau_\lambda(\tau_\lambda = \mu)}{\Delta\tau_\lambda(\tau_\lambda = 1)}, \tag{21}$$

where the function $\Delta\tau_l(\tau_\lambda)$ represents the small additional optical depth present in a faint Fraunhofer line as compared with the neighbouring continuum. If we ignore changes in the second factor on the right of equation (21), it is clear that $R(\mu)/R(1)$ for the faint line wings in a given wave-length region is related to the degree of continuous limb-darkening at that wave-length. An inspection of the limb-darkening curves given by Minnaert (1953) for various wave-lengths shows that the gradient $d\ln B_\lambda/d\tau_\lambda$ increases rapidly towards short wave-lengths, as is to be expected from the increasing sensitivity to temperature of the monochromatic Planck emission function; this fact, incidentally, offers a simple explanation of the general faintness of infra-red Fraunhofer lines. The relative change in the intensity of the continuum from $\mu = 1{\cdot}0$ to $\mu = 0{\cdot}3$ is three times as great in Allen's wave-length region as at λ 15 500; the line broadening shown in Table VI may therefore be taken as a confirmation of Houtgast's conclusion that Allen's data may be satisfactorily accounted for without the assumption of anisotropic turbulence.

5. *Inductive derivation of a new model.*—For lines formed in local thermodynamic equilibrium it is possible to derive the distribution of temperature with τ_λ from limb-darkening curves observed for any given portion of the line profile, provided that the relation between τ_λ and the relevant selective optical depth τ_l is known. This relation is

$$\tau_l(\tau_\lambda) = \int_0^{\tau_\lambda} \{1 + \eta(t_\lambda)\} dt_\lambda, \qquad (22)$$

so that τ_λ can be found from τ_l if $\eta(\tau_\lambda)$ is known. To derive our first model ("Model I"), we assume the form of the line profile to be given by the values of $W/(1 - r_{0\cdot10})$ shown in Table VI; for a given μ, this ratio is nearly independent of the assumed model and of η/n. The observed equivalent widths were converted into values of $r_{0\cdot10}$, and a limb-darkening curve was deduced for each line at the point of the profile corresponding to $\Delta\lambda = 0{\cdot}10$ A, using the values of $I_\lambda(0, \mu)$ derived in Section 4. The results are illustrated in Fig. 6.

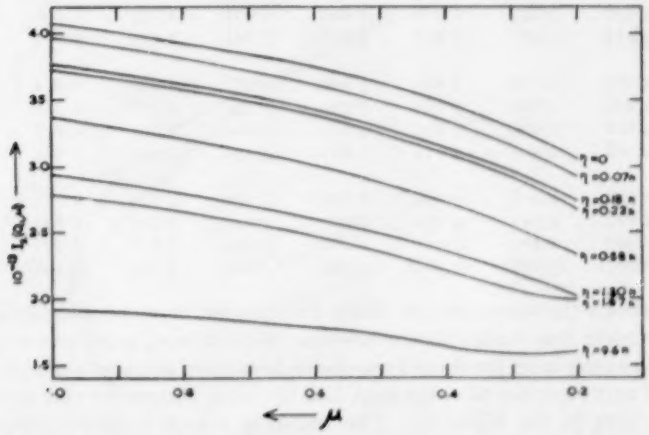

FIG. 6.—*Semi-empirical limb-darkening curves corresponding to the point* $\Delta\lambda = 0{\cdot}10$ *of each line profile.*

To derive the source functions $B_\lambda(\tau_l)$ corresponding to the limb-darkening curves, it is convenient to express $B_\lambda(\tau_l)$ either as a polynomial in τ_l or as a series of exponential integral functions; each expression leads to a corresponding series for $I_\lambda(0,\mu)$ and the coefficients can be found by least squares. In the continuous spectrum, the second type of expansion is greatly preferable (Pierce and Aller, 1951; Peyturaux, 1952), three terms being generally sufficient to represent the observational data well within their r.m.s. error. For the present problem, however, we are concerned with the source function very close to the surface; since the temperature distribution in this region is determined by the blanketing effect rather than by the normal conditions of radiative equilibrium in a nearly grey body, the physical significance of the expansion of the source function in exponential integrals disappears and what is required is purely an interpolation formula valid in the restricted ranges

$$0{\cdot}2 \leqslant \tau_l \leqslant 1{\cdot}0.$$

The data were expanded in series corresponding to both the polynomial and the exponential integral type, the coefficients being obtained by least squares. The various values of μ were assigned equal weight and in each case the expansion was adopted which gave the smallest sum of squares of residuals. The resulting source functions are given in Table VII, together with the type of expansion adopted for each line. The mean sum of squares of residuals is 600 (the unit being the third decimal place in $10^{-13}I_\lambda(0,\mu)$), compared with a mean value of 1000 from the r.m.s. errors in equivalent width. In Table VII, E.I. refers to the three-term exponential integral expansion.

TABLE VII

Source function distribution with selective optical depth τ_l with 10^{13} erg/cm²/sec/dω/cm as unit

τ_l	Continuum E.I. $\eta=0$	15565·38 E.I. $\eta=0{\cdot}07n$	15593·71 E.I. $\eta=0{\cdot}185n$	15566·88 E.I. $\eta=0{\cdot}221n$	15537·71 E.I. $\eta=0{\cdot}585n$	15542·15 quadratic $\eta=1{\cdot}3n$	15531·8 cubic $\eta=1{\cdot}67n$	15662·05 cubic $\eta=9{\cdot}6n$
0·00	(2·058)	(1·879)	(1·712)	(1·645)	(1·472)	(1·643)	(1·749)	(1·660)
0·10	(2·821)	(2·665)	(2·484)	(2·433)	(2·113)	(1·844)	(1·855)	(1·604)
0·20	3·236	3·093	2·906	2·861	2·475	2·037	1·966	1·568
0·30	3·534	3·401	3·211	3·168	2·744	2·223	2·083	1·550
0·40	3·765	3·639	3·446	3·405	2·957	2·456	2·204	1·565
0·50	3·949	3·829	3·636	3·595	3·134	2·736	2·329	1·596
0·60	4·101	3·985	3·792	3·751	3·284	2·891	2·457	1·640
0·70	4·228	4·115	3·923	3·881	3·414	3·040	2·588	1·698
0·80	4·335	4·226	4·034	3·991	3·529	3·180	2·721	1·767
0·90	4·427	4·321	4·131	4·085	3·631	3·313	2·855	1·846
1·00	4·507	4·403	4·215	4·167	3·724	3·612	2·990	2·083
1·25	(4·667)	(4·568)	(4·384)	(4·330)	(3·924)	(3·864)	(3·328)	(2·361)

To convert the values of τ_l in Table VII into the corresponding values of τ_λ, the assumption was made that the relevant values of $n(\tau_\lambda, 0{\cdot}10)$ and of η/n were the same as calculated for these Fraunhofer lines from de Jager's model. τ_l was tabulated as a function of τ_λ for each line by using Simpson's rule to integrate equation (22) in the EDSAC. The resulting source function (Model I) is illustrated in Figs. 7, 8.

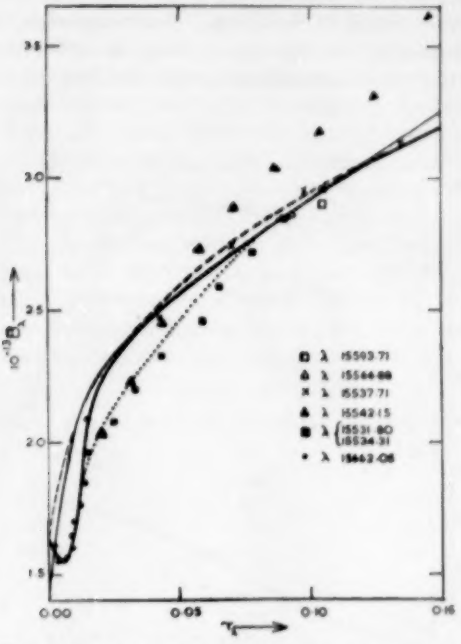

FIG. 7.—*Source function deduced in the range* $0{\cdot}00 < \tau_\lambda < 0{\cdot}15$. *Dotted line : Model I. Heavy full line : Model II. Heavy broken line : Model III. Light full line : de Jager* ($T_e = 4000°$). *Light broken line : Michard.*

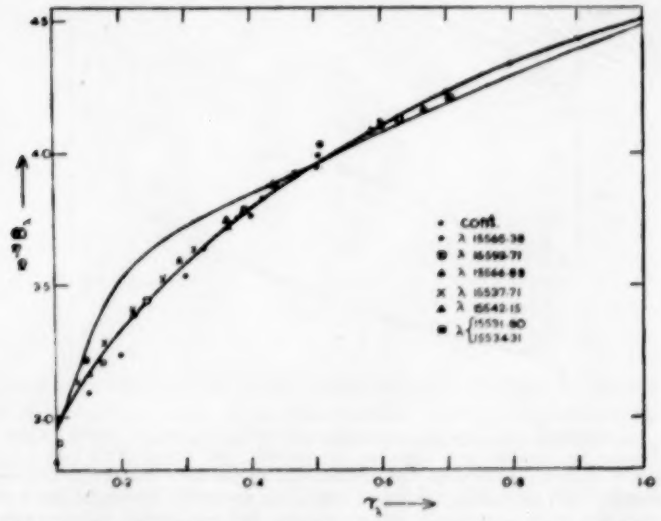

FIG. 8.—*Source function deduced in the range* $0{\cdot}1 < \tau_\lambda < 1{\cdot}0$. *Heavy line : Michard and suggested model. Light line : de Jager.*

To test the accuracy of Model I, the equivalent widths were calculated as a function of μ by the method of Section 4. The comparison is shown in Fig. 9. The agreement, especially for the fainter lines, is rather poor, which is not surprising in view of the approximations used in deriving the model (particularly

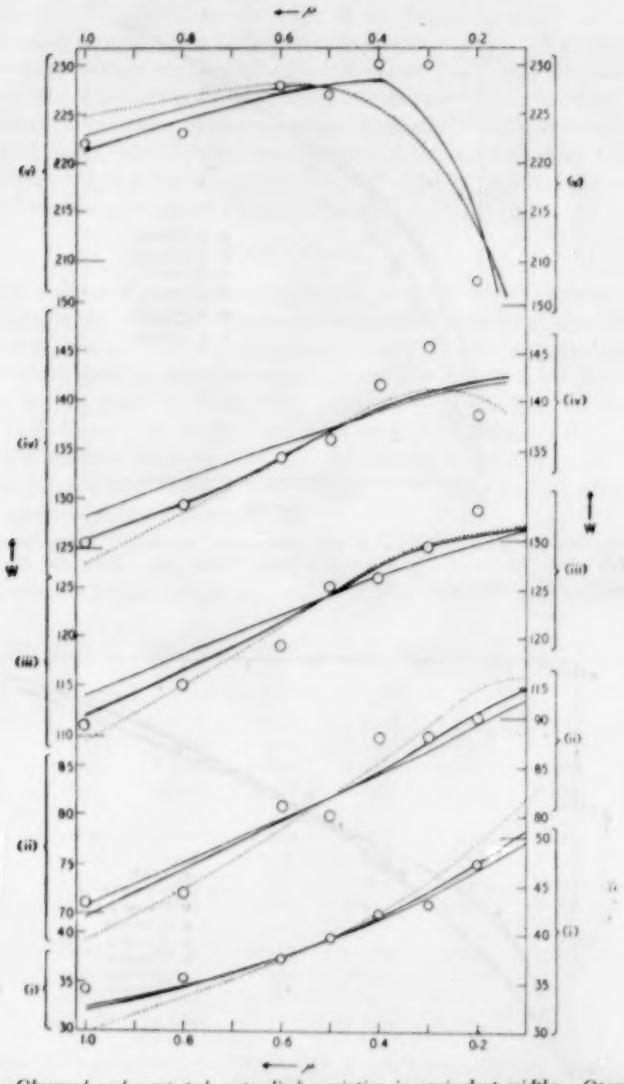

FIG. 9.—*Observed and computed centre-limb variation in equivalent widths. Open circles : observed values for* (*i*) *mean of* λ 15593·71, λ 15566·88 ; (*ii*) λ 15537·71 ; (*iii*) λ 15542·15 ; (*iv*) *mean of* λ 15531·80, λ 15534·31 ; (*v*) λ 15662·05. *Dotted line : Model I for* (*i*) $\eta = 0{\cdot}178n$; (*ii*) $\eta = 0{\cdot}490n$; (*iii*) $\eta = 1{\cdot}009n$; (*iv*) $\eta = 1{\cdot}368n$; (*v*) $\eta = 7{\cdot}08n$. *Heavy full line : Model II for* (*i*) $\eta = 0{\cdot}189n$; (*ii*) $\eta = 0{\cdot}543n$; (*iii*) $\eta = 1{\cdot}245n$; (*iv*) $\eta = 1{\cdot}556n$; (*v*) $\eta = 7{\cdot}76n$. *Light full line : Model III for* (*i*) $\eta = 0{\cdot}197n$; (*ii*) $\eta = 0{\cdot}575n$; (*iii*) $\eta = 1{\cdot}380n$; (*iv*) $\eta = 1{\cdot}738n$; (*v*) $\eta = 9{\cdot}12n$.

the assumption concerning the values of η/κ). For $\tau_\lambda > 0{\cdot}1$, Model I coincides very closely with the temperature distribution of Michard, and the results of Section 4 indicate that the temperature distribution found in this depth range is probably correct. In the outer layers ($\tau_\lambda \leqslant 0{\cdot}1$), the temperature distribution was modified in an attempt to remove the outstanding discrepancies; two new models—Models II and III—were derived in this way (Fig. 7) and the resulting equivalent widths were calculated by a simplified procedure based on the residual intensity at one point of the line profile ($\Delta\lambda = 0{\cdot}05$ A) and on the line-width data obtained from the earlier computations. The results derived from Models II, III are shown in Fig. 9; the equivalent widths derived from Model II show satisfactory agreement with the observational data (within the r.m.s. error), and this model has therefore been adopted. Model II (with $\log P$, $\log P_e$ calculated for our standard chemical composition) is given in Table VIII, and the corresponding continuum intensities and equivalent widths are given in Table IX.

TABLE VIII

Suggested photospheric model (Model II) calculated assuming $A = 10^4$; no helium

τ_{15500}	τ_{8600}	Θ	$\log P$	$\log P_e$
0·000	0·000	1·196		
0·005	0·015	1·227	4·15	−0·27
0·010	0·030	1·180	4·30	−0·07
0·015	0·045	1·077	4·33	+0·13
0·02	0·060	1·054	4·35	0·23
0·03	0·085	1·028	4·44	0·36
0·04	0·100	1·002	4·50	0·45
0·05	0·120	0·989	4·55	0·52
0·06	0·14	0·976	4·62	0·59
0·07	0·16	0·963	4·65	0·65
0·08	0·18	0·950	4·68	0·72
0·10	0·22	0·928	4·72	0·81
0·12	0·25	0·912	4·77	0·91
0·16	0·32	0·890	4·85	1·05
0·20	0·38	0·874	4·87	1·15
0·25	0·47	0·857	4·90	1·25
0·30	0·55	0·842	4·92	1·35
0·40	0·70	0·818	4·96	1·52
0·50	0·85	0·800	4·99	1·65
0·60	0·98	0·785	5·00	1·76
0·80	1·24	0·762	5·03	1·93
1·00	1·49	0·747	5·05	2·04
1·20	1·75	0·734	5·07	2·14
1·40	2·00	0·727	5·08	2·18

6. *Conclusion.*—The calculations of Sections 4, 5 have shown that the present series of observational data is consistent with the photospheric temperature distribution in the deeper layers ($\tau_\lambda \geqslant 0{\cdot}15$; $\tau_0 \geqslant 0{\cdot}30$) derived from the observational data on continuous limb-darkening by Michard; the temperature distribution of Aller and Pierce is in close agreement with that of Michard in these layers if we assume the relation

$$\tau_\theta = 0{\cdot}7\bar{\tau}$$

given by Aller and Pierce (1952). Closer to the surface ($\tau_\lambda < 0{\cdot}15$; $\tau_0 < 0{\cdot}30$), the situation is more complicated. Our Model I begins to depart markedly from the temperature distributions of de Jager and Michard (Fig. 7) for $\tau_\lambda < 0{\cdot}07$ ($\tau_0 < 0{\cdot}16$), while Model II continues to coincide with Michard's distribution down to $\tau_\lambda = 0{\cdot}02$ ($\tau_0 = 0{\cdot}06$). In the range $0{\cdot}02 < \tau_\lambda < 0{\cdot}12$, Model II and the

TABLE IX

Intensity of continuum and equivalent widths calculated from Model II

	$\mu=1{\cdot}0$	$\mu=0{\cdot}8$	$\mu=0{\cdot}6$	$\mu=0{\cdot}5$	$\mu=0{\cdot}4$	$\mu=0{\cdot}3$	$\mu=0{\cdot}2$	$\mu=0{\cdot}1$
(calculated) Continuum	4·084	3·942	3·755	3·636	3·492	3·312	3·071	2·699
(observed)	4·080	3·930	3·737	3·615	3·470	3·288	3·055	
$\eta=(1/8)n$	21·0	23·2	25·9	27·6	29·5	31·8	34·5	38·3
$\eta=(1/4)n$	38·3	41·4	45·8	48·2	50·8	53·3	56·8	60·9
$\eta=(1/2)n$	64·7	69·3	74·0	76·5	79·0	82·1	85·4	87·8
$\eta=n$	99·6	104·6	109·7	112·1	115·8	117·1	119·6	
$\eta=2n$	140·2	144·3	148·0	151·0	153·0	154·3	154·5	
$\eta=4n$	181·5	185·2	188·2	190·0	191·4	189·8	182·0	

models of Michard and de Jager are all closely coincident, so that we may also regard the temperature distribution in this region as well established. More ambiguity arises in the layers for which $\tau_\lambda < 0{\cdot}02$ ($\tau_0 < 0{\cdot}06$), which make a negligible contribution to the intensity of the continuum away from the extreme limb, but are strongly weighted when a Fraunhofer line due to a neutral metal is observed. The temperature inversion obtained by us cannot be dismissed as the result of accidental observational (or truncation) errors, since the sudden drop in equivalent width of the four strongest lines observed from $\mu = 0{\cdot}3$ to $\mu = 0{\cdot}2$ seems to point rather directly to the presence of such a feature although its position at $\tau_\lambda = 0{\cdot}005$ may be wrong by a considerable margin owing to errors in the adopted values of η near the surface. Such errors are to be expected from the difference between the local kinetic temperature near the surface and the effective temperature T_e of radiation incident from deeper solar layers (Woolley and Stibbs, 1953; Böhm, 1954) which results in an enhancement of excitation and ionization in comparison with local thermodynamic equilibrium at the surface temperature T_0. In a photospheric model with a steep temperature gradient, somewhat steeper than in de Jager's model and in our Model II, Böhm finds an enhancement in the ionization of Fe by a factor of 3 for $\tau_0 \leqslant 0{\cdot}01$. The effect on the occupation of the highly excited levels of Fe I, which are relevant in our case, has not been calculated in detail, but the undoubted presence of intense resonance absorption lines in the U.V. region (5·60 ev = λ 2200) suggests that the radiation density at the frequencies relevant for excitation (as opposed to ionization) is likely to depart very little from that corresponding to local thermodynamic equilibrium. As far as the ionization is concerned, it would be of great interest to carry out similar calculations for all the elements, since Böhm's factor 3 is strictly applicable only if there is no significant increase in the electron pressure; if the overall number of ionizing processes in the outer layers of the photosphere were increased by a factor 3, the degree of ionization would be increased somewhat less than this. We conclude that departures from the Saha equation may require an increase by a factor of about 2 in our values of τ_λ close to the surface ($\tau_0 \leqslant 0{\cdot}02$, $\tau_\lambda \leqslant 0{\cdot}01$).

If our conclusion is correct, it would appear that the inversion in the temperature gradient that must occur somewhere in the neighbourhood of the base of the chromosphere actually occurs within the photospheric layers

($\tau_0 = 0{\cdot}015$) and that the average temperature increases monotonically with height above this level. An interesting consequence of this is that we obtain the steep temperature gradient required to account for the increase in Fraunhofer line intensities towards the limb without being compelled to assume a particularly low limb temperature ($T_0 = 4210°$ in Model II). In this way, our temperature distribution may make it easier to account for the discrepancy noted by de Jager (1952) between his T_0 and the value deduced from observations of the continuum close to the limb, but additional computations are needed to test this possibility; furthermore, these data are subject to considerable observational errors.

A further consequence of the new temperature distribution would be the concentration of molecules such as CO in the layer corresponding to the minimum temperature ($\tau_0 = 0{\cdot}015$; $T = 4100°$); the abundances of molecules would be enhanced by the presence of a substantial gas pressure at this level. However, molecular absorption lines would be somewhat masked by the substantial amount of continuous absorption present (especially in the far infra-red; this prediction seems to be consistent with the observed characteristics of the fundamental vibrational band of CO at $\lambda 46\,000$ given by Goldberg and Müller, 1953). It would be of interest to compare the centre-limb variations in the equivalent widths of CO lines with predictions based on Model II.

Finally, if Model II is correct, it must reproduce the observed curves of growth and excitation temperatures of metallic lines. A strict test from this point of view would require a series of elaborate calculations, but the excitation temperatures—at least at the centre of the disk—cannot differ substantially from those of Michard, who expressly corrected his model in the outer photospheric layers to obtain agreement with observation in this respect. It is therefore reasonable to conclude that Model II will give good agreement with observations of line intensities at the centre of the solar disk, although a complete discussion will have to include the effects of temperature heterogeneities.

The writer is particularly indebted to Dr R. R. McMath, for his extension of facilities at the McMath–Hulbert Observatory and for his kindness in making available tracings taken with the Snow Telescope, and to Dr I. S. Bowen for permitting the use of the Snow Telescope for this purpose; he is indebted to Mr W. Livingston for recording the tracings. He is also greatly indebted to Dr M. V. Wilkes, for permitting the use of the EDSAC for this investigation and for instruction in the preparation of programmes, to Professor D. R. Hartree and Dr J. C. P. Miller for advice on numerical procedures, and to Messrs C. B. Haselgrove and K. G. Eickhoff for their assistance in certain aspects of the programming. The investigation was initiated during the writer's stay at the University of Michigan in 1952–3, and it is a pleasure to acknowledge the hospitality of Dr McMath and Dr Leo Goldberg during this period and the instruction and encouragement derived from many discussions with them and with Dr L. H. Aller and Dr O. C. Mohler. Thanks are also due to Dr E. M. Burbidge, Dr G. R. Burbidge, Dr C. de Jager, Professor H. H. Plaskett and Professor R. O. Redman for their interest and advice. Finally the writer is greatly indebted to the U.S. Government for the provision of Smith–Mundt maintenance and Fulbright travel grants, and to the Master and Fellows of Sidney Sussex College, Cambridge, for the award of a Research Fellowship.

Sidney Sussex College,
Cambridge:
1955 *June* 10.

References

Allen, C. W., 1949, *M.N.*, **109**, 173.
Aller, L. H., 1953, *Astrophysics* (New York : Ronald Press Co.), Ch. 8.
Aller, L. H. and Pierce, A. K., 1952, *Ap. J.*, **116**, 176.
Böhm, K. H., 1954, *Zs. f. Ap.*, **35**, 179.
Böhm-Vitense, E., 1954, *Zs. f. Ap.*, **34**, 209.
Chalonge, D. and Kourganoff, V., 1946, *Ann. d'ap.*, **9**, 69.
Chandrasekhar, S., 1950, *Radiative Transfer* (Oxford : Clarendon Press).
Chandrasekhar, S. and Breen, F. H., 1946, *Ap. J.*, **104**, 430.
Chandrasekhar, S. and Münch, G., 1946, *Ap. J.*, **104**, 446.
Claas, W. J., 1951, *Rech. Astr. Obs. Utrecht*, **12**, Part 1.
Goldberg, L., 1950, *Rep Prog. Phys.*, **13**, 24.
Goldberg, L. and Müller, E. A., 1953, *Ap. J.*, **118**, 397.
Harris, D. L., 1948, *Ap. J.*, **108**, 112.
Houtgast, J., 1942, *Dissertation* (Utrecht).
Houtgast, J., 1952, *B.A.N.*, **11**, 475.
Jager, C. de, 1952, *Rech. Astr. Obs. Utrecht*, **13**, Part 1.
Kourganoff, V., 1949, *C.R.*, **228**, 2011.
Labs, D., 1951, *Zs. f. Ap.*, **29**, 199.
Michard, R., 1953, *Ann. d'ap.*, **16**, 217.
Milne, W. E., 1949, *Numerical Calculus* (Princeton), p. 72.
Minnaert, M., 1953, *The Solar System*, **1**; *The Sun*, ed. G. P. Kuiper, p. 88.
Mohler, O. C., Pierce, A. K., McMath, R. R. and Goldberg, L., 1950, *Photometric Atlas of the Near Infra-red Solar Spectrum λ 8465 to λ 25,242* (Ann Arbor : University of Michigan Press).
Mohler, O. C., Pierce, A. K., McMath, R. R. and Goldberg, L., 1953, *Ap. J.*, **117**, 41.
Moore, C. E., 1952, *Atomic Energy Levels*, **2** (Washington : Nat. Bur. Stand. Circ. 467).
Neven, L. and Jager, C. de, 1951, *B.A.N.*, **11**, 291.
Page, R. M., 1951, *Thesis* (Ann Arbor).
Pagel, B. E. J., 1954, *Thesis* (Cambridge).
Panter, S. F. and Foster, J. S., 1937, *Proc. Roy. Soc.* A, **162**, 336.
Peyturaux, R., 1952, *Ann. d'ap.*, **15**, 302.
Pierce, A. K. and Aller, L. H., 1951, *Ap. J.*, **114**, 145.
Scarborough, J. B., 1950, *Numerical Mathematical Analysis* (Baltimore : Johns Hopkins Press), p. 299.
Spitzer, L., 1944, *Ap. J.*, **99**, 1.
Strömgren, B., 1940, *Festschrift für Elis Strömgren* (København : Ejnar Munksgaard), p. 210.
Unsöld, A., 1938, *Physik der Sternatmosphären* (Berlin : Julius Springer), p. 119.
Unsöld, A., 1948, *Ann. d. Phys.*, **3**, 124.
Unsöld, A. and Weidemann, V., 1955, *Vistas in Astronomy* (London: Pergamon Press), p. 254.
Voigt, H. H., 1950, *Zs. f. Ap.*, **27**, 82.
Wilkes, M. V., Wheeler, D. J. and Gill, S., 1951, *The Preparation of Programs for an Electronic Digital Computer* (Cambridge, Mass. : Addison-Wesley Press).
Woolley, R. v. d. R. and Stibbs, D. W. N., 1953, *The Outer Layers of a Star* (Oxford : Clarendon Press), p. 187.

FINITE ATMOSPHERES WITH ISOTROPIC SCATTERING

I. W. Busbridge

(Received 1955 August 12)

Summary

Some transfer problems in plane parallel atmospheres of finite optical thickness τ_1 are considered, the scattering being isotropic with albedo ϖ $(0<\varpi\leqslant 1)$. The equations for Chandrasekhar's X- and Y-functions are obtained by a simple mathematical method, an extension of one originally due to Ambartsumian. The same method is then used to obtain expressions for the emergent intensities at both faces of the atmosphere when there is thermal emission and when it is subject to incident radiation.

---

1. *Introduction.*—Problems concerning the transfer of radiation through plane parallel finite atmospheres are more complicated than the corresponding ones for semi-infinite atmospheres because there are two faces on which incident radiation may fall and through which radiation will emerge. Hitherto the only successful method of tackling such problems has been by means of Chandrasekhar's Principles of Invariance and it is significant of the difficulties involved, that the only people who have worked on such problems are Chandrasekhar himself and a few astrophysicists associated with him at Yerkes.

In two recent papers ((**3**) and (**4**)) I have developed a method which was originally given by Ambartsumian in (**1**) and of which there is an account in (**9**), Section 28. This method has proved to be unexpectedly powerful and in this paper I show that it can be applied to finite atmospheres as well as to semi-infinite ones. Only isotropic scattering with albedo $\varpi(0<\varpi\leqslant 1)$ is considered, but it should not be difficult to adapt the method for other laws of scattering. (See, for example, (**4**) where the scattering is non-coherent. I have also used the method for interlocked multiplet lines.)

Ambartsumian's method only involves simple mathematics. It starts from the form of Milne's first integral equation (Section 2) appropriate to the problem and it depends upon the solution of an auxiliary integral equation (Section 4), which leads directly to the X- and Y-functions. Solving the auxiliary equation is equivalent, in Chandrasekhar's work, to finding expressions for the reflected and transmitted intensities in the "diffuse radiation field" when one surface of the atmosphere is illuminated by axially symmetric radiation inclined at a fixed angle to the inwards drawn normal (see Section 5).

The solution found for a given problem is unique only if the corresponding homogeneous form of Milne's integral equation has no non-null solution of the appropriate order of magnitude. The solutions of the homogeneous equation are investigated in detail in the appendix and the results are summarized in Section 6.

When $0<\varpi<1$, the X- and Y-functions exist and are unambiguous, but when $\varpi=1$ (the conservative case), if $X(\mu)$ and $Y(\mu)$ are solutions of the X- and Y-equations then so are

$$X(\mu)+Q\mu[X(\mu)+Y(\mu)] \quad \text{and} \quad Y(\mu)-Q\mu[X(\mu)+Y(\mu)]$$

for any value of the constant Q. This ambiguity is related to the question of

uniqueness and it is also discussed in the appendix. Throughout the body of the paper, $X(\mu)$ and $Y(\mu)$ will represent the *standard solutions* when $\varpi = 1$, i.e. those solutions which are such that,*

$$x_0 \equiv \tfrac{1}{2}\int_0^1 X(\mu)d\mu = 1, \quad y_0 \equiv \tfrac{1}{2}\int_0^1 Y(\mu)d\mu = 0. \tag{1.1}$$

In every problem it is necessary to discuss the conservative case separately.

With the aid of the auxiliary equation, a number of problems can be solved in terms of the X- and Y-functions. In Sections 7 ($0 < \varpi < 1$) and 8 ($\varpi = 1$) the emergent radiation from an emitting atmosphere is considered. A polynomial representation is used for the Planck function and from this the results found by Horak and Lundquist in (**8**) for a linear Planck function are deduced.

In Sections 9 ($0 < \varpi < 1$) and 10 ($\varpi = 1$), one surface of a non-emitting atmosphere is illuminated by isotropic radiation and the reflected and transmitted intensities are found. The results of these sections can also be used to give the intensities of the emergent radiation from an atmosphere emitting according to the law $E_2(\tau)$ (the second exponential integral), where τ is the optical depth below the upper surface of the atmosphere. By combining the results of Sections 7–10, it is possible to deal with a representation such as

$$a + b\tau + cE_2(\tau)$$

for the Planck function, a form which has been found to give a good representation in the grey case.

Tables of the X- and Y-functions for values of τ_1 (the optical thickness of the atmosphere) and ϖ such that $0 < \tau_1 \leqslant 1$, $0{\cdot}5 \leqslant \varpi \leqslant 1$ have been compiled by Chandrasekhar, Elbert and Franklin (**6**). It is probable that tables for larger values of τ_1 will be needed before much useful numerical work can be done on finite atmospheres.

In this paper details of rigour are omitted. In (**3**) I have treated the same problems rigorously for a semi-infinite atmosphere and in general the treatment for a finite atmosphere is similar. The existence of the X- and Y-functions, at least for sufficiently large τ_1, has been established in (**2**) and I shall therefore treat them as known functions.

2. *Milne's first integral equation.*—When there is isotropic scattering, the equation of transfer is of the form

$$\mu \frac{d}{d\tau} I(\tau, \mu) = I(\tau, \mu) - \tfrac{1}{2}\varpi \int_{-1}^{1} I(\tau, \mu')d\mu' - B_1(\tau), \tag{2.1}$$

where $B_1(\tau)$ may be $(1 - \varpi)$ times the Planck function or it may be some other given function.

Following the notation of Chandrasekhar in (**5**), I shall use $I(\tau, +\mu)$ $(0 < \mu \leqslant 1)$ to denote the intensity of the radiation directed towards the surface $\tau = 0$ and $I(\tau, -\mu)$ $(0 < \mu \leqslant 1)$ for that directed towards the surface $\tau = \tau_1$. Then if radiation of intensity $f_0(\mu)$ is falling on the surface $\tau = 0$ at an angle $\cos^{-1}\mu$ with the inwards normal, and if radiation of intensity $f_1(\mu)$ is similarly falling on the surface $\tau = \tau_1$, the boundary conditions are

$$\left.\begin{aligned} I(0, -\mu) &= f_0(\mu) \quad (0 < \mu \leqslant 1), \\ I(\tau_1, +\mu) &= f_1(\mu) \quad (0 < \mu \leqslant 1). \end{aligned}\right\} \tag{2.2}$$

* All solutions satisfy the equation $x_0 + y_0 = 1$ in the conservative case. Either of the equations (1.1) therefore determines Q.

If we write (2.1) in the form

$$\mu \frac{d}{d\tau} I(\tau, \mu) = I(\tau, \mu) - \mathfrak{J}(\tau), \tag{2.3}$$

where

$$\mathfrak{J}(\tau) = \tfrac{1}{2}\varpi \int_{-1}^{1} I(\tau, \mu')d\mu' + B_1(\tau), \tag{2.4}$$

then the solution of (2.3) subject to the boundary conditions (2.2) is given by (cf. (5), Chap. I, equations (64) and (65))

$$I(\tau, +\mu) = f_1(\mu) \exp[-(\tau_1 - \tau)/\mu] + \exp(\tau/\mu) \int_{\tau}^{\tau_1} \mathfrak{J}(t) \exp(-t/\mu) \frac{dt}{\mu}, \tag{2.5}$$

$$I(\tau, -\mu) = f_0(\mu) \exp(-\tau/\mu) + \exp(-\tau/\mu) \int_{0}^{\tau} \mathfrak{J}(t) \exp(t/\mu) \frac{dt}{\mu}, \tag{2.6}$$

where $0 < \mu \leqslant 1$, $0 \leqslant \tau \leqslant \tau_1$ in each equation. Hence

$$\begin{aligned} \int_{-1}^{1} I(\tau, \mu)d\mu &= \int_{0}^{1} I(\tau, +\mu)d\mu + \int_{0}^{1} I(\tau, -\mu)d\mu \\ &= \int_{0}^{1} f_0(\mu) \exp(-\tau/\mu)\, d\mu + \int_{0}^{1} f_1(\mu) \exp[-(\tau_1 - \tau)/\mu]\, d\mu \\ &\quad + \int_{0}^{\tau_1} \mathfrak{J}(t) E_1(|t - \tau|)\, dt, \end{aligned} \tag{2.7}$$

where

$$E_1(\tau) = \int_{1}^{\infty} \exp(-\tau x) \frac{dx}{x}. \tag{2.8}$$

On substituting from (2.7) into (2.4), we have the following integral equation for the source function $\mathfrak{J}(\tau)$:

$$\begin{aligned} \mathfrak{J}(\tau) = \tfrac{1}{2}\varpi \int_{0}^{\tau_1} \mathfrak{J}(t) E_1(|t - \tau|)\, dt + \tfrac{1}{2}\varpi \int_{0}^{1} f_0(\mu') \exp(-\tau/\mu')\, d\mu' \\ + \tfrac{1}{2}\varpi \int_{0}^{1} f_1(\mu') \exp[-(\tau_1 - \tau)/\mu']\, d\mu' + B_1(\tau). \end{aligned} \tag{2.9}$$

This is the form taken by Milne's first integral equation.

We shall introduce the operator $\bar{\Lambda}$ defined by

$$\bar{\Lambda}_{\tau}\{f(t)\} = \tfrac{1}{2} \int_{0}^{\tau_1} f(t) E_1(|t - \tau|)dt. \tag{2.10}$$

In this, and in all subsequent equations, $0 \leqslant \tau \leqslant \tau_1$. When τ_1 is infinite, $\bar{\Lambda}$ is identical with Hopf's operator Λ. (See (7), and (9), Chap. II.) Equation (2.9) can now be written

$$\mathfrak{J}(\tau) = \varpi \bar{\Lambda}_{\tau}\{\mathfrak{J}(t)\} + B(\tau), \tag{2.11}$$

where

$$\begin{aligned} B(\tau) = B_1(\tau) + \tfrac{1}{2}\varpi \int_{0}^{1} f_0(\mu') \exp(-\tau/\mu')\, d\mu' \\ + \tfrac{1}{2}\varpi \int_{0}^{1} f_1(\mu') \exp[-(\tau_1 - \tau)/\mu']\, d\mu'. \end{aligned} \tag{2.12}$$

This is a known function in any particular problem.

The emergent intensities from the atmosphere are $I(0, +\mu)$ and $I(\tau_1, -\mu)$.

By (2.5) and (2.6), these are given by

$$I(0,+\mu)=f_1(\mu)\exp(-\tau_1/\mu)+\mathfrak{j}_0(\mu^{-1}), \tag{2.13}$$

$$I(\tau_1,-\mu)=f_0(\mu)\exp(-\tau_1/\mu)+\mathfrak{j}_1(\mu^{-1}), \tag{2.14}$$

where

$$\mathfrak{j}_0(s)=s\int_0^{\tau_1}\mathfrak{J}(t)\exp(-st)\,dt, \tag{2.15}$$

$$\mathfrak{j}_1(s)=s\exp(-\tau_1 s)\int_0^{\tau_1}\mathfrak{J}(t)\exp(st)\,dt=s\int_0^{\tau_1}\mathfrak{J}(\tau_1-t)\exp(-st)\,dt. \tag{2.16}$$

In the following sections we shall aim at finding $\mathfrak{j}_0(\mu^{-1})$ and $\mathfrak{j}_1(\mu^{-1})$ when $B(\tau)$ is some standard function.

The functions $\mathfrak{j}_0(s)$ and $\mathfrak{j}_1(s)$ will be called the τ_1-Laplace transforms, or more briefly the τ_1-transforms, of $\mathfrak{J}(\tau)$. From (2.15) and (2.16) we have the important relations

$$\mathfrak{j}_0(s)=-\exp(-s\tau_1)\mathfrak{j}_1(-s),\quad \mathfrak{j}_1(s)=-\exp(-s\tau_1)\mathfrak{j}_0(-s), \tag{2.17}$$

of which we shall make frequent use. We shall always use the corresponding lower case letter with subscripts 0 and 1 to denote the τ_1-transforms. For example, the τ_1-transforms of $J(\tau)$ will be $j_0(s)$ and $j_1(s)$.

Note that, if *

$$B(\tau)=aB^1(\tau)+bB^2(\tau) \tag{2.18}$$

and if

$$J^1(\tau)=\varpi\bar{\Lambda}_\tau\{J^1(t)\}+B^1(\tau), \tag{2.19}$$

$$J^2(\tau)=\varpi\bar{\Lambda}_\tau\{J^2(t)\}+B^2(\tau), \tag{2.20}$$

then a solution of (2.11) is

$$\mathfrak{J}(\tau)=aJ^1(\tau)+bJ^2(\tau), \tag{2.21}$$

and

$$\mathfrak{j}_0(s)=aj_0^1(s)+bj_0^2(s), \tag{2.22}$$

$$\mathfrak{j}_1(s)=aj_1^1(s)+bj_1^2(s). \tag{2.23}$$

Thus the solutions corresponding to standard functions can be added to give solutions (or approximations to the solutions) of more complex problems.

3. *Properties of the operator* $\bar{\Lambda}$.—In deducing (2.21) from (2.19) and (2.20), we have used the fact that the operator $\bar{\Lambda}$ is linear, i.e. if a and b are constants, then

$$\bar{\Lambda}_\tau\{af(t)+bg(t)\}=a\bar{\Lambda}_\tau\{f(t)\}+b\bar{\Lambda}_\tau\{g(t)\}. \tag{3.1}$$

In addition to this $\bar{\Lambda}$ has the following important properties:

I $$\bar{\Lambda}_{\tau_1-\tau}\{f(t)\}=\bar{\Lambda}_\tau\{f(\tau_1-t)\}, \tag{3.2}$$

II $$\frac{d}{d\tau}\bar{\Lambda}_\tau\{f(t)\}=\bar{\Lambda}_\tau\left\{\frac{d}{dt}f(t)\right\}+\tfrac{1}{2}f(0)E_1(\tau)-\tfrac{1}{2}f(\tau_1)E_1(\tau_1-\tau), \tag{3.3}$$

the function $f(t)$ being subject to appropriate conditions. (Cf. (7), p.34.)

To prove I, we have, by the definition (2.10),

$$\bar{\Lambda}_{\tau_1-\tau}\{f(t)\}=\tfrac{1}{2}\int_0^{\tau_1-\tau}f(t)E_1(\tau_1-\tau-t)\,dt+\tfrac{1}{2}\int_{\tau_1-\tau}^{\tau_1}f(t)E_1(t-\tau_1+\tau)\,dt.$$

* Because of the subscripts 0 and 1, it is necessary to write other subscripts as superscripts. As no powers of functions are involved, there is no risk of confusion.

On putting $t=\tau_1-u$, we get

$$\overline{\Lambda}_{\tau_1-\tau}\{f(t)\}=\tfrac{1}{2}\int_{\tau}^{\tau_1}f(\tau_1-u)E_1(u-\tau)\,du+\tfrac{1}{2}\int_0^{\tau}f(\tau_1-u)E_1(\tau-u)\,du$$
$$=\overline{\Lambda}_{\tau}\{f(\tau_1-u)\}.$$

To prove II, put $t=\tau-u$ in the integral over $(0,\tau)$ and $t=\tau+u$ in the integral over (τ,τ_1) in the definition (2.10) of $\overline{\Lambda}_{\tau}\{f(t)\}$. Then

$$\overline{\Lambda}_{\tau}\{f(t)\}=\tfrac{1}{2}\int_0^{\tau}f(\tau-u)E_1(u)du+\tfrac{1}{2}\int_0^{\tau_1-\tau}f(\tau+u)E_1(u)\,du. \tag{3.4}$$

By the usual formula for differentiation under the integral sign,

$$\frac{d}{d\tau}\overline{\Lambda}_{\tau}\{f(t)\}=\tfrac{1}{2}\int_0^{\tau}\frac{d}{d\tau}f(\tau-u)E_1(u)\,du+\tfrac{1}{2}f(0)E_1(\tau)$$
$$+\tfrac{1}{2}\int_0^{\tau_1-\tau}\frac{d}{d\tau}f(\tau+u)E_1(u)\,du-\tfrac{1}{2}f(\tau_1)E_1(\tau_1-\tau),$$

and this (cf. (3·4)) is (3.3).

4. *The auxiliary equation and the X- and Y-functions.*—The auxiliary equation is

$$J(\tau,\sigma)=\varpi\overline{\Lambda}_{\tau}\{J(t,\sigma)\}+\exp(-\sigma\tau)\quad(0<\varpi\leqslant 1). \tag{4.1}$$

Just as in (3), Theorem III, it can be shown that, when $0<\varpi<1$, (4.1) has a solution which is bounded for $\sigma\geqslant 0$ and $0\leqslant\tau\leqslant\tau_1$, the bounds being independent of τ_1. We shall use $J(\tau,\sigma)$ to denote this solution. When $\varpi=1$, $J(\tau,\sigma)$ is ambiguous in the same way that $X(\mu)$ and $Y(\mu)$ are ambiguous. This difficulty will be dealt with in the appendix. For the present it is enough to say that $J(\tau,\sigma)$ is a solution of (4.1).

Differentiate (4.1) with respect to τ, using (3.3). Then

$$\frac{\partial}{\partial\tau}J(\tau,\sigma)=\varpi\overline{\Lambda}_{\tau}\left\{\frac{\partial}{\partial t}J(t,\sigma)\right\}+\tfrac{1}{2}\varpi J(0,\sigma)E_1(\tau)$$
$$-\tfrac{1}{2}\varpi J(\tau_1,\sigma)E_1(\tau_1-\tau)-\sigma\exp(-\sigma\tau).$$

Hence

$$\frac{\partial}{\partial\tau}J(\tau,\sigma)+\sigma J(\tau,\sigma)=\varpi\overline{\Lambda}_{\tau}\left\{\frac{\partial}{\partial t}J(t,\sigma)+\sigma J(t,\sigma)\right\}$$
$$+\tfrac{1}{2}\varpi J(0,\sigma)E_1(\tau)-\tfrac{1}{2}\varpi J(\tau_1,\sigma)E_1(\tau_1-\tau). \tag{4.2}$$

We next obtain expressions for $E_1(\tau)$ and $E_1(\tau_1-\tau)$ from (4.1). Multiplying (4.1) by σ^{-1} and integrating with respect to σ over $(1,\infty)$, we have (on writing x for σ)*

$$\int_1^{\infty}J(\tau,x)\frac{dx}{x}=\varpi\overline{\Lambda}_{\tau}\left\{\int_1^{\infty}J(t,x)\frac{dx}{x}\right\}+E_1(\tau). \tag{4.3}$$

On replacing τ by $\tau_1-\tau$ and using (3.2), we get

$$\int_1^{\infty}J(\tau_1-\tau,x)\frac{dx}{x}=\varpi\overline{\Lambda}_{\tau}\left\{\int_1^{\infty}J(\tau_1-t,x)\frac{dx}{x}\right\}+E_1(\tau_1-\tau). \tag{4.4}$$

From (4.2) subtract $\tfrac{1}{2}\varpi J(0,\sigma)$ times (4.3) and add $\tfrac{1}{2}\varpi J(\tau_1,\sigma)$ times (4.4). Since the operator $\overline{\Lambda}$ is linear, we see that

$$\frac{\partial}{\partial\tau}J(\tau,\sigma)+\sigma J(\tau,\sigma)-\tfrac{1}{2}\varpi J(0,\sigma)\int_1^{\infty}J(\tau,x)\frac{dx}{x}$$
$$+\tfrac{1}{2}\varpi J(\tau_1,\sigma)\int_1^{\infty}J(\tau_1-\tau,x)\frac{dx}{x}=CJ(\tau), \tag{4.5}$$

* An integration with respect to σ commutes with $\overline{\Lambda}$, which is independent of σ. In general we shall invert orders of integration without comment.

where $J(\tau)$ satisfies the equation

$$J(\tau)=\varpi\overline{\Lambda}_{\tau}\{J(t)\} \tag{4.6}$$

and C is a constant which may depend on σ.

The solutions of (4.6) are discussed in the appendix. As we shall show that $C=0$, the value of $J(\tau)$ does not matter.

Let
$$R(s,\sigma)=\int_0^{\tau_1}\exp(-st)J(t,\sigma)\,dt. \tag{4.7}$$

Then we have the important relations

$$R(s,\sigma)=R(\sigma,s), \tag{4.8}$$

$$\exp(-s\tau_1)R(-s,\sigma)=\exp(-\sigma\tau_1)R(-\sigma,s). \tag{4.9}$$

To prove (4.8), multiply (4.1) by $J(\tau,s)$ and integrate with respect to τ over $(0,\tau_1)$. Then

$$\begin{aligned}\int_0^{\tau_1}J(\tau,s)J(\tau,\sigma)\,d\tau&=\tfrac{1}{2}\varpi\int_0^{\tau_1}J(\tau,s)\,d\tau\int_0^{\tau_1}J(t,\sigma)E_1(|t-\tau|)\,dt+R(\sigma,s)\\&=\tfrac{1}{2}\varpi\int_0^{\tau_1}J(t,\sigma)\,dt\int_0^{\tau_1}J(\tau,s)E_1(|\tau-t|)\,d\tau+R(\sigma,s)\\&=\int_0^{\tau_1}J(t,\sigma)J(t,s)\,dt-R(s,\sigma)+R(\sigma,s)\end{aligned}$$

(by interchange of s and σ, t and τ in the first line) and hence we have (4.8).

To prove (4.9), write $\tau_1-\tau$ for τ in (4.1). Then

$$J(\tau_1-\tau,\sigma)=\varpi\overline{\Lambda}_{\tau_1-\tau}\{J(t,\sigma)\}+\exp[-\sigma(\tau_1-\tau)].$$

Hence

$$\begin{aligned}\int_0^{\tau_1}J(\tau,s)J(\tau_1-\tau,\sigma)\,d\tau&=\tfrac{1}{2}\varpi\int_0^{\tau_1}J(\tau,s)\,d\tau\int_0^{\tau_1}J(t,\sigma)E_1(|t+\tau-\tau_1|)\,dt\\&\quad+\exp(-\sigma\tau_1)\int_0^{\tau_1}\exp(\sigma\tau)J(\tau,s)\,d\tau\\&=\tfrac{1}{2}\varpi\int_0^{\tau_1}J(t,\sigma)\,dt\int_0^{\tau_1}J(\tau,s)E_1(|\tau+t-\tau_1|)\,d\tau\\&\quad+\exp(-\sigma\tau_1)R(-\sigma,s)\\&=\int_0^{\tau_1}J(t,\sigma)J(\tau_1-t,s)\,dt-\exp(-s\tau_1)R(-s,\sigma)\\&\quad+\exp(-\sigma\tau_1)R(-\sigma,s).\end{aligned}$$

But (writing $t=\tau_1-\tau$)

$$\int_0^{\tau_1}J(t,\sigma)J(\tau_1-t,s)\,dt=\int_0^{\tau_1}J(\tau_1-\tau,\sigma)J(\tau,s)\,d\tau,$$

and so (4.9) follows.

Now multiply (4.5) by $\exp(-s\tau)$ and integrate with respect to τ over $(0,\tau_1)$. Since

$$\begin{aligned}\int_0^{\tau_1}J(\tau_1-\tau,x)\exp(-s\tau)\,d\tau&=\int_0^{\tau_1}J(t,x)\exp[-s(\tau_1-t)]\,dt\\&=\exp(-s\tau_1)R(-s,x),\end{aligned} \tag{4.10}$$

we have (after integrating the first term by parts)

$$\exp(-s\tau_1)J(\tau_1,\sigma)-J(0,\sigma)+sR(s,\sigma)+\sigma R(s,\sigma)-\tfrac{1}{2}\varpi J(0,\sigma)\int_1^\infty R(s,x)\frac{dx}{x}$$
$$+\tfrac{1}{2}\varpi J(\tau_1,\sigma)\exp(-s\tau_1)\int_1^\infty R(-s,x)\frac{dx}{x}=Cs^{-1}j_0(s),$$

where $j_0(s)$ is the first τ_1-transform of $J(\tau)$. (See equation (2.15). This may be written

$$(s+\sigma)R(s,\sigma)-Cs^{-1}j_0(s)=J(0,\sigma)\left\{1+\tfrac{1}{2}\varpi\int_1^\infty R(s,x)\frac{dx}{x}\right\}$$
$$-J(\tau_1,\sigma)\exp(-s\tau_1)\left\{1+\tfrac{1}{2}\varpi\int_1^\infty R(-s,x)\frac{dx}{x}\right\}. \qquad (4.11)$$

Put $\tau=0$ and write s for σ in (4.1). Then we have

$$\begin{aligned}J(0,s)&=\tfrac{1}{2}\varpi\int_0^{\tau_1}J(t,s)E_1(t)\,dt+1\\&=1+\tfrac{1}{2}\varpi\int_0^{\tau_1}J(t,s)\,dt\int_1^\infty\exp(-xt)\frac{dx}{x}\\&=1+\tfrac{1}{2}\varpi\int_1^\infty R(x,s)\frac{dx}{x}\qquad\text{(by (4.7))}\\&=1+\tfrac{1}{2}\varpi\int_1^\infty R(s,x)\frac{dx}{x}\qquad(4.12)\end{aligned}$$

by (4.8).

Again, putting $\tau=\tau_1$ in (4.1), we have

$$\begin{aligned}J(\tau_1,s)&=\tfrac{1}{2}\varpi\int_0^{\tau_1}J(t,s)E_1(\tau_1-t)\,dt+\exp(-s\tau_1)\\&=\exp(-s\tau_1)+\tfrac{1}{2}\varpi\int_0^{\tau_1}J(t,s)\,dt\int_1^\infty\exp[-(\tau_1-t)x]\frac{dx}{x}\\&=\exp(-s\tau_1)+\tfrac{1}{2}\varpi\int_1^\infty\exp(-\tau_1x)R(-x,s)\frac{dx}{x}\\&=\exp(-s\tau_1)\left\{1+\tfrac{1}{2}\varpi\int_1^\infty R(-s,x)\frac{dx}{x}\right\}\qquad(4.13)\end{aligned}$$

by (4.9). Hence (4.11), (4.12) and (4.13) give

$$(s+\sigma)R(s,\sigma)-Cs^{-1}j_0(s)=J(0,\sigma)J(0,s)-J(\tau_1,\sigma)J(\tau_1,s).$$

Since, however, $R(s,\sigma)=R(\sigma,s)$, we must have $C=A\sigma^{-1}j_0(\sigma)$, where A may be zero. Hence

$$(s+\sigma)R(s,\sigma)-As^{-1}\sigma^{-1}j_0(s)j_0(\sigma)=J(0,s)J(0,\sigma)-J(\tau_1,\sigma)J(\tau_1,s). \qquad (4.14)$$

From (4.12) and (4.13) we have the important relations

$$\left.\begin{aligned}J(\tau_1,-s)&=\exp(s\tau_1)J(0,s),\\J(0,-s)&=\exp(s\tau_1)J(\tau_1,s).\end{aligned}\right\} \qquad (4.15)$$

Write $-s$ for s in (4.14) and use (4.15) and (2.17).

Then on multiplying by $\exp(-s\tau_1)$, we have

$$(s-\sigma)\exp(-s\tau_1)R(-s,\sigma)+As^{-1}\sigma^{-1}j_1(s)j_0(\sigma)=J(0,s)J(\tau_1,\sigma)-J(0,\sigma)J(\tau_1,s). \qquad (4.16)$$

Since $\exp(-s\tau_1)R(-s,\sigma)=\exp(-\sigma\tau_1)R(-\sigma,s)$, either $A=0$ or

$$j_1(s)j_0(\sigma)=-j_1(\sigma)j_0(s).$$

In this we can put $\sigma=s$ and we get $j_0(s)\equiv 0$ or $j_1(s)\equiv 0$ and either implies that $J(\tau)\equiv 0$. Hence (4.14) and (4.16) become

$$(s+\sigma)R(s,\sigma)=J(0,s)J(0,\sigma)-J(\tau_1,s)J(\tau_1,\sigma), \tag{4.17}$$

$$(s-\sigma)\exp(-s\tau_1)R(-s,\sigma)=J(0,s)J(\tau_1,\sigma)-J(0,\sigma)J(\tau_1,s). \tag{4.18}$$

From (4.12) and (4.17), (4.13) and (4.18), we have the following integral equations for $J(0,s)$ and $J(\tau_1,s)$:

$$J(0,s)=1+\tfrac{1}{2}\varpi\int_1^\infty\{J(0,s)J(0,x)-J(\tau_1,s)J(\tau_1,x)\}\frac{dx}{x(s+x)}, \tag{4.19}$$

$$J(\tau_1,s)=\exp(-s\tau_1)+\tfrac{1}{2}\varpi\int_1^\infty\{J(0,s)J(\tau_1,x)-J(0,x)J(\tau_1,s)\}\frac{dx}{x(s-x)}. \tag{4.20}$$

Now put $s=1/\mu$, $x=1/\mu'$ and write

$$X(\mu)=J(0,\mu^{-1}),\quad Y(\mu)=J(\tau_1,\mu^{-1}). \tag{4.21}$$

Then (4.19) and (4.20) become the X- and Y-equations:

$$X(\mu)=1+\tfrac{1}{2}\varpi\mu\int_0^1\{X(\mu)X(\mu')-Y(\mu)Y(\mu')\}\frac{d\mu'}{\mu+\mu'}, \tag{4.22}$$

$$Y(\mu)=\exp(-\tau_1/\mu)+\tfrac{1}{2}\varpi\mu\int_0^1\{Y(\mu)X(\mu')-X(\mu)Y(\mu')\}\frac{d\mu'}{\mu-\mu'} \tag{4.23}$$

These are (5), Chap. VIII, equations (1) and (2) with $\Psi(\mu)=\frac{1}{2}\varpi$.

The existence of $X(\mu)$ and $Y(\mu)$ when $0<\varpi<1$ follows from (4.21) and the existence of $J(\tau,\sigma)$.

In the appendix it is shown that, when $\varpi=1$, the function $J(\tau,\sigma)$ can be chosen so that the functions defined by (4.21) are the standard solutions, i.e. those satisfying (1.1). We shall assume that this has been done.

From (4.17), (4.18) and (4.21), we have

$$R(\mu^{-1},\mu_0^{-1})=\frac{\mu\mu_0}{\mu+\mu_0}\{X(\mu)X(\mu_0)-Y(\mu)Y(\mu_0)\}, \tag{4.24}$$

$$\exp(-\tau_1/\mu)R(-\mu^{-1},\mu_0^{-1})=\frac{\mu\mu_0}{\mu_0-\mu}\{X(\mu)Y(\mu_0)-Y(\mu)X(\mu_0)\}. \tag{4.25}$$

Note that the relation

$$Y(\mu)=\exp(-\tau_1/\mu)X(-\mu) \tag{4.26}$$

comes from (4.15).

5. *Diffuse reflection and transmission.*—If the surface $\tau=0$ is illuminated by axially symmetric radiation at an angle $\cos^{-1}\mu_0$ ($0<\mu_0\leqslant 1$) with the inwards drawn normal and if F is the intrinsic flux of the incident radiation, then (see (9), section 31.2) with the notation of Section 2

$$f_0(\mu)=\tfrac{1}{2}F\delta(\mu-\mu_0), \tag{5.1}$$

where δ is Dirac's δ-function. By the properties of the δ-function

$$\int_0^1 f_0(\mu)\exp(-\tau/\mu)\,d\mu=\tfrac{1}{2}F\exp(-\tau/\mu_0).$$

If $f_1(\mu)=0$ and $B_1(\tau)=0$, (2.11) and (2.12) give

$$\mathfrak{J}(\tau)=\varpi\bar{\Lambda}_\tau\{\mathfrak{J}(t)\}+\tfrac{1}{4}\varpi F\exp(-\tau/\mu_0). \tag{5.2}$$

Comparing this with (4.1) we see that a solution of (5.2) is

$$\mathfrak{J}(\tau) = \tfrac{1}{4}\varpi F J(\tau, \mu_0^{-1}). \tag{5.3}$$

From (2.13), (2.15) and (5.3),

$$I(0, +\mu) = \tfrac{1}{4}\varpi F \int_0^{\tau_1} J(t, \mu_0^{-1}) \exp(-t/\mu) \frac{dt}{\mu}$$

$$= \tfrac{1}{4}\varpi F \mu^{-1} R(\mu^{-1}, \mu_0^{-1})$$

by (4.7). Hence (4.24) gives

$$I(0, +\mu) = \tfrac{1}{4}\varpi F \frac{\mu_0}{\mu + \mu_0} \{X(\mu)X(\mu_0) - Y(\mu)Y(\mu_0)\}. \tag{5.4}$$

From (2.14), (2.16), (5.1) and (5.3),

$$I(\tau_1, -\mu) = \tfrac{1}{4}F\delta(\mu - \mu_0)\exp(-\tau_1/\mu_0) + \exp(-\tau_1/\mu)\,\tfrac{1}{4}F\varpi\mu^{-1}R(-\mu^{-1}, \mu_0^{-1}).$$

The first term on the right gives the "reduced incident radiation" and the second term, by (4.25), gives the following expression for the transmitted intensity in the "diffuse radiation field":

$$\tfrac{1}{4}F\varpi \frac{\mu_0}{\mu - \mu_0} \{X(\mu_0)Y(\mu) - Y(\mu_0)X(\mu)\}. \tag{5.5}$$

The expressions (5.4) and (5.5) are those given in (**5**), Chap. VIII, equations (108) and (109).

6. *The homogeneous Milne equation.*—It is important to determine whether the equation

$$J(\tau) = \varpi \overline{\Lambda}_\tau \{J(t)\} \tag{6.1}$$

has any solutions other than $J(\tau) \equiv 0$, for if $\mathfrak{J}^1(\tau)$ and $\mathfrak{J}^2(\tau)$ are solutions of the non-homogeneous equation (2.11), then $\mathfrak{J}^1(\tau) - \mathfrak{J}^2(\tau)$ satisfies (6.1) and

$$\mathfrak{J}^2(\tau) = \mathfrak{J}^1(\tau) + CJ(\tau), \tag{6.2}$$

where C is an arbitrary constant.

The investigation of (6.1) is rather long and it depends on some relations between the X- and Y-functions which I have proved in (**2**). I give below the main results, leaving all details to the appendix.

As in the semi-infinite case, we have to consider the *characteristic equation*

$$\frac{\varpi}{2C} \ln \frac{1 + C}{1 - C} = 1. \tag{6.3}$$

If $0 < \varpi < 1$, this has two roots $C = \pm k$ $(0 < k < 1)$. When $\varpi = 1$ it has the single root $C = 0$. The values of k corresponding to different values of ϖ are given in (**5**), Table I.

When $0 < \varpi < 1$, the functions $X(z)$ and $Y(z)$ of the complex variable z have simple poles at the points $z = \pm 1/k$. Let

$$L = \lim_{z \to 1/k} \frac{X(z)}{Y(z)}, \tag{6.4}$$

so that L is the quotient of the residues of $X(z)$ and $Y(z)$ at $z = 1/k$. Then the τ_1-transforms corresponding to the non-null solution $J(\tau)$ of (6.1) are given by

$$j_0(\mu^{-1}) = \frac{A}{1 - k\mu} \{X(\mu) - LY(\mu)\} + \frac{B}{1 + k\mu} \{LX(\mu) - Y(\mu)\}, \tag{6.5}$$

$$j_1(\mu^{-1}) = \frac{A}{1 + k\mu} \{LX(\mu) - Y(\mu)\} + \frac{B}{1 - k\mu} \{X(\mu) - LY(\mu)\}, \tag{6.6}$$

where A and B are arbitrary constants.

For all A and B other than some special values such as $A=B=0$, $J(\tau)$ has a multiple of $\exp(k\tau)$ as its term of largest magnitude for large τ. Thus (6.5) and (6.6) must be added to the emergent intensities found for any given problem unless it is physically impossible for the source function $\mathfrak{S}(\tau)$ to increase at exponential rate. The constants A and B must be determined in some other way, e.g. by the flux through the surfaces $\tau=0$ and $\tau=\tau_1$.

When $\varpi=1$, the τ_1-transforms are given by

$$j_0(\mu^{-1})=AX(\mu)-BY(\mu), \tag{6.7}$$

$$j_1(\mu^{-1})=BX(\mu)-AY(\mu), \tag{6.8}$$

where A and B are again arbitrary. Here $X(\mu)$ and $Y(\mu)$ are the standard solutions.

In this case $J(\tau)$ is only $O(\tau)$ for large τ and the addition of (6.7) and (6.8) to the emergent intensities found for a given problem is likely to be more important than in the non-conservative case.

7. *An emitting atmosphere* $(0<\varpi<1)$.—In this section we shall take $f_0(\mu)=0$, $f_1(\mu)=0$ and

$$B_1(\tau)=a_0\frac{\tau^n}{n!}+a_1\frac{\tau^{n-1}}{(n-1)!}+\ldots+a_n \tag{7.1}$$

in (2.12). Because we can deal with recurrence relations, it is as easy to work with (7.1) as with $B_1(\tau)=a_0\tau+a_1$. In the latter case, we have to deal with $B_1(\tau)=a_0$ first, and the work is nearly doubled.

Let $\mathfrak{S}(\tau)=J^n(\tau)$ when $B_1(\tau)$ has the value (7.1). Then the Milne equation (2.11) becomes

$$J^n(\tau)=\varpi\bar{\Lambda}_\tau\{J^n(t)\}+a_0\frac{\tau^n}{n!}+a_1\frac{\tau^{n-1}}{(n-1)!}+\ldots+a_n, \tag{7.2}$$

where $n=0, 1, 2, \ldots$. For convenience define $J^{-1}(\tau)$ to be identically zero.

From (7.2), by the differentiation formula (3.3),

$$\frac{d}{d\tau}J^n(\tau)=\varpi\Lambda_\tau\left\{\frac{d}{dt}J^n(t)\right\}+\tfrac{1}{2}\varpi J^n(0)E_1(\tau)-\tfrac{1}{2}\varpi J^n(\tau_1)E_1(\tau_1-\tau)$$
$$+a_0\frac{\tau^{n-1}}{(n-1)!}+\ldots+a_{n-1},$$

the polynomial being absent when $n=0$. Hence

$$\frac{d}{d\tau}J^n(\tau)-J^{n-1}(\tau)=\varpi\bar{\Lambda}_\tau\left\{\frac{d}{dt}J^n(t)-J^{n-1}(t)\right\}+\tfrac{1}{2}\varpi J^n(0)E_1(\tau)-\tfrac{1}{2}\varpi J^n(\tau_1)E_1(\tau_1-\tau).$$

Because $J^{-1}(\tau)\equiv 0$, this holds for $n=0$. If we now subtract $\frac{1}{2}\varpi J^n(0)$ times (4.3) and add $\frac{1}{2}\varpi J^n(\tau_1)$ times (4.4), we get the homogeneous Milne equation

$$\frac{d}{d\tau}J^n(\tau)-J^{n-1}(\tau)-\tfrac{1}{2}\varpi J^n(0)\int_1^\infty J(\tau,x)\frac{dx}{x}+\tfrac{1}{2}\varpi J^n(\tau_1)\int_1^\infty J(\tau_1-\tau,x)\frac{dx}{x}$$
$$=\varpi\bar{\Lambda}_\tau\left\{\frac{d}{dt}J^n(t)-J^{n-1}(t)-\tfrac{1}{2}\varpi J^n(0)\int_1^\infty J(t,x)\frac{dx}{x}+\tfrac{1}{2}\varpi J^n(\tau_1)\int_1^\infty J(\tau_1-t,x)\frac{dx}{x}\right\}, \tag{7.3}$$

and a solution of this is

$$\frac{d}{d\tau}J^n(\tau)-J^{n-1}(\tau)-\tfrac{1}{2}\varpi J^n(0)\int_1^\infty J(\tau,x)\frac{dx}{x}$$
$$+\tfrac{1}{2}\varpi J^n(\tau_1)\int_1^\infty J(\tau_1-\tau,x)\frac{dx}{x}=0. \tag{7.4}$$

This holds for $n=0, 1, 2, \ldots$

Multiply (7.4) by $\exp(-s\tau)$ and integrate with respect to τ over $(0, \tau_1)$, integrating the first term by parts. Then, with the usual notation for τ_1-transforms,

$$\exp(-s\tau_1)J^n(\tau_1) - J^n(0) + j_0^n(s) - s^{-1}j_0^{n-1}(s) - \tfrac{1}{2}\varpi J^n(0)\int_1^\infty R(s,x)\frac{dx}{x} + \tfrac{1}{2}\varpi J^n(\tau_1)\exp(-s\tau_1)\int_1^\infty R(-s,x)\frac{dx}{x} = 0. \quad (7.5)$$

In this we have used (4.7) and (4.10). By (4.12) and (4.13), we have

$$j_0^n(s) - s^{-1}j_0^{n-1}(s) = J^n(0)J(0,s) - J^n(\tau_1)J(\tau_1,s). \quad (7.6)$$

On putting $-s$ for s and using (2.17) and (4.15), we get

$$j_1^n(s) + s^{-1}j_1^{n-1}(s) = J^n(\tau_1)J(0,s) - J^n(0)J(\tau_1,s). \quad (7.7)$$

If we now write $s = 1/\mu$ and use (4.21), (7.6) and (7.7) become

$$j_0^n(\mu^{-1}) - \mu j_0^{n-1}(\mu^{-1}) = J^n(0)X(\mu) - J^n(\tau_1)Y(\mu), \quad (7.8)$$

$$j_1^n(\mu^{-1}) + \mu j_1^{n-1}(\mu^{-1}) = J^n(\tau_1)X(\mu) - J^n(0)Y(\mu). \quad (7.9)$$

Since $J^{-1}(\tau) \equiv 0$, therefore $j_0^{-1}(s) = 0$, $j_1^{-1}(s) = 0$ and these equations hold for $n = 0, 1, 2, \ldots$ Solving, we get

$$j_0^n(\mu^{-1}) = X(\mu)\sum_{r=0}^{n} J^r(0)\mu^{n-r} - Y(\mu)\sum_{r=0}^{n} J^r(\tau_1)\mu^{n-r}, \quad (7.10)$$

$$j_1^n(\mu^{-1}) = X(\mu)\sum_{r=0}^{n} J^r(\tau_1)(-\mu)^{n-r} - Y(\mu)\sum_{r=0}^{n} J^r(0)(-\mu)^{n-r}. \quad (7.11)$$

We have now to find the $2n+2$ constants $J^r(0), J^r(\tau_1) (r = 0, 1, \ldots, n)$. Put $\tau = 0$ and $\tau = \tau_1$ in (7.2). Then

$$\begin{aligned} J^n(0) &= \tfrac{1}{2}\varpi\int_0^{\tau_1} J^n(t)E_1(t)\,dt + a_n \\ &= \tfrac{1}{2}\varpi\int_0^{\tau_1} J^n(t)\,dt\int_1^\infty \exp(-xt)\frac{dx}{x} + a_n \\ &= \tfrac{1}{2}\varpi\int_1^\infty j_0^n(x)\frac{dx}{x^2} + a_n \qquad \text{(by (2.15))} \\ &= \tfrac{1}{2}\varpi\int_0^1 j_0^n(\mu^{-1})\,d\mu + a_n. \end{aligned} \quad (7.12)$$

$$\begin{aligned} J^n(\tau_1) &= \tfrac{1}{2}\varpi\int_0^{\tau_1} J^n(t)E_1(\tau_1 - t)\,dt + \sum_{r=0}^{n} a_r\frac{{\tau_1}^{n-r}}{(n-r)!} \\ &= \tfrac{1}{2}\varpi\int_0^{\tau_1} J^n(t)\,dt\int_1^\infty \exp[-(\tau_1 - t)x]\frac{dx}{x} + \sum_{r=0}^{n} a_r\frac{{\tau_1}^{n-r}}{(n-r)!} \\ &= \tfrac{1}{2}\varpi\int_1^\infty j_1^n(x)\frac{dx}{x^2} + \sum_{r=0}^{n} a_r\frac{{\tau_1}^{n-r}}{(n-r)!} \qquad \text{(by (2.16))} \\ &= \tfrac{1}{2}\varpi\int_0^1 j_1^n(\mu^{-1})\,d\mu + \sum_{r=0}^{n} a_r\frac{{\tau_1}^{n-r}}{(n-r)!}. \end{aligned} \quad (7.13)$$

Let

$$\left.\begin{aligned} x_r &= \tfrac{1}{2}\varpi\int_0^1 \mu^r X(\mu)\,d\mu = \tfrac{1}{2}\varpi\alpha_r, \\ y_r &= \tfrac{1}{2}\varpi\int_0^1 \mu^r Y(\mu)\,d\mu = \tfrac{1}{2}\varpi\beta_r. \end{aligned}\right\} \quad (7.14)$$

These definitions agree with those of (5), Chap. VIII, with $\Psi(\mu)=\frac{1}{2}\varpi$. By Theorem 2 of the same reference

$$(1-x_0)^2-y_0^2=1-\varpi. \tag{7.15}$$

(When $\varpi=1$, this leads to the relation $x_0+y_0=1$ and hence to the conditions (1.1) for the standard solutions.)

On substituting from (7.10) and (7.11) into (7.12) and (7.13), we obtain the equations

$$J^n(0)-\sum_{r=0}^{n}J^r(0)x_{n-r}+\sum_{r=0}^{n}J^r(\tau_1)y_{n-r}=a_n, \tag{7.16}$$

$$J^n(\tau_1)-\sum_{r=0}^{n}J^r(\tau_1)(-1)^{n-r}x_{n-r}+\sum_{r=0}^{n}J^r(0)(-1)^{n-r}y_{n-r}=\sum_{r=0}^{n}a_r\frac{\tau_1^{n-r}}{(n-r)!}. \tag{7.17}$$

From these equations with $n=0, 1, 2, \ldots$, $J^0(0)$, $J^0(\tau_1)$, $J^1(0)$, $J^1(\tau_1)$, ... can be evaluated in turn. Then (by (2.13) and (2.14)) the corresponding emergent intensities are given by (7.10) and (7.11).

When $n=0$, equations (7.16) and (7.17) become

$$\left.\begin{aligned}J^0(0)(1-x_0)+J^0(\tau_1)y_0&=a_0,\\ J^0(0)y_0+J^0(\tau_1)(1-x_0)&=a_0.\end{aligned}\right\} \tag{7.18}$$

Hence, by (7.15),

$$J^0(0)=J^0(\tau_1)=a_0(1-x_0-y_0)/(1-\varpi). \tag{7.19}$$

From (7.16) and (7.17), with $n=1$,

$$J^1(0)(1-x_0)+J^1(\tau_1)y_0-J^0(0)x_1+J^0(\tau_1)y_1=a_1,$$

$$J^1(0)y_0+J^1(\tau_1)(1-x_0)-J^0(0)y_1+J^0(\tau_1)x_1=a_0\tau_1+a_1.$$

From these equations, (7.19) and (7.15), we get

$$\left.\begin{aligned}(1-\varpi)J^1(0)&=a_1(1-x_0-y_0)+a_0(x_1-y_1-\tau_1y_0),\\ (1-\varpi)J^1(\tau_1)&=a_1(1-x_0-y_0)-a_0[x_1-y_1-\tau_1(1-x_0)].\end{aligned}\right\} \tag{7.20}$$

Hence (7.10) and (7.11), with $n=1$, give for the emergent intensities corresponding to linear emission

$$I(0,+\mu)=\frac{X(\mu)}{1-\varpi}\{(a_0\mu+a_1)(1-x_0-y_0)+a_0(x_1-y_1-\tau_1y_0)\}$$
$$-\frac{Y(\mu)}{1-\varpi}\{(a_0\mu+a_1)(1-x_0-y_0)-a_0[x_1-y_1-\tau_1(1-x_0)]\}, \tag{7.21}$$

$$I(\tau_1,-\mu)=\frac{X(\mu)}{1-\varpi}\{(-a_0\mu+a_1)(1-x_0-y_0)-a_0[x_1-y_1-\tau_1(1-x_0)]\}$$
$$-\frac{Y(\mu)}{1-\varpi}\{(-a_0\mu+a_1)(1-x_0-y_0)+a_0(x_1-y_1-\tau_1y_0)\}. \tag{7.22}$$

These values agree with those found by Horak and Lundquist in (8). They have used the moments α_r and β_r instead of x_r and y_r and have not made use of (7.15).

8. *An emitting atmosphere* ($\varpi=1$).—When $\varpi=1$, the coefficients of $J^n(0)$ and $J^n(\tau_1)$ in (7.16) and (7.17) are zero by (1.1). The equations are then obviously wrong. For example, the equations (7.18) can only be satisfied if $a_0=0$.

In this case we have to use the general solution of the homogeneous Milne equation (7.3), *viz.

$$\frac{d}{d\tau}J^n(\tau)-J^{n-1}(\tau)-\tfrac{1}{2}J^n(0)\int_1^\infty J(\tau,x)\frac{dx}{x}$$
$$+\tfrac{1}{2}J^n(\tau_1)\int_1^\infty J(\tau_1-\tau,x)\frac{dx}{x}=J(\tau), \tag{8.1}$$

where, from (6.7) and (6.8),

$$\left.\begin{aligned} j_0(\mu^{-1})&=A_nX(\mu)-B_nY(\mu),\\ j_1(\mu^{-1})&=B_nX(\mu)-A_nY(\mu).\end{aligned}\right\} \tag{8.2}$$

Then an additional term $s^{-1}j_0(s)$ has to be inserted on the right of (7.5), and $\mu j_0(\mu^{-1}), -\mu j_1(\mu^{-1})$ have to be added, respectively, on the right of (7.8) and (7.9). Equations (7.10) and (7.11) become, by (8.2),

$$j_0^n(\mu^{-1})=X(\mu)\sum_{r=0}^{n}J^r(0)\mu^{n-r}-Y(\mu)\sum_{r=0}^{n}J^r(\tau_1)\mu^{n-r}$$
$$+\mu X(\mu)\sum_{r=0}^{n}A_r\mu^{n-r}-\mu Y(\mu)\sum_{r=0}^{n}B_r\mu^{n-r},$$
$$j_1^n(\mu^{-1})=X(\mu)\sum_{r=0}^{n}J^r(\tau_1)(-\mu)^{n-r}-Y(\mu)\sum_{r=0}^{n}J^r(0)(-\mu)^{n-r}$$
$$-\mu X(\mu)\sum_{r=0}^{n}B_r(-\mu)^{n-r}+\mu Y(\mu)\sum_{r=0}^{n}A_r(-\mu)^{n-r}.$$

Write

$$C_0=A_0, D_0=B_0, C_r=A_r+J^{r-1}(0), D_r=B_r+J^{r-1}(\tau_1)\ (r\geqslant 1).$$

Then these equations become

$$j_0^n(\mu^{-1})=J^n(0)X(\mu)-J^n(\tau_1)Y(\mu)+X(\mu)\sum_{r=0}^{n}C_r\mu^{n-r+1}-Y(\mu)\sum_{r=0}^{n}D_r\mu^{n-r+1}, \tag{8.3}$$

$$j_1^n(\mu^{-1})=J^n(\tau_1)X(\mu)-J^n(0)Y(\mu)+X(\mu)\sum_{r=0}^{n}D_r(-\mu)^{n-r+1}-Y(\mu)\sum_{r=0}^{n}C_r(-\mu)^{n-r+1}. \tag{8.4}$$

The equations (7.12) and (7.13) (with $\varpi=1$) are unchanged. On substituting for $j_0^n(\mu^{-1})$ and $j_1^n(\mu^{-1})$ from (8.3) and (8.4) and using the conditions $x_0=1, y_0=0$, the terms containing $J^n(0)$ and $J^n(\tau_1)$ disappear and we are left with

$$\sum_{r=0}^{n}C_rx_{n-r+1}-\sum_{r=0}^{n}D_ry_{n-r+1}=-a_n, \tag{8.5}$$

$$\sum_{r=0}^{n}D_r(-1)^{n-r+1}x_{n-r+1}-\sum_{r=0}^{n}C_r(-1)^{n-r+1}y_{n-r+1}=-\sum_{r=0}^{n}a_r\frac{\tau_1^{n-r}}{(n-r)!}. \tag{8.6}$$

These hold for $n=0, 1, 2, \ldots$ and the constants $C_0, D_0, C_1, D_1, \ldots$ can be determined successively. Then the τ_1-transforms of $J^n(\tau)$ are given by (8.3) and (8.4), $J^n(0)$ and $J^n(\tau_1)$ being arbitrary.

When $n=0$, (8.5) and (8.6) become

$$C_0x_1-D_0y_1=-a_0,$$
$$C_0y_1-D_0x_1=-a_0.$$

---

* Had this been done in Section 7, after elaborate reductions, we should have obtained the same emergent intensities plus those given by (6.5) and (6.6).

Hence

$$C_0 = -D_0 = -a_0/(x_1 + y_1). \tag{8.7}$$

However, by (5), Chapter VIII, Theorem 8, with $\Psi(\mu) = \frac{1}{2}$,

$$x_1^2 - y_1^2 = \tfrac{1}{3}, \tag{8.8}$$

and so (8.7) can be written

$$C_0 = -D_0 = -3a_0(x_1 - y_1). \tag{8.9}$$

When $n = 1$, (8.5) and (8.6) become

$$\begin{aligned} C_1x_1 + C_0x_2 - D_1y_1 - D_0y_2 &= -a_1, \\ C_1y_1 - C_0y_2 - D_1x_1 + D_0x_2 &= -a_0\tau_1 - a_1, \end{aligned}$$

and on using (8.9) and (8.8) we get

$$\left.\begin{aligned} C_1 &= 3a_0(x_2 + y_2) - 3a_1(x_1 - y_1) + 3a_0\tau_1y_1, \\ D_1 &= 3a_0(x_2 + y_2) + 3a_1(x_1 - y_1) + 3a_0\tau_1x_1. \end{aligned}\right\} \tag{8.10}$$

Hence (8.3) and (8.4) give for the emergent intensities corresponding to linear emission

$$\begin{aligned} I(0, +\mu) = j_0^1(\mu^{-1}) &= J^1(0)X(\mu) - J^1(\tau_1)Y(\mu) + 3\mu X(\mu)\{a_0(x_2 + y_2 + \tau_1y_1) \\ &\quad - (a_1 + a_0\mu)(x_1 - y_1)\} - 3\mu Y(\mu)\{a_0(x_2 + y_2 + \tau_1x_1) + (a_1 + a_0\mu)(x_1 - y_1)\}, \end{aligned} \tag{8.11}$$

$$\begin{aligned} I(\tau_1, -\mu) = j_1^1(\mu^{-1}) &= J^1(\tau_1)X(\mu) - J^1(0)Y(\mu) - 3\mu X(\mu)\{a_0(x_2 + y_2 + \tau_1x_1) \\ &\quad + (a_1 - a_0\mu)(x_1 - y_1)\} + 3\mu Y(\mu)\{a_0(x_2 + y_2 + \tau_1y_1) - (a_1 - a_0\mu)(x_1 - y_1)\}. \end{aligned} \tag{8.12}$$

The constants $J^1(0)$ and $J^1(\tau_1)$ are arbitrary as long as the Milne equation (7.2) alone is considered. They can be evaluated by the method used by Horak and Lundquist in (8), of which the following is a modification.

Let

$$F(\tau) = 2\int_{-1}^{1} \mu I(\tau, \mu)\, d\mu, \quad K(\tau) = \tfrac{1}{2}\int_{-1}^{1} \mu^2 I(\tau, \mu)\, d\mu. \tag{8.13}$$

Then it follows from the equation of transfer (2.1), in the usual way, that

$$\frac{d}{d\tau}F(\tau) = -4B_1(\tau), \quad \frac{d}{d\tau}K(\tau) = \tfrac{1}{4}F(\tau). \tag{8.14}$$

From these we easily obtain the relations

$$F(\tau_1) - F(0) = -4\int_0^{\tau_1} B_1(t)\, dt, \tag{8.15}$$

$$\begin{aligned} 2[K(\tau_1) - K(0)] &- \tfrac{1}{4}\tau_1[F(\tau_1) + F(0)] \\ &= \int_0^{\tau_1} \left\{ \int_\tau^{\tau_1} B_1(t)\, dt - \int_0^{\tau} B_1(t)\, dt \right\} d\tau. \end{aligned} \tag{8.16}$$

With the initial conditions given by (2.2), these can be written

$$\begin{aligned} \tfrac{1}{2}\int_0^1 \mu\{I(0, +\mu) + I(\tau_1, -\mu)\}\, d\mu &\\ = \tfrac{1}{2}\int_0^1 \mu\{f_0(\mu) + f_1(\mu)\}\, d\mu &+ \int_0^{\tau_1} B_1(t)\, dt, \end{aligned} \tag{8.17}$$

$$\begin{aligned} \tfrac{1}{2}\int_0^1 (\mu^2 + \tfrac{1}{2}\tau_1\mu)\{I(\tau_1, -\mu) - I(0, +\mu)\}\, d\mu &= \tfrac{1}{2}\int_0^1 (\tfrac{1}{2}\tau_1\mu - \mu^2)\{f_1(\mu) - f_0(\mu)\}\, d\mu \\ + \tfrac{1}{2}\int_0^{\tau_1} \left\{ \int_\tau^{\tau_1} B_1(t)\, dt - \int_0^{\tau} B_1(t)\, dt \right\} d\tau. & \end{aligned} \tag{8.18}$$

On putting $B_1(\tau)=a_0\tau+a_1, f_0(\mu)=f_1(\mu)=0$, and substituting for $I(0,+\mu)$ and $I(\tau_1,-\mu)$ from (8.11) and (8.12), we obtain two equations giving, respectively, $J^1(0)+J^1(\tau_1)$ and $J^1(0)-J^1(\tau_1)$ from which we obtain the following values:

$$J^1(0)=a_0\{3(x_1-y_1)[x_4+y_4+\tfrac{1}{2}\tau_1(x_3+y_3)]-\tfrac{1}{24}\tau_1^3\}/\Delta + 3a_0[\tau_1y_2+\tfrac{1}{4}\tau_1^2(x_1+y_1)-x_3+y_3]+3a_1\Delta, \tag{8.19}$$

$$J^1(\tau_1)=-a_0\{3(x_1-y_1)[x_4+y_4+\tfrac{1}{2}\tau_1(x_3+y_3)]-\tfrac{1}{24}\tau_1^3\}/\Delta + 3a_0[\tau_1x_2+\tfrac{1}{4}\tau_1^2(x_1+y_1)+x_3-y_3]+3a_1\Delta, \tag{8.20}$$

where
$$\Delta=x_2+y_2+\tfrac{1}{2}\tau_1(x_1+y_1). \tag{8.21}$$

The equations (8.11), (8.12) and (8.19)–(8.21) give the final solution for linear emission.

9. *Isotropic illumination of the surface* $\tau=0 (0<\varpi<1)$.—Suppose that the surface $\tau=0$ is illuminated by isotropic radiation of unit intensity. Then $f_0(\mu)=1$, $f_1(\mu)=0$ and, if the atmosphere is not emitting, $B_1(\tau)=0$. Hence (2.12) gives

$$\begin{aligned}B(\tau)&=\tfrac{1}{2}\varpi\int_0^1\exp(-\tau/\mu')\,d\mu'\\&=\tfrac{1}{2}\varpi\int_1^\infty\exp(-\tau x)\frac{dx}{x^3}\\&=\tfrac{1}{2}\varpi E_2(\tau).\end{aligned}$$

Let $\mathfrak{B}(\tau)=\Phi^2(\tau)$ when $B(\tau)$ has this value. Then the Milne equation (2.11) is

$$\Phi^2(\tau)=\varpi\overline{\Lambda}_\tau\{\Phi^2(t)\}+\tfrac{1}{2}\varpi E_2(\tau). \tag{9.1}$$

We could solve the general equation

$$\Phi^n(\tau)=\varpi\overline{\Lambda}_\tau\{\Phi^n(t)\}+\tfrac{1}{2}\varpi E_n(\tau), \tag{9.2}$$

as has been done in (3) for the semi-infinite case, but little use is likely to be made of the solution for $n>2$. When $n=1$, the solution is easily obtained from the equation (4.3), but as $E_1(\tau)\to\infty$ as $\tau\to0$, this solution has no practical value.

Since $(d/d\tau)E_2(\tau)=-E_1(\tau)$, (9.1) gives, on differentiating with respect to τ,

$$\frac{d}{d\tau}\Phi^2(\tau)=\varpi\overline{\Lambda}_\tau\left\{\frac{d}{dt}\Phi^2(t)\right\}+\tfrac{1}{2}\varpi\Phi^2(0)E_1(\tau)-\tfrac{1}{2}\varpi\Phi^2(\tau_1)E_1(\tau_1-\tau)-\tfrac{1}{2}\varpi E_1(\tau).$$

Hence by (4.3) and (4.4)

$$\frac{d}{d\tau}\Phi^2(\tau)-\tfrac{1}{2}\varpi[\Phi^2(0)-1]\int_1^\infty J(\tau,x)\frac{dx}{x}+\tfrac{1}{2}\varpi\Phi^2(\tau_1)\int_1^\infty J(\tau_1-\tau,x)\frac{dx}{x}$$
$$=\varpi\overline{\Lambda}_\tau\left\{\frac{d}{dt}\Phi^2(t)-\tfrac{1}{2}\varpi[\Phi^2(0)-1]\int_1^\infty J(t,x)\frac{dx}{x}+\tfrac{1}{2}\varpi\Phi^2(\tau_1)\int_1^\infty J(\tau_1-t,x)\frac{dx}{x}\right\}, \tag{9.3}$$

and a solution of this is

$$\frac{d}{d\tau}\Phi^2(\tau)-\tfrac{1}{2}\varpi[\Phi^2(0)-1]\int_1^\infty J(\tau,x)\frac{dx}{x}+\tfrac{1}{2}\varpi\Phi^2(\tau_1)\int_1^\infty J(\tau_1-\tau,x)\frac{dx}{x}=0. \tag{9.4}$$

Multiply (9.4) by $\exp(-s\tau)$ and integrate with respect to τ over $(0,\tau_1)$, integrating the first term by parts. On introducing the τ_1-transforms of $\Phi^2(\tau)$, we have

$$\Phi^2(\tau_1)\exp(-s\tau_1)-\Phi^2(0)+\phi_0^2(s)-\tfrac{1}{2}\varpi[\Phi^2(0)-1]\int_1^\infty R(s,x)\frac{dx}{x}$$
$$+\tfrac{1}{2}\varpi\Phi^2(\tau_1)\exp(-s\tau_1)\int_1^\infty R(-s,x)\frac{dx}{x}=0, \tag{9.5}$$

and by (4.12) and (4.13) this can be written

$$\phi_0^2(s) = \Phi^2(0)J(0,s) - \Phi^2(\tau_1)J(\tau_1,s) - [J(0,s) - 1]. \tag{9.6}$$

On writing $-s$ for s and using (2.17) and (4.15), we get

$$\phi_1^2(s) = \Phi^2(\tau_1)J(0,s) - \Phi^2(0)J(\tau_1,s) + J(\tau_1,s) - \exp(-\tau_1 s), \tag{9.7}$$

and hence, by (4.21),

$$\phi_0^2(\mu^{-1}) = \Phi^2(0)X(\mu) - \Phi^2(\tau_1)Y(\mu) + 1 - X(\mu), \tag{9.8}$$

$$\phi_1^2(\mu^{-1}) = \Phi^2(\tau_1)X(\mu) - \Phi^2(0)Y(\mu) + Y(\mu) - \exp(-\tau_1/\mu). \tag{9.9}$$

Put $\tau = 0$ and $\tau = \tau_1$ in (9.1). Since $E_2(0) = 1$, we have (proceeding as in (7.12) and (7.13))

$$\Phi^2(0) = \tfrac{1}{2}\varpi \int_0^1 \phi_0^2(\mu^{-1})\, d\mu + \tfrac{1}{2}\varpi, \tag{9.10}$$

$$\Phi^2(\tau_1) = \tfrac{1}{2}\varpi \int_0^1 \phi_1^2(\mu^{-1})\, d\mu + \tfrac{1}{2}\varpi E_2(\tau_1). \tag{9.11}$$

On substituting for $\phi_0^2(\mu^{-1})$ and $\phi_1^2(\mu^{-1})$ from (9.8) and (9.9), we get

$$\Phi^2(0)(1 - x_0) + \Phi^2(\tau_1)y_0 = \varpi - x_0, \tag{9.12}$$

$$\begin{aligned}\Phi^2(0)y_0 + \Phi^2(\tau_1)(1 - x_0) &= y_0 - \tfrac{1}{2}\varpi E_2(\tau_1) + \tfrac{1}{2}\varpi E_2(\tau_1) \\ &= y_0.\end{aligned} \tag{9.13}$$

Hence, by (7.15),

$$\Phi^2(0) = x_0, \quad \Phi^2(\tau_1) = y_0, \tag{9.14}$$

and (9.8) and (9.9) become

$$\phi_0^2(\mu^{-1}) = 1 - (1 - x_0)X(\mu) - y_0 Y(\mu), \tag{9.15}$$

$$\phi_1^2(\mu^{-1}) = y_0 X(\mu) + (1 - x_0)Y(\mu) - \exp(-\tau_1/\mu). \tag{9.16}$$

From (2.13) and (2.14), the emergent intensities are

$$I(0, +\mu) = \phi_0^2(\mu^{-1}) = 1 - (1 - x_0)X(\mu) - y_0 Y(\mu), \tag{9.17}$$

$$I(\tau_1, -\mu) = \phi_1^2(\mu^{-1}) + \exp(-\tau_1/\mu) = y_0 X(\mu) + (1 - x_0)Y(\mu). \tag{9.18}$$

If we have an atmosphere emitting according to the law $\frac{1}{2}\varpi E_2(\tau)$ and with no incident radiation, the Milne equation is again (9.1), but the emergent intensities are simply $\phi_0^2(\mu^{-1})$ and $\phi_1^2(\mu^{-1})$. These are given by (9.15) and (9.16).

10. *Isotropic illumination of the surface* $\tau = 0$ ($\varpi = 1$).—When $\varpi = 1$, equation (9.4) has to be replaced by

$$\frac{d}{d\tau}\Phi^2(\tau) - \tfrac{1}{2}[\Phi^2(0) - 1]\int_1^\infty J(\tau, x)\frac{dx}{x} + \tfrac{1}{2}\Phi^2(\tau_1)\int_1^\infty J(\tau_1 - \tau, x)\frac{dx}{x} = J(\tau), \tag{10.1}$$

where the τ_1-transforms of $J(\tau)$ are given by (6.7) and (6.8). Then $s^{-1}j_0(s)$ has to be inserted on the right of (9.5), and (9.8) and (9.9) have to be replaced by

$$\phi_0^2(\mu^{-1}) = \Phi^2(0)X(\mu) - \Phi^2(\tau_1)Y(\mu) + 1 - X(\mu) + \mu[AX(\mu) - BY(\mu)], \tag{10.2}$$

$$\phi_1^2(\mu^{-1}) = \Phi^2(\tau_1)X(\mu) - \Phi^2(0)Y(\mu) + Y(\mu) - \exp(-\tau_1/\mu) - \mu[BX(\mu) - AY(\mu)]. \tag{10.3}$$

Equations (9.10) and (9.11) (with $\varpi = 1$) are unchanged. On substituting from (10.2) and (10.3) and using the conditions $x_0 = 1$, $y_0 = 0$, we get

$$Ax_1 - By_1 = 0, \quad Ay_1 - Bx_1 = 0$$

and hence $A=B=0$. The emergent intensities are therefore

$$I(0,+\mu)=\phi_0(\mu^{-1})=CX(\mu)-DY(\mu)+1, \tag{10.4}$$

$$I(\tau_1,-\mu)=\phi_1(\mu^{-1})+\exp(-\tau_1/\mu)=DX(\mu)-CY(\mu), \tag{10.5}$$

where $C=\Phi^2(0)-1$, $D=\Phi^2(\tau_1)$.

The constants C and D can be evaluated by (8.17) and (8.18). In this case $B_1(\tau)=0$, $f_0(\mu)=1$, $f_1(\mu)=0$ and it is easily found that

$$C=-D=-\tfrac{1}{2}[x_2+y_2+\tfrac{1}{2}\tau_1(x_1+y_1)]^{-1}. \tag{10.6}$$

Equations (10.4)–(10.6) give the solution of the problem.

For an atmosphere emitting according to the law $\frac{1}{2}E_2(\tau)$ and with no incident radiation, the emergent intensities are $\phi_0^2(\mu^{-1})$ and $\phi_1^2(\mu^{-1})$. These are given by (10.4) and (10.5) but with different constants C and D, which have to be evaluated similarly from (8.17) and (8.18).

APPENDIX

11. *The homogeneous Milne equation.*—For the homogeneous equation

$$J(\tau)=\varpi\overline{\Lambda}_\tau\{J(t)\} \quad (0<\varpi\leqslant 1), \tag{11.1}$$

we proceed as in the preceding sections. Differentiating with respect to τ, we have

$$\frac{d}{d\tau}J(\tau)=\varpi\overline{\Lambda}_\tau\left\{\frac{d}{dt}J(t)\right\}+\tfrac{1}{2}\varpi J(0)E_1(\tau)-\tfrac{1}{2}\varpi J(\tau_1)E_1(\tau_1-\tau).$$

On subtracting $\frac{1}{2}\varpi J(0)$ times (4.3) and adding $\frac{1}{2}\varpi J(\tau_1)$ times (4.4), we get another homogeneous Milne equation, from which it follows that

$$\frac{d}{d\tau}J(\tau)-\tfrac{1}{2}\varpi J(0)\int_1^\infty J(\tau,x)\frac{dx}{x}+\tfrac{1}{2}\varpi J(\tau_1)\int_1^\infty J(\tau_1-\tau,x)\frac{dx}{x}=CJ(\tau), \tag{11.2}$$

where C is an arbitrary constant.

Multiply (11.2) by $\exp(-s\tau)$ and integrate with respect to τ over $(0,\tau_1)$, integrating the first term by parts. Then by (4.7) and (4.10)

$$J(\tau_1)\exp(-s\tau_1)-J(0)+j_0(s)-\tfrac{1}{2}\varpi J(0)\int_1^\infty R(s,x)\frac{dx}{x}$$

$$+\tfrac{1}{2}\varpi J(\tau_1)\exp(-s\tau_1)\int_1^\infty R(-s,x)\frac{dx}{x}=Cs^{-1}j_0(s).$$

By (4.12) and (4.13) this can be written

$$j_0(s)(1-Cs^{-1})=J(0)J(0,s)-J(\tau_1)J(\tau_1,s). \tag{11.3}$$

Writing $-s$ for s and using (2.17) and (4.15), we have

$$j_1(s)(1+Cs^{-1})=J(\tau_1)J(0,s)-J(0)J(\tau_1,s). \tag{11.4}$$

Finally, on putting $s=1/\mu$ and using (4.21), (11.3) and (11.4) become

$$j_0(\mu^{-1})(1-C\mu)=J(0)X(\mu)-J(\tau_1)Y(\mu), \tag{11.5}$$

$$j_1(\mu^{-1})(1+C\mu)=J(\tau_1)X(\mu)-J(0)Y(\mu). \tag{11.6}$$

If we now put $\tau = 0$ and $\tau = \tau_1$ in (11.1) and proceed as in (7.12) and (7.13), we get

$$J(0) = \tfrac{1}{2}\varpi \int_0^1 j_0(\mu^{-1})\, d\mu, \tag{11.7}$$

$$J(\tau_1) = \tfrac{1}{2}\varpi \int_0^1 j_1(\mu^{-1})\, d\mu. \tag{11.8}$$

Hence on substituting for $j_0(\mu^{-1})$ and $j_1(\mu^{-1})$ from (11.5) and (11.6), we obtain the equations

$$J(0)\left\{1 - \tfrac{1}{2}\varpi \int_0^1 \frac{X(\mu)}{1 - C\mu}\, d\mu\right\} + J(\tau_1)\tfrac{1}{2}\varpi \int_0^1 \frac{Y(\mu)}{1 - C\mu}\, d\mu = 0, \tag{11.9}$$

$$J(0)\tfrac{1}{2}\varpi \int_0^1 \frac{Y(\mu)}{1 + C\mu}\, d\mu + J(\tau_1)\left\{1 - \tfrac{1}{2}\varpi \int_0^1 \frac{X(\mu)}{1 + C\mu}\, d\mu\right\} = 0. \tag{11.10}$$

Unless C is a root of the equation,

$$F(1/C) = 0, \tag{11.11}$$

where

$$F(z) \equiv \left\{1 - \tfrac{1}{2}\varpi \int_0^1 \frac{zX(\mu)}{z - \mu}\, d\mu\right\}\left\{1 - \tfrac{1}{2}\varpi \int_0^1 \frac{zX(\mu')}{z + \mu'}\, d\mu'\right\} - \tfrac{1}{4}\varpi^2 \int_0^1 \frac{zY(\mu)}{z - \mu}\, d\mu \int_0^1 \frac{zY(\mu')}{z + \mu'}\, d\mu', \tag{11.12}$$

the only solution of (11.9) and (11.10) is $J(0) = J(\tau_1) = 0$. This gives $j_0(s) \equiv 0$ and hence $J(\tau) \equiv 0$.

We shall now show that $F(z) \equiv \mathfrak{C}(z)$, where

$$\mathfrak{C}(z) = 1 - \tfrac{1}{2}\varpi z \ln \frac{z + 1}{z - 1}, \tag{11.13}$$

so that (11.11) is equation (6.3). If $0 < \varpi < 1$, then $C = \pm k$, and if $\varpi = 1$, then $C = 0$.

In (**2**) I have obtained the following relations between the X- and Y- functions (see (**2**), equations (2.4), (2.6) and (2.7) with $\Psi(z) = \frac{1}{2}\varpi$):

$$\mathfrak{C}(z) = \frac{1}{X(z)}\left\{1 - \tfrac{1}{2}\varpi \int_0^1 \frac{zX(\mu)}{z - \mu}\, d\mu\right\} - \frac{\exp(-\tau_1/z)}{X(z)Y(z)} + \frac{\exp(-\tau_1/z)}{Y(z)}\left\{1 - \tfrac{1}{2}\varpi \int_0^1 \frac{zX(\mu')}{z + \mu'}\, d\mu'\right\}, \tag{11.14}$$

$$X(z)\mathfrak{C}(z) = 1 - \tfrac{1}{2}\varpi \int_0^1 \frac{zX(\mu)}{z - \mu}\, d\mu - \tfrac{1}{2}\varpi \exp(-\tau_1/z) \int_0^1 \frac{zY(\mu')}{z + \mu'}\, d\mu', \tag{11.15}$$

$$Y(z)\mathfrak{C}(z) = \exp(-\tau_1/z)\left\{1 - \tfrac{1}{2}\varpi \int_0^1 \frac{zX(\mu')}{z + \mu'}\, d\mu'\right\} - \tfrac{1}{2}\varpi \int_0^1 \frac{zY(\mu)}{z - \mu}\, d\mu. \tag{11.16}$$

From (11.15) and (11.16),

$$\tfrac{1}{4}\varpi^2 \int_0^1 \frac{zY(\mu)}{z - \mu}\, d\mu \int_0^1 \frac{zY(\mu')}{z + \mu'}\, d\mu' = \left\{X(z)\mathfrak{C}(z) - 1 + \tfrac{1}{2}\varpi \int_0^1 \frac{zX(\mu)}{z - \mu}\, d\mu\right\} \times \left\{Y(z)\mathfrak{C}(z)\exp(\tau_1/z) - 1 + \tfrac{1}{2}\varpi \int_0^1 \frac{zX(\mu')}{z + \mu'}\, d\mu'\right\}.$$

Hence, by (11.12),

$$F(z) = X(z)\mathfrak{C}(z)\left\{1 - \tfrac{1}{2}\varpi \int_0^1 \frac{zX(\mu')}{z + \mu'}\, d\mu'\right\} - X(z)Y(z)[\mathfrak{C}(z)]^2 \exp(\tau_1/z) + Y(z)\mathfrak{C}(z)\exp(\tau_1/z)\left\{1 - \tfrac{1}{2}\varpi \int_0^1 \frac{zX(\mu)}{z - \mu}\, d\mu\right\}. \tag{11.17}$$

On multiplying (11.14) by $X(z)Y(z)\mathfrak{C}(z)\exp(\tau_1/z)$, it is seen that the right-hand side of (11.17) reduces to $\mathfrak{C}(z)$.

First consider the case $0<\varpi<1$. Then $\mathfrak{C}(z)$ has simple zeros at $z=\pm 1/k$ and (see (2)) both $X(z)$ and $Y(z)$ have simple poles at $z=\pm 1/k$. Let r_x, r_y be the residues at $z=1/k$ and let

$$L=\frac{r_x}{r_y}=\lim_{z\to 1/k}\frac{X(z)}{Y(z)}. \tag{11.18}$$

The equations (4.22) and (4.23) hold when μ is replaced by the complex variable z. Writing them in the form

$$\frac{X(z)}{Y(z)}\left\{1-\tfrac{1}{2}\varpi\int_0^1\frac{zX(\mu')}{z+\mu'}\,d\mu'\right\}+\tfrac{1}{2}\varpi\int_0^1\frac{zY(\mu')}{z+\mu'}\,d\mu'=\frac{1}{Y(z)},$$

$$\frac{X(z)}{Y(z)}\tfrac{1}{2}\varpi\int_0^1\frac{zY(\mu)}{z-\mu}\,d\mu+\left\{1-\tfrac{1}{2}\varpi\int_0^1\frac{zX(\mu)}{z-\mu}\,d\mu\right\}=\frac{\exp(-\tau_1/z)}{Y(z)},$$

and letting $z\to 1/k$, we have

$$L\left\{1-\tfrac{1}{2}\varpi\int_0^1\frac{X(\mu')}{1+k\mu'}\,d\mu'\right\}+\tfrac{1}{2}\varpi\int_0^1\frac{Y(\mu')}{1+k\mu'}\,d\mu'=0, \tag{11.19}$$

$$L\tfrac{1}{2}\varpi\int_0^1\frac{Y(\mu)}{1-k\mu}\,d\mu+\left\{1-\tfrac{1}{2}\varpi\int_0^1\frac{X(\mu)}{1-k\mu}\,d\mu\right\}=0. \tag{11.20}$$

On comparing these with (11.9) and (11.10), we see that $J(\tau_1)/J(0)=L$ if $C=k$, and $J(0)/J(\tau_1)=L$ if $C=-k$. If $C=k$, (11.5) and (11.6) give

$$\left.\begin{aligned} j_0(\mu^{-1})&=\frac{A}{1-k\mu}\{X(\mu)-LY(\mu)\},\\ j_1(\mu^{-1})&=\frac{A}{1+k\mu}\{LX(\mu)-Y(\mu)\},\end{aligned}\right\} \tag{11.21}$$

where $A=J(0)$ and A is arbitrary. If $C=-k$, then

$$\left.\begin{aligned} j_0(\mu^{-1})&=\frac{B}{1+k\mu}\{LX(\mu)-Y(\mu)\},\\ j_1(\mu^{-1})&=\frac{B}{1-k\mu}\{X(\mu)-LY(\mu)\},\end{aligned}\right\} \tag{11.22}$$

where $B=J(\tau_1)$ and B is arbitrary. But the sum of two solutions of (11.1) is also a solution and therefore the general non-null solution of (11.1) has the τ_1-transforms

$$j_0(\mu^{-1})=\frac{A}{1-k\mu}\{X(\mu)-LY(\mu)\}+\frac{B}{1+k\mu}\{LX(\mu)-Y(\mu)\}, \tag{11.23}$$

$$j_1(\mu^{-1})=\frac{A}{1+k\mu}\{LX(\mu)-Y(\mu)\}+\frac{B}{1-k\mu}\{X(\mu)-LY(\mu)\}. \tag{11.24}$$

These are (6.5) and (6.6).

Next consider the function $J(\tau)$ corresponding to (11.23) and (11.24). Since $j_0(s)$ is the ordinary Laplace transform of the function equal to $J(\tau)$ in $(0,\tau_1)$ and to zero in (τ_1,∞), therefore

$$J(\tau)=\frac{1}{2\pi i}\int_{\gamma-i\infty}^{\gamma+i\infty}\frac{j_0(s)}{s}\exp(\tau s)\,ds\quad(0\leqslant\tau<\tau_1), \tag{11.25}$$

where the line $R(s)=\gamma$ lies to the right of all the poles of $j_0(s)/s$.

Near $z = 1/k$,

$$X(z) = \frac{r_x}{z - 1/k} + x(z), \quad Y(z) = \frac{r_y}{z - 1/k} + y(z), \tag{11.26}$$

where $x(z)$ and $y(z)$ are regular at $z = 1/k$. Hence, by (11.18),

$$X(s^{-1}) - LY(s^{-1}) = x(s^{-1}) - Ly(s^{-1}),$$

$$LX(s^{-1}) - Y(s^{-1}) = \frac{r_x^2 - r_y^2}{r_y} \frac{ks}{k - s} + Lx(s^{-1}) - y(s^{-1}).$$

Thus $X(s^{-1}) - LY(s^{-1})$ is regular at $s = k$, while $LX(s^{-1}) - Y(s^{-1})$ has a simple pole there. It now follows from (11.23) with μ replaced by $1/s$ that $j_0(s)/s$ has a simple pole at $s = k$ except when A and B are such that the coefficient of $(s - k)^{-1}$ is zero. On evaluating $J(\tau)$ from (11.25) by contour integration, we get a multiple of $\exp(k\tau)$ arising from the residue at $s = k$ and this is the term of greatest magnitude for large τ.

When $\varpi = 1$, the working is simpler. Since $C = 0$, equations (11.9) and (11.10) become

$$\left.\begin{aligned} J(0)(1 - x_0) + J(\tau_1) y_0 &= 0, \\ J(0) y_0 + J(\tau_1)(1 - x_0) &= 0. \end{aligned}\right\} \tag{11.27}$$

Let $X(\mu)$, $Y(\mu)$ denote any solutions of the X- and Y-equations and let $X_s(\mu)$, $Y_s(\mu)$ denote the standard solutions. For $X(\mu)$ and $Y(\mu)$ we have the relation $x_0 + y_0 = 1$ and the equations (11.27) give

$$J(\tau_1) = -J(0), \tag{11.28}$$

and so (11.5) and (11.6) give

$$\left.\begin{aligned} j_0(\mu^{-1}) &= A\{X(\mu) + Y(\mu)\}, \\ j_1(\mu^{-1}) &= -A\{X(\mu) + Y(\mu)\}, \end{aligned}\right\} \tag{11.29}$$

where $A = J(0)$ and A is arbitrary. For $X_s(\mu)$ and $Y_s(\mu)$ we have $x_0 = 1$, $y_0 = 0$ and the constants $J(0)$ and $J(\tau_1)$ become indeterminate by (11.27). Then

$$\left.\begin{aligned} j_0(\mu^{-1}) &= AX_s(\mu) - BY_s(\mu), \\ j_1(\mu^{-1}) &= BX_s(\mu) - AY_s(\mu), \end{aligned}\right\} \tag{11.30}$$

where $A = J(0)$, $B = J(\tau_1)$ and these are arbitrary. Since $X(\mu) + Y(\mu) = X_s(\mu) + Y_s(\mu)$ (see Section 1), the solution (11.29) is only a special case of (11.30). In the body of the paper we have dropped the suffix s and (11.30) agrees with (6.7) and (6.8).

In (**2**) I have shown that $X_s(z)$ and $Y_s(z)$ are $O(z)$ for large z. Hence $j_0(s)$ is $O(s^{-1})$ for small s and $j_0(s)/s$ has a double pole at $s = 0$. The contribution to $J(\tau)$ arising from the residue at this pole, when evaluating (11.25) by contour integration, is of the form $\alpha\tau + \beta$ and so $J(\tau)$ is $O(\tau)$ for large τ.

We now turn to the question of the choice of $J(\tau, \sigma)$ in Section 4, when $\varpi = 1$, and the corresponding ambiguity in $X(\mu)$ and $Y(\mu)$.

The equation (4.1) has the solution

$$J(\tau, \sigma) + CJ(\tau), \tag{11.31}$$

where C may depend upon σ. Is it possible to choose C so that the subsequent analysis will hold with $J(\tau, \sigma)$ replaced by (11.31)? By (4.7), $R(s, \sigma)$ will be replaced by

$$R_1(s, \sigma) = R(s, \sigma) + Cs^{-1} j_0(s),$$

and in order that we may have

$$R_1(s,\sigma) = R_1(\sigma,s),$$

we must have $C = A'\sigma^{-1}j_0(\sigma)$, where A' is independent of σ and s. Hence

$$R_1(s,\sigma) = R(s,\sigma) + A's^{-1}\sigma^{-1}j_0(s)j_0(\sigma). \tag{11.32}$$

If $j_0(\mu^{-1})$ is given by (11.29), then

$$j_0(s)j_1(\sigma) = j_0(\sigma)j_1(s)$$

and it is easily verified, with the aid of (2.17), that the condition

$$\exp(-s\tau_1)R_1(-s,\sigma) = \exp(-\sigma\tau_1)R_1(-\sigma,s)$$

is also satisfied by (11.32). Hence $J(\tau,\sigma)$ may be replaced by

$$J(\tau,\sigma) + A'\sigma^{-1}j_0(\sigma)J(\tau), \tag{11.33}$$

where $j_0(\sigma)$ is given by (11.29) and $J(\tau)$ is the corresponding source function.

It now follows from (4.21) that $X(\mu)$ and $Y(\mu)$ may be replaced, respectively, by

$$X(\mu) + A'\mu j_0(\mu^{-1})J(0) \text{ and } Y(\mu) + A'\mu j_0(\mu^{-1})J(\tau_1).$$

Hence, by (11.28) and (11.29), $X(\mu)$ and $Y(\mu)$ may be replaced by

$$X(\mu) + Q\mu[X(\mu) + Y(\mu)], \quad Y(\mu) - Q\mu[X(\mu) + Y(\mu)],$$

where $Q = AA'J(0)$. By choice of Q, these functions are $X_s(\mu)$ and $Y_s(\mu)$, and then (11.33), with $A' = Q/J(0)A$, becomes the correct $J(\tau,\sigma)$ for the analysis of Section 4.

St Hugh's College,
Oxford:
1955 *July* 26.

References

(1) V. A. Ambartsumian, *Ast. J. of the Soviet Union*, **19**, 30, 1942.
(2) I. W. Busbridge, *Ap. J.*, **122**, 327, 1955.
(3) I. W. Busbridge, *Quart. J.* (Oxford) (2), **6**, 218, 1955.
(4) I. W. Busbridge, *M.N.*, **115**, 661, 1955.
(5) S. Chandrasekhar, *Radiative Transfer*, Oxford, 1950.
(6) S. Chandrasekhar, D. Elbert and A. Franklin, *Ap. J.*, **115**, 244, 1952.
(7) E. Hopf, *Mathematical Problems of Radiative Equilibrium*, Cambridge Tracts, No. 31, 1934.
(8) H. G. Horak and C. A. Lundquist, *Ap. J.*, **116**, 477, 1952, and **119**, 42, 1954.
(9) V. Kourganoff, *Basic Methods in Transfer Problems*, Oxford, 1952.

THE OXFORD 35 m SOLAR TELESCOPE

H. H. Plaskett

(Received 1955 October 7)

Summary

A new telescope for solar work with an equivalent focal length of 35·2 m is described. It is an ordinary Cassegrain reflector used at the coudé focus. The optical requirements for satisfactory performance are listed and some of the mechanical features briefly described. The performance is assessed from a Hartmann test.

Introduction.—For some time there has been a need at Oxford for a solar telescope giving a larger scale than the existing instrument (**4**). As a result of savings made during the war and a generous benefaction from Professor D. A. Jackson, enough money was available to build a high-dispersion spectroscope, and in 1948 the University Grants Committee made available a sum of £16,300 for a telescope and a building to house it and the spectroscope. Specifications were drawn up for an enlarged version of the 19·8 m telescope with 81 cm diameter flats for the coelostat and secondary mirror. Fused silica blanks of this size were not, however, available in this country at that time, and a provisional estimate indicated that two blanks of this size in low-expansion glass would cost £2000—too high a proportion of the money available. Accordingly it was decided to depart from conventional solar-telescope design, and to build an *f*/70 Cassegrain reflector with a principal mirror 51 cm in diameter.

Optical requirements.—For a variety of reasons it is essential in a reflector designed for solar work to have large-aperture Cassegrain and coudé mirrors. These act as central stops in the optical system and affect the diffraction pattern. Theodore Dunham* has recently calculated the distribution of light in the diffraction disk for various relative diameters of the central stop. With his permission I quote in Table I under each central stop first the value of z_1/π,

TABLE I

Diffraction patterns

	Relative diameter of central stop							
	0·0		0·5		0·6		0·7	
	z_1/π	%	z_1/π	%	z_1/π	%	z_1/π	%
Dark ring 1	**1·22**	**83·8**	1·00	47·8	0·95	37·1	0·89	26·8
Dark ring 2	2·23	91·0	**2·29**	**83·0**	2·16	71·7	2·05	56·0
Dark ring 3	3·24	93·8	3·50	90·2	**3·39**	**87·3**	3·21	76·2
Dark ring 4	4·24	95·3	4·13	90·4	4·52	90·2	**4·38**	**86·5**

where $z_1\lambda/\pi D$ is the angular radius of the dark ring, and secondly the percentage of the total light of the image which is concentrated inside the dark ring. For no central stop Rayleigh arbitrarily defines the observable image as that part of the Airy disk which lies within the first dark ring and contains 83·8 per cent of the light. If the relative diameter of the central stop is 0·6 we get a little more

* An abstract appears in *J.O.S.A.*, **41**, 290, 1951.

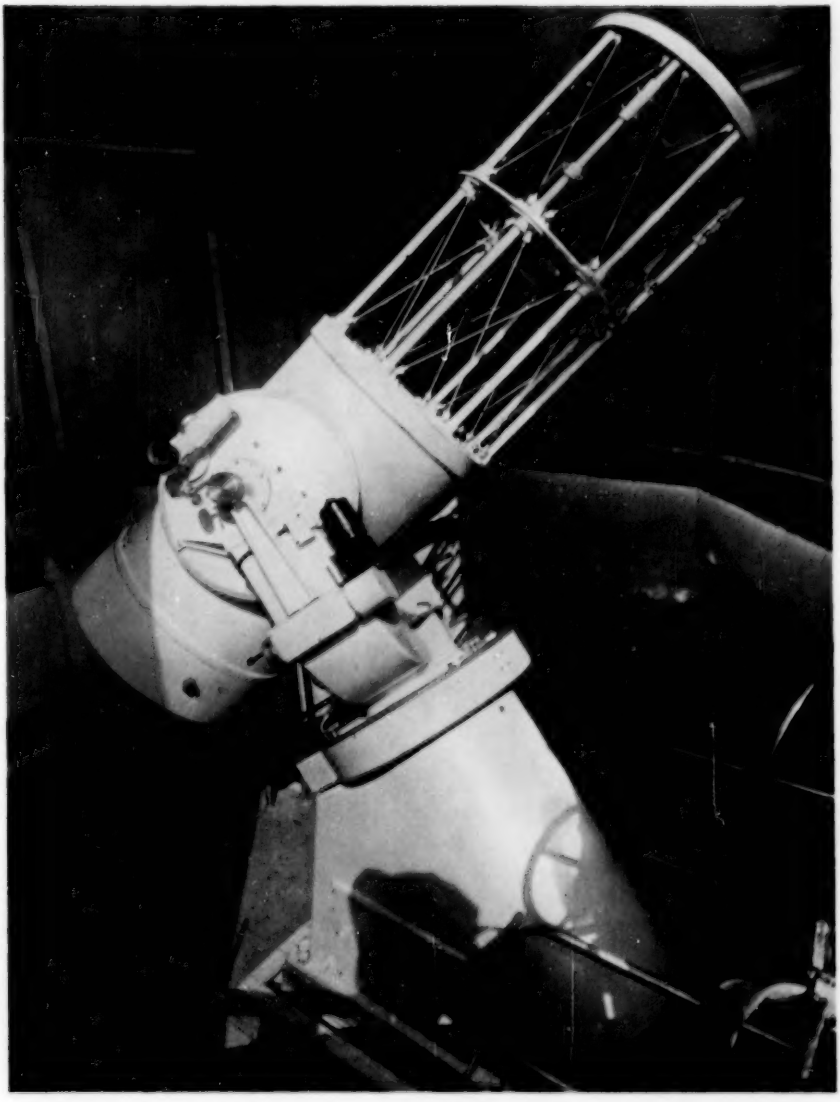

The telescope from the south-west.

The tower and the dome from the west with the spectroscope tunnel seen on the right-hand side.

than Rayleigh's percentage of light within the third dark ring, and consequently an observable image with angular radius

$$3{\cdot}39\lambda/D = 0''{\cdot}78$$

for a diameter, D, of the principal mirror of 50·8 cm and a wave-length of 5600 A. In solar work we cannot afford to have a resolving power smaller than 0″·78 (comparable with the radius of the tremor disk in superlatively good seeing), and consequently the effective diameters of the Cassegrain and coudé mirrors must not exceed 30·4 cm, that is 0·6 of the diameter of the main mirror.

For reasons of economy the dome has to be kept as small as possible, and this in turn means that the focal ratio of the main mirror must not exceed $f/5$. At this focal ratio the flux of radiation in the focal plane of the main mirror, that is in the vicinity of the Cassegrain mirror and its supports, is sufficiently intense to make the paint-work smoke and thus to produce bad seeing in the telescope from the convection currents resulting from this local heating. To eliminate this possibility the Cassegrain must have a clear aperture so large that no matter what part of the solar image is on the axis of the telescope, that is on the slit of the spectroscope, the extra-focal patch from the main mirror will never fall off the reflecting surface of the Cassegrain mirror. In this way, apart from the minute fraction absorbed by the aluminium coating, all the high-intensity flux from the main mirror is reflected by the Cassegrain and none falls on the rim of its cell or its supports to produce local heating. To meet this requirement the Cassegrain mirror must have a minimum clear aperture of 21·7 cm. The actual clear aperture given the mirror is 22·1 cm (8·70 in.) with an outside diameter of the cell of 24·1 cm (9·50 in.).

In a telescope designed for solar spectroscopy it is necessary only to ensure full illumination of the image over the height of the slit. As indicated above, the Cassegrain mirror is (though for quite other reasons) more than sufficiently large to give full illumination over the whole solar image. The limitation on full illumination comes from the first coudé mirror, distant 11·94 m (470·25 in.) from the focal plane of the $f/70$ telescope. The diameter of the extra-focal patch on the first coudé for an axial image will therefore be 17·1 cm (6·73 in.). To ensure full illumination over the height of the spectroscope slit, approximately 5 cm, the coudé mirror must be large enough to accept the full extra-focal patch for a central ray making an angle of 2′·35 with the optical axis. This requires a minimum clear (projected) circular aperture of 17·7 cm. Further, with this clear aperture points on the image radially distant as much as 16′·3 from the optical axis will suffer only 12·2 per cent vignetting; in other words the limbs of the centred solar image in the focal plane will always be clearly visible.

The first coudé mirror which directs the light from the Cassegrain down the polar axis is used at angles of incidence as high as 56°·75, corresponding to a declination of +23°·50. The reflecting surface is therefore given an elliptical cross section with a major axis 32·8 cm (12·90 in.) and a minor axis 17·8 cm (7·00 in.), that is, just more than sufficient to give full illumination over the whole height of the spectroscope slit for this declination and *a fortiori* for all smaller declinations. A point to be watched is that with decreasing declinations the ends of the major axis of the coudé mirror move out of the shadow of the Cassegrain cell and reflect parallel light direct from the Sun into the focal plane. To avoid this, lobes are attached to the north and south sides of the Cassegrain cell, giving

to it an elliptical cross section with a major axis of 29·2 cm (11·50 in.) and a minor axis of 24·1 cm (9·50 in.). The shadow of this enlarged Cassegrain cell prevents parallel light from the Sun reaching the coudé, no matter what part of the solar image is on the slit, provided $\delta > -21°.8$. This declination limitation could be removed by slightly increasing the lobes on the Cassegrain cell, but at Oxford it is no limitation since at these declinations the Sun has too small an altitude for useful observation.

The elliptical central stop with axes of 29·2 cm and 24·1 cm given by the Cassegrain cell corresponds closely enough, as far as the diffraction image is concerned, to a circular stop with a diameter of $(29{\cdot}2 \times 24{\cdot}1)^{1/2} = 26{\cdot}5$ cm, or 0·52 of the diameter of the main mirror. The effective central stop of the telescope is, however, provided by the coudé mirror and cell. The mirror, one fifth of the way towards the focus of the paraboloid, provides a central stop 25 per cent larger than its geometrical dimensions. The edge of this mirror towards the Cassegrain is cut away, so that for $\delta = +23°.5$ the mirror and cell together present an effective central stop of 18·8 cm (7·40 in.) diameter which is lost inside the central stop of the Cassegrain cell and its lobes. The axis about which the coudé rotates lies in the plane of the reflecting surface so that, as the declination decreases, the mirror remains centred in the beam, but the north and south edges project into the beam. The extreme occurs at $\delta = -23°.5$ when the effective stop presented by the coudé has a major axis of 37·2 cm (14·64 in.) and a minor axis, provided by the Cassegrain cell, of 24·1 cm (9·50 in.). This corresponds closely enough, as far as diffraction is concerned, to a circular stop of the same area and a diameter of 29·4 cm (11·79 in.). This is 0·59 of the diameter of the main mirror, and is just within our maximum allowable central stop which gives a diffraction image of $0''.78$ angular radius.

The fourth and final mirror, the second coudé, is not in the telescope proper but is mounted in the south prolongation of its polar axis. It accepts the beam from the first coudé at an angle of incidence of 45° and turns it to run horizontally to the west. This second coudé is some 3 m from the focal plane of the telescope, that is the slit of the spectroscope, and has to be large enough to give full illumination over the full height of the slit, which is easy, but also large enough to accept at least part of the extra-focal patch from the limb of the centred Sun. This is necessary both for guiding and for finding the heliographic coordinates of the point under observation on the Sun. The second coudé is given a clear aperture of 38·1 cm (15 in.), and this is more than sufficient, except in the plane of incidence, to accept all the light from the first coudé. The limitation of aperture in the plane of incidence does not prevent the limbs of the Sun being seen in these position angles, but they are highly vignetted.

Telescope design.—A telescope to meet the foregoing requirements was designed and constructed by Messrs. Grubb, Parsons & Co. under the supervision of its managing director, Mr G. M. Sisson. Plate 7 shows a photograph of the telescope in position in the dome, Plate 8 a photograph of the tower with the spectroscope tunnel seen stretching westwards and Fig. 1 is a meridian section through the tower showing the general arrangement. The telescope is designed to do just what is required but no more; hence the large polar axis to pass unimpeded the beam from the first coudé, the short tines of the fork since the telescope is only to be used within declination limits $\pm 23°.5$, and the dome shutter pivoting at the top.

The principal mirror is figured on a fused silica blank of 54·6 cm (21·5 in.) diameter and 8·9 cm (3·50 in.) thick. It is supported on six "wobbly" pads mounted in pairs at the vertices of a triangular frame. This frame is adjustable for squaring-on, and the three edge supports are made as far as possible friction free so that the mirror does not bind when this adjustment is being made. The supports and the mirror are mounted in a massive cell which is bolted to the centre piece. Two trunnions (one of which can be seen in Plate 7) in the side of the cell fit into a yoke carried by a block and tackle from the dome. The mirror and cell can thus be easily lowered through a trap door down to the ground floor of the tower for aluminizing.

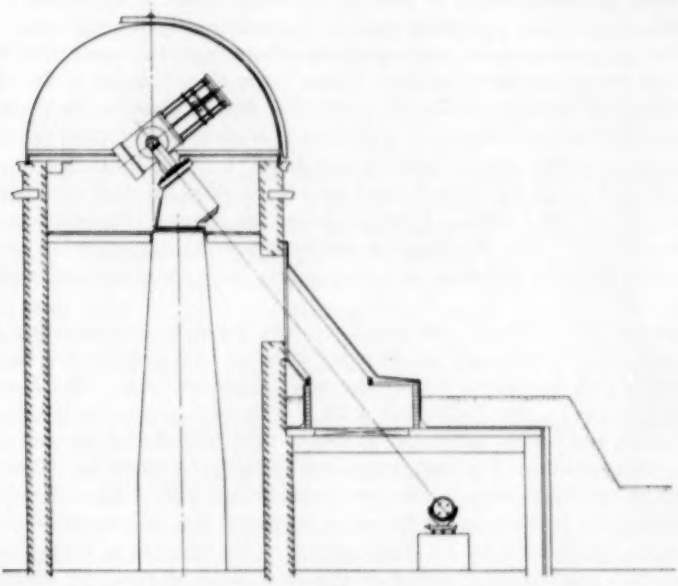

FIG. 1.—*A diagrammatic sketch to scale of the whole telescope. The height from the basement floor to the top of the dome is* 10·2 *m, or nearly* 34 *feet.*

The Cassegrain mirror cell and its focusing mount are supported by webs from a stubby and very stiff structural steel-work tube. The mirror is figured from a fused silica blank of 23·2 cm (9·12 in.) diameter, 4·1 cm (1·62 in.) thick. The cell which carries it is provided with squaring-on screws.

The first coudé mirror is carried in a cell on a stout spindle through the declination axis. The half-speed drive is provided by phosphor-bronze tapes, spring loaded to a high tension, and moving over cylindrical rollers. The mirror with an optically plane surface of elliptical cross section (axes 32·8 and 17·8 cm) is made from a fused silica blank 6·0 cm (2·35 in.) thick with its leading edge cut away so as to offer the minimum central obstruction to the light beam. Many of the problems of design and construction of the telescope seemed to centre about the coudé mirror. Its awkward shape made figuring with full-size tools very difficult, and that there was ultimately a succesful outcome must be attributed to the skill and experience of Mr G. E. Manville, the chief optician of the firm. Mechanically too the large mass of the coudé and cell increases sensitivity to

deflectional and torsional oscillations of the spindle. When in mid-1953 the mirrors were finally installed in the telescope, low-period oscillations of the coudé with an amplitude of a few seconds of arc were in fact found. They appeared to arise from heavy traffic on a nearby road. These oscillations were finally eliminated by Mr Sisson, partly as a result of increasing the spring loading of the tapes and so increasing the natural frequency of the system, and partly by supporting the spindle near the cell by two flat steel strips carried from the centre piece.

The telescope is driven by a synchronous motor through a large worm and 60 cm diameter worm wheel. The long focal length of 35·2 m is a severe test of the accuracy of the cutting and the mounting of these parts, but in actual use no evidence has been found of periodic or other errors in the drive. By the usual differential gear a guiding motion (approximately diurnal rate) can be applied in right ascension, or a setting motion of ten times this rate can be brought into action by an auxiliary motor. These gears are enclosed in an oil bath. The guiding and setting motions are controlled from a panel at the focal plane; this panel also carries buttons for a guiding motion in declination, for focusing the Cassegrain mirror and for rotating the dome.

The second coudé mirror is figured on a fused silica blank of 41 cm (16·1 in.) diameter, 7·6 cm (3 in.) thick. The mirror and cell have an altazimuth mounting with fine motions. Like the telescope proper this mounting is fixed to a concrete pier, isolated from the building, and erected on a large concrete mat 2·6 m below ground level.

Hartmann test.—Though the associated long-focus spectroscope has not yet been completed, the telescope has been in use since 1954 July for low-dispersion spectroscopy and interferometry of the solar chromosphere. The large solar image of 32·4 cm (12·8 in.) diameter with a scale of 1 mm = 5″·9 is well suited for such work and for spectroscopic studies of solar granulation, as well as many other problems, and such investigations are likely to be aided by the brilliance of the image resulting from an effective focal ratio of *f*/88. The rotation of the image, though an inconvenience for some purposes, is a gain in others, and can in any event be arrested by an image rotator. No changes of focal length are observed with continuous exposure to the Sun, showing both the effectiveness of the low-expansion fused silica mirrors and the small amount of heat absorbed by the aluminium coating of the Cassegrain. A noteworthy feature is the small depth of focus, and this coupled with solar definition varying from moderate to good suggests that performance is limited by the seeing rather than the optical properties of the telescope.

To find the latter, Hartmann plates were made in 1955 April of Procyon, Regulus and Arcturus. The Hartmann diaphragm had holes diametrically opposite each other in pairs on one or two azimuths per zone. The holes were made as small as possible (5·1 cm diameter), only 1/700th the focal length instead of the minimum 1/400th recommended by Hartmann (**2**), but even so several trials were made before a satisfactory diaphragm could be constructed in which the holes were not obstructed by the Cassegrain webs, or the supports of the coudé spindle. The positions of the holes are shown in the first two columns of Table II, where r is the radius of the zone in cm and ϕ is the azimuth measured counterclockwise from the east declination axis of the telescope. The remaining six columns, one for each photographic plate, give the residuals $f-\bar{f}$ in mm, where f is the focal setting for a given r and ϕ, and $\bar{f}$ is a provisional mean focal

setting for the plate as a whole. The column headings give the star, the angle of incidence, i_1, of the first coudé, and the angle, ϕ_0, of the west side of the plane of incidence of coudé II measured counterclockwise from the main-mirror side of the plane of incidence of coudé I.

TABLE II

Values of $(f-\bar{f})$ in mm as a function of r and ϕ

		Procyon		Regulus		Arcturus	
r	ϕ	$i_1=47^\circ\cdot67$	$47^\circ\cdot67$	$51^\circ\cdot09$	$51^\circ\cdot09$	$54^\circ\cdot71$	$54^\circ\cdot71$
		$\phi_0=117^\circ\cdot3$	$123^\circ\cdot8$	$93^\circ\cdot3$	$97^\circ\cdot5$	$42^\circ\cdot3$	$44^\circ\cdot6$
16·8	50°	−35·0	−19·5	−36·3	−44·6	−37·8	−43·4
	130	−51·7	−58·9	−49·5	−39·3	−45·7	−41·9
19·3	75	+27·2	+34·7	+41·3	+29·1	+14·9	+ 2·7
21·8	15	+21·6	+19·2	+17·1	+12·9	+22·8	+21·1
	105	+49·3	+45·1	+54·6	+58·5	+44·7	+48·5

In an ideal telescope these residuals would be constant within the errors of the determination. An inspection of Table II reveals, however, two systematic trends. First the focal settings for azimuth 105° are always greater than for azimuth 15°, indicating astigmatism, and secondly the focal settings steadily increase from the innermost to the outermost zone, indicating zonal aberration.

The most likely origin of the astigmatism is to be found in the two coudé mirrors since these may have a slight curvature. If such a mirror has a radius of curvature ρ, its focal length in the plane of incidence is $\frac{1}{2}\rho\cos i$, and perpendicular to the plane of incidence is $\rho/2\cos i$, where i is the angle of incidence (**5**). In any other azimuth (**3**) making an angle α with the plane of incidence the focal length is

$$\frac{1}{f_\alpha}=\frac{2}{\rho}\left(\frac{\cos^2\alpha}{\cos i}+\sin^2\alpha\cos i\right)=\frac{a}{\rho}.$$

Knowing the focal lengths in terms of the radii of curvature, ρ_1 for coudé I and ρ_2 for coudé II, the object distance, l, for coudé I and the distance c between coudé I and II, we can apply the paraxial formula to find the image position for the azimuth α. For another azimuth β the focal length of a given coudé will be

$$\frac{1}{f_\beta}=\frac{2}{\rho}\left(\frac{\cos^2\beta}{\cos i}+\sin^2\beta\cos i\right)=\frac{b}{\rho}.$$

Denoting the difference in image positions for these two azimuths by γ, and neglecting squares and higher powers of the small quantities ρ_1^{-1} and ρ_2^{-1}, we find an equation of condition

$$\sigma\rho_1^{-1}+\tau\rho_2^{-1}=\gamma$$

where $\sigma=(b_1-a_1)l^2+\gamma(a_1+b_1)l$; $\tau=(a_2-b_2)(l+c)^2-\gamma(a_2+b_2)(l+c)$,

the suffix 1 referring to coudé I and 2 to coudé II. From zones $r=16{\cdot}8$ cm and 21·8 cm we thus have 12 observation equations from Table II to solve by least squares to find the curvatures of the two coudé mirrors. The coefficients σ and τ may be readily calculated for each equation from the data given in Table II, bearing in mind that the angle of incidence, i_2, for coudé II is always 45°. Solving we find

$$\rho_1^{-1}=-(1{\cdot}24\pm0{\cdot}28)\times10^{-6}\,\text{cm}^{-1}\ ;\qquad \rho_2^{-1}=+(0{\cdot}00\pm0{\cdot}41)\times10^{-6}\,\text{cm}^{-1}.$$

Coudé II is thus flat within the errors of measurement, and coudé I is convex with a radius of curvature of some 8 km—a good "flat" on any ordinary standards.

Unfortunately coudé I is used at high angles of incidence and is at a considerable distance from the focal plane. In Table III are given the differences, γ_0, in focal setting for the resulting line images and the path differences in units of $\lambda = 5600$ A, computed from the appropriate formula, for various declinations. It is unlikely

TABLE III

Effect of convexity of coudé I

δ	i_1	γ_0 mm	ϵ
+20°	55°	42·0	1·2λ
0	45	25·4	0·7λ
−20	35	14·4	0·4λ

TABLE IV

Zonal aberration

r	$f_r-\bar{f}$ mm	T' mm	$\lvert T'/\rho \rvert$
16·8	−45·0	−0·22	1·6
19·3	+ 9·8	+0·05	0·4
21·8	+34·6	+0·21	1·6

that solar seeing is sufficiently good for astigmatic path differences of as much as $\lambda/2$ ever to impair the definition or affect the contrast, and it is at least fortunate that the best solar seeing at Oxford occurs in the early spring and the late autumn when the astigmatism from Table III approaches this limit. Nevertheless there can be little doubt that an improvement in the performance of the telescope, particularly in the three summer months, would result if the radius of curvature of coudé I could be at least doubled.

To find the zonal aberration we must eliminate from the focal settings in Table II the known effect of astigmatism. The minimum focal setting, $f_0(r)$, for any zone r occurs at right angles to the plane of incidence of coudé I, that is at $\phi = 0$. At any other azimuth we shall have

$$f_\phi(r) = f_0(r) + \gamma_0 \sin^2\phi.$$

Knowing γ_0 for the angle of incidence i_1, as computed for example for Table III, we can find for each entry in Table II the value of $f_0(r)$. Then $f_r = f_0(r) + \frac{1}{2}\gamma_0$ is the desired focal setting for the zone r which is independent of the astigmatism. Taking the mean of these values f_r for each zone on a given plate and selecting a focal setting $\bar{f}$ for which the disk of least confusion is a minimum, we can find mean values of $f_r - \bar{f}$ for the six plates. The results are given in Table IV, where $T' = r(f_r - \bar{f})/F$ is the lateral aberration and T'/ρ is its ratio to the expected Airy disk inside the third dark ring. The path differences are given by

$$\epsilon = \frac{1}{F}\int_{16\cdot8}^{r} T'\,dr,$$

and are found never to exceed 0·2 λ, that is just inside the Rayleigh limit. Further, since T'/ρ is comparable with unity, both of the criteria of Danjon and Couder (1) are satisfied and the telescope may be regarded as having negligible zonal aberration.

In conclusion I wish to express to Mr Sisson, Mr Manville and their assistants at Grubb, Parsons my appreciation for the thought and care which they have given to making the telescope a success. To Mr E. H. Swain and Mr J. M. Miller, former University Surveyors, and to Mr T. R. Davies, the Clerk of Works, I wish to add my thanks for the design and construction of a tower and tunnel perfectly tailored to fit the telescope and its accompanying spectroscope.

University Observatory,
Oxford:
1955 *October* 6.

References

(1) A. Danjon and A. Couder, *Lunettes et Télescopes*, p. 522, Paris, 1935.
(2) J. Hartmann, *Zs. f. Instk.*, **24**, 1, 1904.
(3) L. C. Martin, *Introduction to Applied Optics* I, p. 280, London, 1930.
(4) H. H. Plaskett, *M.N.*, **99**, 219, 1939; *Comm. Univ. Obs. Oxford*, No. 14.
(5) Lord Rayleigh, *Collected Papers* I, 437, 1884.

THE SECOND-ORDER THEORY OF THE FIGURE OF JUPITER

P. J. Message

(Communicated by Sir Harold Jeffreys

(Received 1955 April 12)

Summary

The second-order hydrostatic theory of a rotating planet is applied to each of the four models of the mass distribution in Jupiter proposed by W. H. Ramsey and B. Miles. The coefficients in the external field of the planet are found in each case. An inequality relating these coefficients given by Sampson for the ellipsoidal planet is extended to cover the case of a planet with second-order departure from the true ellipsoidal form, it being shown that a real planet must be of this type. Using the general nature of the dependence of the coefficient of the fourth harmonic on that of the second found from the models, and the value of the latter coefficient derived from observations of the great satellite motions, an estimate of the secular motion of the node of the fifth satellite is made which is close to the observed value.

---

1. The hydrostatic theory of a rotating planet to the second order has been treated by Sir Harold Jeffreys.* The planet is taken as symmetrical about its axis of revolution, the general surface of constant density having the equation

$$r = r'\{1 - \tfrac{4}{45}e^2 + (e' + \tfrac{2}{3}e^2)L_2 + (\tfrac{3}{2}e^2 + 4\kappa)L_4 + O(e^3)\}, \tag{1}$$

where, with r the distance from the centre and ϕ' the latitude,

$$\left.\begin{aligned} L_2 &= \tfrac{1}{3} - \sin^2\phi' = -\tfrac{2}{3}P_2, \\ L_4 &= \sin^4\phi' - \tfrac{6}{7}\sin^2\phi' + \tfrac{3}{35} = \tfrac{8}{35}P_4. \end{aligned}\right\} \tag{2}$$

r' is the radius of the sphere of equal volume, equal to b, say, for the outer surface of the planet. $e'(r')$ is related to the ellipticity e of the surface defined by (1) by

$$e' = e - \tfrac{5}{42}e^2, \tag{3}$$

and its square may be interchanged with e^2, to the accuracy desired. $\kappa(r')$ measures the departure of the surface (1) from the true ellipsoidal form.

With ω the angular velocity of rotation, M the mass of the planet, and f the constant of gravitation put

$$m = \omega^2 b^3/fM. \tag{4}$$

The potential function is then given by

$$U = \frac{4\pi}{3}f\left\{\frac{1}{2}\int_{r'=r_1}^{b}\rho d(3r'^2) + \frac{r_1^3}{r}\rho_0 + \frac{3}{5}\left(\frac{Sr_1^5}{r^3} + r^2T\right)L_2 + \left(\frac{3}{2}\frac{Pr_1^7}{r^5} + \frac{4}{3}\frac{Qr^4}{r_1^2}\right)L_4\right. \tag{5}$$

---

* Sir Harold Jeffreys, *M.N.*, **113**, 97–105, 1953.

where

$$\left.\begin{aligned}
\rho_0 &= \frac{1}{r_1^3}\int_{r'=0}^{r_1}\rho d(r'^3)=\bar{\rho} \quad \text{for} \quad r_1=b,\\
S &= \frac{1}{r_1^5}\int_{r'=0}^{r_1}\rho d\{r'^5(e'+\tfrac{2}{7}e^2)\},\\
T &= \int_{r'=r_1}^{b}\rho d(e'+\tfrac{16}{21}e^2),\\
P &= \frac{1}{r_1^7}\int_{r'=0}^{r_1}\rho d\{r'^7(e^2+\tfrac{8}{9}\kappa)\},\\
Q &= r_1^2\int_{r'=r_1}^{b}\rho d\left(\frac{\kappa}{r'^2}\right).
\end{aligned}\right\} \tag{6}$$

The condition that the surface (1) is a level surface leads to de Sitter's equations, as corrected by Jeffreys:

$$(e'+\tfrac{2}{7}e^2)\rho_0-\tfrac{3}{5}(S+T)-\tfrac{1}{2}\bar{\rho}m=\tfrac{4}{21}e(\bar{\rho}m-3T), \tag{7}$$

$$(3e^2-8\kappa)\rho_0-6e'S+3P+\tfrac{8}{3}Q=0. \tag{8}$$

2. *The mass distribution models.*—W. H. Ramsey and B. Miles* have given four models for the distribution of mass within Jupiter. They were found from the theoretical relation between the pressure and density of solid hydrogen, allowance being made for admixture of helium, the proportion varying between the models. In the models J_1, J_2, J_3, the heavier elements are supposed concentrated at the centre, J_1 having the most massive central particle and J_3 the least. J_4 has no massive central particle. Sir Harold Jeffreys allowed me to use values of the density in the models which had been sent to him by W. H. Ramsey. I found it necessary to extrapolate the values to values of r' smaller than those for which it had been given. The form of the compressibility used in the extrapolation was

$$k=\rho\frac{dp}{d\rho}=\alpha p+k_0, \tag{9}$$

as given by W. H. Ramsey†, where α varies from 5/3 for a perfect Fermi gas to 5 for heavy atoms. $\alpha=2$ was adopted as being reasonable for hydrogen, and leading to a case of Laplace's hypothesis:

$$k\propto\rho^2. \tag{10}$$

In the process the mass of the central particle in J_1 was re-estimated as $(4\pi/3)\times 70{\cdot}9\times 10^{27}$ gm. Those in J_2, J_3 were unaltered.

For J_1, J_2 and J_3 the density is given to three decimal places for the greater part of the planet, so the uncertainty of its specification may be taken as $\pm 0{\cdot}001$. At the surface $\rho\simeq 0{\cdot}10$, and is thus specified to ± 1 per cent. For most of the planet $\rho\simeq 1$, and so is specified to $\pm 0{\cdot}1$ per cent. In the case of J_4 only two decimal places are given, so the surface value is specified to only ± 10 per cent.

3. *The ellipticity.*—If we put

$$\eta=\frac{r'}{e'}\frac{de'}{dr'}, \tag{11}$$

two differentiations of (7) lead to

$$r'\frac{d\eta}{dr'}+\eta^2+5\eta+2(1+\eta)\frac{r'}{\rho_0}\frac{d\rho_0}{dr'}=10\Delta, \tag{12}$$

* W. H. Ramsey, *M.N.*, **111**, 427–447, 1951; and B. Miles and W. H. Ramsey, *M.N.*, **112** 234–243, 1952.

† W. H. Ramsey, *M.N., Geophys. Suppl.*, **6**, 42, 1950

where $$10\Delta = \frac{2\epsilon'}{21}\left\{(17+2\eta)r'\frac{d\eta}{dr'} + 2\eta^3 + 13\eta^2 + 4\eta + \frac{r'}{\rho_0}\frac{d\rho_0}{dr'}(6+7\eta-2\eta^2)\right\}, \quad (13)$$

which in turn leads to de Sitter's equation:

$$\sqrt{(1+\eta)} = \frac{5}{r'^5\rho_0}\int_0^{r'}\rho_0 r'^4 F(\eta)dr', \quad (14)$$

where $$F(\eta) = (1+\tfrac{1}{2}\eta - \tfrac{1}{10}\eta^2 + \Delta)/\sqrt{(1+\eta)}. \quad (15)$$

An examination of the influence of Δ on η shows it to affect it by 0·2 per cent or less, so it was neglected.

For the models with a central particle we have, if m^* is its mass,

$$\rho_0 \sim \frac{3m^*}{4\pi r'^3} \quad \text{as} \quad r' \to 0, \quad (16)$$

which, substituted in (12), gives

$$\eta \to 3 \quad \text{as} \quad r' \to 0. \quad (17)$$

For the models J_1, J_2, J_3, (14) was solved by iteration, using this initial value of η. The solution is given in Tables I–IV. The values for $r' = b$ thus obtained were (the suffix "s" indicating surface values):

	J_1	J_2	J_3
$\eta_s =$	1·658	1·485	1·306

Where there is no central particle (12) shows

$$\eta \to 0 \quad \text{as} \quad r' \to 0. \quad (18)$$

The integration for J_4 with this initial value has been carried out by Ramsey and Miles. They obtain $\eta_s = 1{\cdot}099$.

Differentiating (6) and eliminating S_s with the original equation leads to

$$e_s' = \frac{5m}{2(2+\eta_s)} + \frac{5(2\eta_s^2 - \eta_s + 5)m^2}{21(2+\eta_s)^3}. \quad (19)$$

De Sitter* gives the ratio of the mass of the system of Jupiter to that of the Sun as $1047{\cdot}40 \pm 0{\cdot}03$. Sampson†, from the semi-durations of satellite eclipses, gives the angular equatorial semi-diameter of Jupiter at mean distance as $18''{\cdot}92$. Micrometer measures give about $19''{\cdot}2$, but these are probably increased by irradiation. I take $a_0 = 18''{\cdot}92 \pm 0''{\cdot}20$. The period of rotation is observed from spots to be $9^h\,50^m\,30^s$ at the equator and $9^h\,55^m\,5^s$ to $9^h\,55^m\,42^s$ in temperate latitudes. By analogy with the Earth there is a strong atmospheric current at high altitudes, in the same direction as the axial rotation, and as the spots observed are almost certainly atmospheric phenomena the period of rotation of the solid planet is likely to be nearer the larger of these two. Hence I take $9^h\,55^m \pm 2^m{\cdot}5$. With Struve's value 0·065 for the ellipticity, (5) gives

$$m = \frac{\omega^2 a_0^3(1-e_s)}{fM}$$

$$= 0{\cdot}08339(1 \pm 0{\cdot}010).$$

---

* W. de Sitter, *Proc. Roy. Akad. Sci. Amst.*, **10**, 710–729, 1908.

† R. A. Sampson, *Harvard Annals*, **52**, Pt. 2, 333, 1909.

(19) then gives:

J_1	J_2	J_3	J_4

$e_s' = 0{\cdot}05729(1 \pm 0{\cdot}011), 0{\cdot}06013(1 \pm 0{\cdot}011), 0{\cdot}06339(1 \pm 0{\cdot}011), 0{\cdot}06763(1 \pm 0{\cdot}020)$,

and hence by means of the values of e_s from (3), m is corrected to:

$m = 0{\cdot}08404(1 \pm 0{\cdot}010), 0{\cdot}08379(1 \pm 0{\cdot}010), 0{\cdot}08349(1 \pm 0{\cdot}010), 0{\cdot}08318(1 \pm 0{\cdot}010)$.

These values give from (19), correct to the second order,

$e_s' = 0{\cdot}05774(1 \pm 0{\cdot}011), 0{\cdot}06042(1 \pm 0{\cdot}011), 0{\cdot}06347(1 \pm 0{\cdot}011), 0{\cdot}06739(1 \pm 0{\cdot}011)$.

From (11) we have
$$\ln e_s' - \ln e' = \int_{r'}^{b} \frac{\eta}{r'} dr', \tag{20}$$
whence $e'(r')$ is determined throughout the planet, the values being given in Tables I–IV.

4. *The departure from the ellipsoidal form.*—Put
$$\left.\begin{aligned} P_1 &= \frac{1}{r_1^7} \int_{r'=0}^{r_1} \rho d(r'^7 e^2), \\ P_2 &= \frac{1}{r_1^7} \int_{r'=0}^{r_1} \rho d(r'^7 \kappa); \end{aligned}\right\} \tag{21}$$
then equation (8) becomes
$$\kappa(r') = \kappa_1(r') + \frac{1}{3\rho_0(r')}(P_2 + Q), \tag{22}$$
where
$$\kappa_1(r') = \frac{3}{8}\left\{e^2 + \frac{1}{\rho_0}(P_1 - 2e'S)\right\}. \tag{23}$$
Since P_2, Q are linear operators on the function $\kappa(r')$, we may write (22) as
$$(r\kappa') = \kappa_1(r') + \mathscr{L}(\kappa) \tag{22a}$$
where $\mathscr{L}$ is a linear operator. Put
$$\left.\begin{aligned} \delta_1\kappa &= \mathscr{L}(\kappa_1), \\ \delta_n\kappa &= \mathscr{L}(\delta_{n-1}\kappa) \text{ for } n > 1. \end{aligned}\right\} \tag{24}$$
Then if λ is the greatest eigenvalue of $\mathscr{L}$ we have
$$\delta_n\kappa/\delta_{n-1}\kappa \to \lambda \quad \text{as} \quad n \to \infty.$$
If $|\lambda| < 1$, we have $\delta_n\kappa \to 0$ as $n \to \infty$, and hence, putting
$$\kappa_n = \kappa_1 + \sum_{r=1}^{n-1} \delta_r\kappa, \tag{25}$$
$$\kappa_n - \kappa_1 - \mathscr{L}(\kappa_n) = -\delta_{n+1}\kappa \text{ which} \to 0 \text{ as } n \to \infty,$$
so that since κ_n converges, it converges to κ, the solution of (22). It was found that $\delta_3\kappa/\delta_2\kappa$ was constant to the desired accuracy ($\delta_2\kappa/\delta_1\kappa$ in the case of J_4), so
$$\sum_{r=3}^{\infty} \delta_r\kappa \simeq \sum_{r=0}^{\infty} \lambda^r \delta_3\kappa$$
$$= \delta_3\kappa/(1-\lambda). \tag{26}$$
Therefore
$$\kappa \simeq \kappa_1 + \delta_1\kappa + \delta_2\kappa + \delta_3\kappa/(1-\lambda). \tag{27}$$
An examination of (22) as $r' \to 0$ shows $\kappa(0) = 0$. Hence the functions $\kappa(r')$ were found, and are given in Tables I–IV, the surface values being

	J_1	J_2	J_3	J_4
$1/\lambda =$	6·15	5·7	5·2	5·0
$10^4\kappa_s =$	$5{\cdot}76 \pm 0{\cdot}13$	$5{\cdot}33 \pm 0{\cdot}12$	$4{\cdot}65 \pm 0{\cdot}10$	$3{\cdot}59 \pm 0{\cdot}15$

TABLE I

Model J_1, central particle 15·5 per cent of total mass

r'	ρ	η	e'	$10^4\kappa$
10^9 cm	g cm^{-3}			
6·99	0·089	1·658	0·05774	5·76
6·95	0·121	1·642	0·05719	5·60
6·9	0·171	1·604	0·05653	5·44
6·7	0·240	1·512	0·05400	4·78
6·5	0·279	1·449	0·05164	4·20
6·3	0·309	1·354	0·04942	3·73
6·1	0·333	1·261	0·04738	3·35
5·949	{0·350 0·768}		0·04580	3·11
5·6	0·940	1·138	0·04282	2·73
5·2	1·150	1·121	0·03940	2·35
4·8	1·370	1·132	0·03600	2·04
4·4	1·601	1·171	0·03258	1·76
4·0	1·844	1·242	0·02905	1·49
3·6	2·095	1·346	0·02535	1·24
3·2	2·373	1·489	0·02133	0·98
2·8	2·676	1·674	0·01727	0·73
2·4	3·019	1·898	0·01313	0·47
2·0	3·425	2·150	0·00907	0·23
1·6	3·96	2·411	0·00545	0·10
1·2	4·97	2·638	0·00264	0·03
0·8	6·93	2·835	0·00088	0·00
0·4	12·80	2·956	0·00011	0·00
0·0	...	3·000	0·00000	0·00

TABLE II

Model J_2, central particle 10·5 per cent of total mass

r'	ρ	η	e'	$10^4\kappa$
10^9 cm	g cm^{-3}			
6·99	0·095	1·485	0·06042	5·33
6·95	0·132	1·466	0·05991	5·18
6·9	0·185	1·426	0·05929	5·03
6·7	0·261	1·353	0·05692	4·37
6·5	0·303	1·243	0·05473	3·88
6·3	0·335	1·158	0·05271	3·43
6·1	0·361	1·046	0·05090	3·10
6·003	{0·372 0·808}		0·05007	3·00
5·6	1·024	0·934	0·04682	2·57
5·2	1·248	0·901	0·04376	2·25
4·8	1·481	0·897	0·04072	1·99
4·4	1·722	0·915	0·03764	1·78
4·0	1·969	0·967	0·03442	1·59
3·6	2·222	1·053	0·03095	1·38
3·2	2·490	1·183	0·02714	1·22
2·8	2·774	1·360	0·02291	1·00
2·4	3·082	1·590	0·01827	0·74
2·0	3·432	1·924	0·01326	0·46
1·6	3·863	2·239	0·00833	0·21
1·2	4·48	2·570	0·00417	0·06
0·8	5·52	2·828	0·00138	0·01
0·4	8·28	2·954	0·00019	0·00
0·0	...	3·000	0·00000	0·00

TABLE III

Model J_3, central particle 5·2 per cent of total mass

r'	ρ	η	e'	$10^4\kappa$
10^9 cm	g cm^{-3}			
6·99	0·101	1·306	0·06347	4·65
6·95	0·143	1·284	0·06300	4·50
6·9	0·200	1·242	0·06243	4·37
6·7	0·281	1·152	0·06026	3·76
6·5	0·326	1·055	0·05828	3·26
6·3	0·361	0·927	0·05650	2·92
6·1	0·389	0·819	0·05495	2·60
6·051	{0·395 0·851}		0·05466	2·57
5·6	1·112	0·692	0·05198	2·20
5·2	1·354	0·643	0·04954	1·93
4·8	1·601	0·614	0·04712	1·73
4·4	1·853	0·606	0·04469	1·58
4·0	2·100	0·624	0·04215	1·48
3·6	2·352	0·670	0·03939	1·40
3·2	2·606	0·758	0·03633	1·35
2·8	2·862	0·897	0·03246	1·28
2·4	3·121	1·110	0·02783	1·14
2·0	3·391	1·416	0·02213	0·89
1·6	3·693	1·819	0·01544	0·57
1·2	4·078	2·304	0·00851	0·21
0·8	4·71	2·710	0·00304	0·03
0·4	6·48	2·940	0·00045	0·00
0·0	...	3·000	0·00000	0·00

TABLE IV

Model J_4, no central particle

r'	ρ	η	e'	$10^4\kappa$
10^9 cm	g cm^{-3}			
6·99	0·11	1·099	0·06739	3·6
6·96	0·14	1·065	0·06708	3·5
6·9	0·22	1·034	0·06647	3·3
6·8	0·27	0·977	0·06550	3·0
6·7	0·30	0·926	0·06459	2·7
6·5	0·36	0·801	0·06292	2·3
6·3	0·39	0·691	0·06147	1·9
6·1	{0·42 0·89}	0·565	0·06024	1·7
6·0	0·96	0·533	0·05970	1·6
5·5	1·28	0·416	0·05731	1·2
5·0	1·60	0·324	0·05534	0·8
4·5	1·92	0·254	0·05369	0·5
4·0	2·23	0·195	0·05230	0·5
3·5	2·53	0·143	0·05115	0·4
3·0	2·80	0·118	0·05015	0·3
2·5	3·05	0·105	0·04912	0·2
2·0	3·27	0·047	0·04831	0·1
1·5	3·43	0·025	0·04785	0·1
1·0	3·56	0·020	0·04742	0·1
0·0	3·66	0·000	0·04688	0·0

5. *The external field.*—This is given from (5) with $r_1 = b$:

$$V = fM\left\{\frac{1}{r} + \frac{Jb^2}{r^3}L_2 + \frac{Db^4}{r^5}L_4 + O(e_s^3)\right\}, \tag{28}$$

where

$$\left.\begin{aligned} J &= \frac{3}{5\bar{\rho}}S_2 = \frac{3}{5\bar{\rho}b^5}\int_{r'=0}^{b}\rho d\{r'^5(e' + \tfrac{2}{7}e^3)\},\\ D &= \frac{3}{2\bar{\rho}}P_2 = \frac{3}{2\bar{\rho}b^7}\int_{r'=0}^{b}\rho d\{r'^7(e^2 + \tfrac{8}{9}\kappa)\};\end{aligned}\right\} \tag{29}$$

whence by direct calculation we have the following values:

	J_1	J_2	J_3	J_4
J =	0·01569(1 ± 0·014),	0·01853(1 ± 0·014),	0·02193(1 ± 0·014),	0·02627(1 ± 0·06)
D =	0·00177(1 ± 0·023),	0·00217(1 ± 0·023),	0·00267(1 ± 0·023),	0·00334(1 ± 0·04)

Now from (7), (8), with surface values, using (29),

$$\left.\begin{aligned} J &= e'_s - \tfrac{1}{2}m + \tfrac{2}{7}e^2_s - \tfrac{4}{21}me_s\\ D &= \tfrac{7}{2}e^2_s - \tfrac{5}{2}me'_s + 4\kappa_s\end{aligned}\right\} \tag{30}$$

whence we have

	J_1	J_2	J_3	J_4
J =	0·01575(1 ± 0·012),	0·01860(1 ± 0·012),	0·02187(1 ± 0·012),	0·02603(1 ± 0·05)
D =	0·00184(1 ± 0·022),	0·00225(1 ± 0·022),	0·00271(1 ± 0·022),	0·00332(1 ± 0·083)

Weighted, these give

	J_1	J_2	J_3	J_4
J =	0·01572 ± 0·00020,	0·01857 ± 0·00024,	0·02190 ± 0·00028,	0·02613 ± 0·00131
D =	0·00181 ± 0·00004,	0·00221 ± 0·00005,	0·00269 ± 0·00006,	0·00334 ± 0·00015
D/J^2 =	7·32 ± 0·35	6·41 ± 0·31	5·61 ± 0·27	4·89 ± 0·71

It is noticed that D/J^2 varies approximately linearly with J^{-1}. Equation (1), with $r' = b$, $\phi' = 0$, gives

$$b = a_0(1 - \tfrac{1}{3}e'_s - \tfrac{19}{126}e^2_s - \tfrac{12}{35}\kappa_s), \tag{31}$$

giving, in astronomical units,

	J_1	J_2	J_3	J_4
$10^4 b$ =	4·677 ± 0·011	4·673 ± 0·011	4·668 ± 0·011	4·662 ± 0·011
$10^9 Jb^2$ =	3·439 ± 0·088	4·055 ± 0·104	4·772 ± 0·122	5·678 ± 0·310
$10^{16} Db^4$ =	0·866 ± 0·043	1·054 ± 0·052	1·277 ± 0·063	1·577 ± 0·070

6. *Comparison with observation.*—De Sitter collected and reduced several series of observations of the great satellites from 1891 to 1924, and certain older eclipse observations. In his 1931 George Darwin lecture* he gave, from the secular motions, the coefficients of the great inequalities and the period of the libration, equations for the masses of the satellites and the coefficient Jb^2. A least-squares solution by Professor Brouwer, communicated by letter to Sir Harold Jeffreys, gives

$$Jb^2 = 5{\cdot}028 \times 10^{-9}.$$

This corresponds to a degree of central condensation intermediate between J_3 and J_4, being much closer to J_3. Linear interpolation of D/J^2 gives 5·41 and hence $Db^4 = 1{\cdot}37 \times 10^{-16}$.

The most significant dynamical effect of the figure of the planet is the secular motion of the orbit of the fifth satellite. We have, where ϖ, θ are the longitudes

* W. de Sitter, *M.N.*, **91**, 706–738, 1931.

of the apse and node respectively, from the figure of the planet

$$\frac{d\varpi}{dt} = n\{Jb^2/a^2 - \tfrac{1}{2}J^2b^4/a^4 + \tfrac{9}{7}Db^4/a^4\} \qquad (32)$$

$$\frac{d\theta}{dt} = -n\{Jb^2/a^2 - \tfrac{3}{2}J^2b^4/a^4 + \tfrac{9}{7}Db^4/a^4\}.$$

H. Struve*, from Barnard's observations between 1892 and 1905, gives the semi-major axis as $47''{\cdot}965$, and the mean daily motion in longitude as $722^\circ{\cdot}63175$. Hence, with $Jb^2 = 5{\cdot}028 \times 10^{-9}$, $Db^4 = 1{\cdot}37 \times 10^{-16}$, the contributions to the secular motions are, per Julian year,

	$\frac{d\varpi}{dt}$	$\frac{d\theta}{dt}$
from Jb^2	$906^\circ{\cdot}61$	$-906^\circ{\cdot}61$
from J^2b^4	$-\ 1^\circ{\cdot}61$	$4^\circ{\cdot}72$
from Db^4	$14^\circ{\cdot}5$	$-\ 14^\circ{\cdot}5$
from satellite I	$0^\circ{\cdot}39$	$-\ 0^\circ{\cdot}39$
from the other satellites	$0^\circ{\cdot}04$	$-\ 0^\circ{\cdot}04$
Total	$919^\circ{\cdot}9$	$-916^\circ{\cdot}8$

A. J. J. van Woerkom†, discussing observations from 1892 to 1921 and in 1949, considers the eccentricity too small for any estimate of the apse motion to be made, and finds for the node

$$\frac{d\theta}{dt} = -914^\circ{\cdot}62 \pm 0^\circ{\cdot}36.$$

The difference between the observed and calculated values would correspond to $0{\cdot}012$ in $Jb^2 \times 10^{-9}$ or to $0{\cdot}21$ in $Db^4 \times 10^{-16}$. The former is a tenth of the uncertainty of the value calculated for the model J_3, and the latter less than four times the corresponding uncertainty. The agreement offers support for the dependence of D/J^2 deduced from Miles and Ramsey's models, and strongly favours the model J_3.

7. *The nature of κ and D/J^2.*—Sampson,‡ in the introduction to his theory of the four great satellites, shows that the equation of hydrostatic equilibrium cannot be satisfied for a perfectly ellipsoidal body with uniform rotation unless it is homogeneous in density. Thus for a real body, which has positive compressibility and whose density therefore increases towards the centre, there will be departure from the ellipsoidal form. That this departure must appear in the second order can be deduced from the equation for κ. From (23),

$$\kappa_1(r') = \frac{3}{8\rho_0 r_1^7}\int_{r'=0}^{r_1} \rho d\{(r')^3(r_1e'(r_1) - r'e'(r'))^2\}$$

$$= -\frac{3}{8\rho_0 r_1^7}\int_{r'=0}^{r_1} (r')^5\{r_1e'(r_1) - r'e'(r')\}^2 d\rho$$

$$> 0 \qquad \text{for} \qquad 0 < r' \leqslant b,$$

* H. Struve, *Sitz. Ber. Preuss. Akad. Wiss.*, **2**, 790, 1906.
† A. J. J. van Woerkom, *Astron. Papers of the Amer. Ephem.*, **12**, Pt. 1, 1950.
‡ R. A. Sampson, *Mem. R.A.S.*, **63**, 14–16, 1921.

since ρ is a strictly decreasing function of r' and the form $e' \propto 1/r'$ for the ellipticity violates both the possible initial values for η. Also, from (22),

$$\begin{aligned}\mathscr{L}\{f(r')\} &= \frac{1}{3\rho_0}\left\{\frac{1}{r_1^2}\int_{r'=0}^{r_1}\rho d((r')^2 f) + r_1^2\int_{r'=r_1}^{b}\rho d(f/(r')^2)\right\}\\ &= \frac{1}{3\rho_0}\left\{\frac{r_1^2}{b^2}f(b)\rho_b - r_1^2\int_{r'=r_1}^{b} f/(r')^2 d\rho - \frac{1}{r_1^2}\int_{r'=0}^{r_1}(r')^2 f d\rho\right\}\\ &> 0 \quad \text{for} \quad 0<r'\leqslant b \quad \text{if} \quad f>0 \quad \text{for} \quad 0<r'<b,\end{aligned}$$

Thus in turn $\delta_1\kappa>0$, $\delta_2\kappa>0, \ldots$, and hence

$$\kappa(r')>0 \qquad \text{for} \qquad 0<r'<b. \tag{33}$$

Sampson derives an inequality ($n \geqslant m^2$ in his notation) for which the following proof is extended to cover the case of non-zero κ. Consider the function of the arbitrary variable λ

$$\begin{aligned}F(\lambda) &= \rho_0 + 2\lambda S + \lambda^2 P\\ &= \frac{1}{r_1^3}\int_{r'=0}^{r_1}\rho d\left[(r')^3\left\{1+2\lambda\left(\frac{r'}{r_1}\right)^2\left(e'+\frac{2}{7}e^2\right)+\lambda^2\left(\frac{r'}{r_1}\right)^4\left(e^2+\frac{8}{9}\kappa\right)\right\}\right]\\ &= \frac{1}{r_1^3}\int_{r'=0}^{r_1}\rho d\left[(r')^3\left\{\left(1+\lambda\left(\frac{r'}{r_1}\right)^2\left(e'+\frac{2}{7}e^2\right)\right)^2+\frac{8}{9}\lambda^2\left(\frac{r'}{r_1}\right)^4\kappa\right\}\right]\\ &= \rho(r_1)\left[\left\{1+\lambda\left(e'+\frac{2}{7}e^2\right)\right\}^2+\frac{8}{9}\lambda^2\kappa\right]\\ &\quad -\int_{r'=0}^{r_1}\left(\frac{r'}{r_1}\right)^3\left[\left\{1+\lambda\left(\frac{r'}{r_1}\right)^2\left(e'+\frac{2}{7}e^2\right)\right\}^2+\frac{8}{9}\lambda^2\left(\frac{r'}{r_1}\right)^4\kappa\right]d\rho.\end{aligned}$$

The second term is strictly positive, unless the body is homogeneous, when it vanishes for all r_1. The first term is positive or zero. For the homogeneous body, having $\kappa=0$, it vanishes, for given r_1, for just one value of λ. Hence $F=0$ has no real root for λ except in the case of the homogeneous body, when the roots are equal. Thus

$$P\rho_0 \geqslant S^2, \tag{34}$$

with equality only if the body is homogeneous. Taking surface values and using (29) we have

$$D/J^2 \geqslant 25/6, \tag{35}$$

with equality only if the body is homogeneous.

I should like to record my gratitude to Sir Harold Jeffreys for having initiated and guided my work, and to the Council of Gonville and Caius College for a Research Studentship which made it possible.

Gonville and Caius College,
Cambridge:
1955 *April* 5.

GREENWICH OBSERVATIONS OF THE HORIZONTAL AND VERTICAL DIAMETERS OF THE SUN

P. J. D. Gething

(Communicated by the Astronomer Royal)

(Received 1955 June 17)

Summary

It has been claimed that the Greenwich observations of the horizontal diameter of the Sun are in agreement with those made at Campidoglio and Monte Mario in indicating a real variation of diameter with a period of about 22 years. It is shown in the present paper that this conclusion cannot be justified from the data considered. A more detailed analysis of the Greenwich measurements of both the horizontal and vertical diameters in the period 1915 to 1936 is given, in which corrections are applied for irradiation and personality differences between observers. The resulting diameters show comparatively large variations from year to year. These variations do not necessarily represent real changes in the size of the Sun; they may be due to variations in the mean personality correction. No definite relationship can be established between the apparent variations in diameters and other phenomena, such as the sunspot cycle.

---

1. *Introduction.*—Numerous authors claim to have detected variations in the diameter of the Sun, whereas other investigators, such as Auwers (**1**), failed to find any variation, or to detect any significant difference between the equatorial and polar diameters. The results of various series of observations have not been in good agreement, some authors finding an eight-year period, others an eleven-year period and others a twenty-two-year period, while estimates of the amplitude of the fundamental oscillation have ranged from a few hundredths to a few tenths of a second of arc, with extreme ranges of up to two seconds. Some authors (**1**–**4**) have examined heliometer measurements of the polar and equatorial diameters and others (**5**–**7**) the horizontal diameters at transit. Poor (**8**) has discussed measurements of photographic plates.

The series of measurements made with the transit circle at Campidoglio (and later at Monte Mario) deserves special mention (**6, 7, 9**–**16**). An image of the Sun about one metre in diameter is projected onto a screen, and the passage of each R.A. limb is timed across seven wires by four observers using the eye-and-ear method. The technique of obtaining four observations at each transit, introduced by Respighi in 1876, has two advantages: it decreases the probable error of a yearly mean because of the increased number of observations, and it enables differences of personal equation between observers to be calculated easily. On the other hand, the eye-and-ear observations across fixed wires would be expected to be inferior in accuracy to observations obtained with a self-recording moving-wire micrometer, and to involve greater personality differences.

This series of observations seems to provide strong evidence for an oscillation with a period of 22 years and an amplitude of a few tenths of a second of arc in the horizontal diameter. It has been claimed (**17**) that the Greenwich observations support this conclusion, providing evidence of an oscillation of about the same period and phase. A comparison of the two sets of observations, given below, offers no support to this claim.

The Greenwich results for the period 1851 to 1939 obtained with the Airy Transit Circle are given in Table I. The table exhibits the mean horizontal and vertical semi-diameters obtained from all the O–C diameter residuals published in the annual volumes of Greenwich Observations. It must be emphasized that corrections for personality have not been applied. Some of the data have been published previously (**18, 19**), some are taken from computations undertaken by R. T. Cullen for an unpublished investigation. The results have been tabulated in the form of semi-diameters to facilitate comparison with the Italian results.

TABLE I

Yearly mean horizontal and vertical radii of the Sun observed at Greenwich

Year	Horizontal semi-diameter	Number of observations	Vertical semi-diameter	Number of observations
	"		"	
1851·5	961·46	87	961·26	106
1852·5	1·74	103	1·60	112
1853·5	1·82	78	1·53	86
1854·5	1·19	109	1·18	111
1855·5	1·33	84	1·50	93
1856·5	1·12	104	1·24	109
1857·5	1·33	113	1·32	123
1858·5	1·33	126	1·36	132
1859·5	1·26	109	1·32	125
1860·5	1·19	72	1·00	72
1861·5	1·12	108	1·34	113
1862·5	0·91	81	1·26	87
1863·5	0·98	103	1·18	107
1864·5	1·26	105	1·28	111
1865·5	1·33	104	1·31	117
1866·5	1·26	95	1·26	103
1867·5	1·05	73	1·12	83
1868·5	1·26	111	1·16	126
1869·5	0·98	79	1·02	93
1870·5	0·98	106	1·18	119
1871·5	1·05	103	1·50	104
1872·5	0·98	107	1·50	109
1873·5	1·05	102	1·58	108
1874·5	1·12	94	1·74	95
1875·5	1·05	96	1·52	104
1876·5	1·05	99	1·30	96
1877·5	1·12	75	1·31	75
1878·5	1·12	77	1·15	72
1879·5	1·19	61	1·16	64
1880·5	1·26	99	1·13	104
1881·5	1·19	107	1·36	108
1882·5	1·26	87	1·48	97
1883·5	1·47	113	1·38	122
1884·5	1·32	100	1·44	100
1885·5	1·42	110	1·46	123

TABLE I—*cont.*

Year	Horizontal semi-diameter	Number of observations	Vertical semi-diameter	Number of observations
	″		″	
1886·5	961·46	115	961·43	121
1887·5	1·38	125	1·30	132
1888·5	1·33	84	1·26	96
1889·5	1·23	109	1·03	118
1890·5	1·28	124	1·23	141
1891·5	1·20	120	1·18	130
1892·5	1·02	136	1·11	139
1893·5	1·30	167	1·44	172
1894·5	1·09	149	1·23	158
1895·5	1·19	177	1·24	188
1896·5	1·02	147	1·20	147
1897·5	1·16	160	1·29	170
1898·5	0·99	143	1·12	150
1899·5	1·13	162	1·20	179
1900·5	1·07	145	1·10	154
1901·5	1·06	159	1·27	173
1902·5	0·92	119	1·08	145
1903·5	0·78	138	0·77	158
1904·5	0·96	139	0·98	150
1905·5	0·93	118	0·98	129
1906·5	0·90	113	0·97	117
1907·5	0·88	138	0·92	139
1908·5	1·11	130	1·16	139
1909·5	1·14	128	1·28	137
1910·5	1·02	122	1·12	136
1911·5	1·08	154	1·43	167
1912·5	0·84	131	1·22	144
1913·5	1·06	137	1·34	147
1914·5	1·10	148	1·40	163
1915·5	1·10	103	1·39	127
1916·5	0·95	111	1·07	125
1917·5	0·90	137	1·04	163
1918·5	0·98	124	0·90	137
1919·5	0·92	116	1·14	129
1920·5	0·98	127	1·04	140
1921·5	1·02	150	1·19	159
1922·5	0·96	114	1·16	118
1923·5	0·82	114	1·06	125
1924·5	0·72	112	1·16	122
1925·5	0·65	99	0·84	112
1926·5	0·79	131	0·91	140
1927·5	0·46	130	0·92	139
1928·5	0·64	135	0·92	149
1929·5	0·84	146	1·10	151
1930·5	0·66	115	0·84	131
1931·5	0·56	118	0·94	123
1932·5	0·72	116	1·04	126
1933·5	0·82	147	0·98	157
1934·5	0·74	133	1·04	146
1935·5	0·68	110	1·06	118
1936·5	0·46	107	1·06	114
1937·5	0·48	94	0·98	102
1938·5	0·56	121	1·24	131
1939·5	0·54	75	1·12	97

The values given in Table I do not agree exactly with those given by Miss Giannuzzi (**17**). The means in Table I were obtained by giving each observation unit weight, whereas Miss Giannuzzi first formed monthly means and then gave these equal weight in forming the annual means. The differences between the two sets of values obtained by these two different procedures are small in general. The Italian results for the horizontal semi-diameter are given in Table XI of the paper by Gialanella (**7**).

The two series of observations are compared in Fig. 1. The upper graph shows the two series of measurements of horizontal semi-diameters and the lower graph shows the Greenwich measurements in the vertical co-ordinate; measurements of the vertical diameter were not made at Campidoglio. The diagram also shows the dates of sunspot maxima and minima for the purposes of comparison.

An examination of the upper graph fails to show any obvious agreement between the variations found at the two observatories. Miss Giannuzzi, however, claimed that the Greenwich observations of horizontal diameter contained an oscillation with a period of between 22 and 24 years, agreeing in period and phase with an oscillation found from the Italian results. The conclusions she reached from her study of the Greenwich observations were as follows:

(i) There appears to be a secular drift in the Greenwich semi-diameters from about 1890 onwards, the semi-diameter decreasing at the rate of about 0″·01 per year; the drift is removed before the results are analysed.

(ii) A periodic analysis by a special method suggested the existence of two oscillations, one with a period between 22 and 24 years (mentioned above), and the other with a period between 6 and 8 years. Periods of about 22 years and 8 years have already been detected in the Campidoglio results; it is suggested by Miss Giannuzzi that the 22-year period represents a real oscillation of the horizontal diameter, since there is agreement in the phase as well as in period, whereas the 8-year period may be of atmospheric origin, since there is no agreement in phase.

(iii) Although the 22-year oscillations agree approximately in period and phase, there is a discrepancy in amplitude, the Greenwich oscillation having an amplitude between 0″·1 and 0″·2 and the oscillation found from the Italian results having an amplitude between 0″·2 and 0″·5.

In view of Miss Giannuzzi's results, the following tests were applied to the results plotted in Fig. 1:

(i) *Correlation.*—The correlation coefficient between the horizontal semi-diameters for the years 1876 to 1936 and the Italian results for the same period is −0·26, or −0·07 after removal of the secular drift from the Greenwich observations.

(ii) *Analysis for period.*—Inconclusive results were obtained from a normal periodogram analysis. The horizontal semi-diameters showed a suggestion of a seven-year period, and the vertical semi-diameters showed a suggestion of a ten-year period, but the evidence was not convincing in either case.

(iii) *Amplitude of variations.*—It is clear from a cursory inspection of Fig. 1 that the variations in the Greenwich semi-diameters are considerably smaller than those in the Campidoglio results. The standard deviation of the Campidoglio measures from their mean is nearly three times the standard deviation of the Greenwich measures from the Greenwich mean. This result is in reasonable

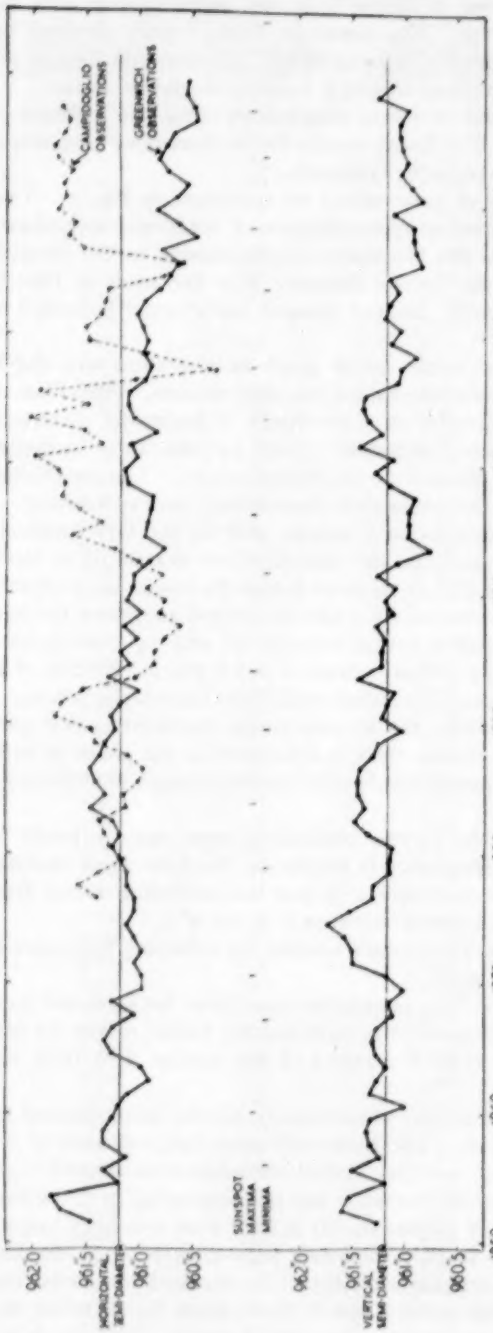

FIG. 1.—*Greenwich observations, uncorrected for irradiation and personality differences, of the horizontal and vertical semi-diameters of the Sun. The Campidoglio results for the horizontal semi-diameter are also shown.*

agreement with Miss Giannuzzi's conclusion given as (iii) above, but it is important evidence *against* the hypothesis that the variations represent real changes in the Sun's size, which would be expected to affect both series of measurements equally.

In the above discussion of the Greenwich observations, no account has been taken of the differing personal equations of observers and the differing distributions of the dates of observations from year to year; apparent changes in the annual means might arise from either of these two causes. The personal equations are systematic differences between observations of diameter made by different observers. Clearly, if an observer with a personal equation which is large compared with the mean of other observers' personalities obtains a large number of observations in one year and a small number in the next year, the mean semi-diameter will show a consequent change which does not represent a real change in the size of the Sun. Similarly, the annual term in the measurements made by each observer, i.e. the "irradiation" term found by Cullen (**20**), can give rise to apparent changes in mean diameter if the distribution of observations changes appreciably from year to year.

2. *The Greenwich observations from 1915 to 1937.*—In view of the importance of personality corrections and of the irradiation term, it was decided to attempt an analysis in which allowance could be made for their effects. Apart from these difficulties, the transit circle appears to be particularly suitable for the measurement of the horizontal diameter since the quantity measured, effectively the time interval between the passage of the two vertical limbs past a fixed point, is not affected by instrumental changes. The measured vertical diameters, however, could be affected to a small extent by changes in the scale values of the ZD micrometer and of the microscope micrometers used in obtaining the circle readings.

The observations obtained by five regular observers with exceptionally long periods of service between the years 1915 and 1936 provided the most suitable data. The introduction of the impersonal R.A. micrometer in 1915 forms a suitable starting point, since the personality of each observer in measuring the R.A. limbs probably changed with the new method of observing; it is possible that the personalities for measurements in the vertical direction also changed because of the consequent changes in observing technique. The total number of observations obtained by the five observers showed a sharp drop after 1936, owing to retirements from observing duties or to transfers to other instruments. There is therefore a poor "connection" with the new observers who replaced them. The names of the observers, the initials by which their observations are identified, and their periods of service as regular transit-circle observers are as follows:

Mr Witchell (W), 1902–1934,
Mr Cullen (RC), 1903–1935,
Mr Acton (HA), 1912–1937,
Mr Barton (HB), 1921–1937,
Mr Symms (LS), 1922–1937.

It was decided to collect the observations of both the horizontal and vertical diameters in order to compare the variations in the two co-ordinates.

The published observations of solar diameter are in the form of residuals, either (C–O) or (O–C), between the observed diameter O, and the computed

diameter C published in the Nautical Almanac for the time of transit. The first step was to correct each residual for the irradiation term found by Cullen (**20**). This is an annual term in the measured diameters, both horizontal and vertical, varying approximately with the secant of the Sun's zenith distance; the Sun is observed large in summer and small in winter.

After corrections for irradiation had been applied, yearly means were formed for each observer. These means will be referred to as "individual means". The yearly means were then examined for personality differences by the method described below. The appropriate personality corrections required to refer all observations to a standard observer were then applied, and a mean formed for each year, by combining with appropriate weights the corrected individual means; this mean will be referred to as the "combined mean" for that year. The results are tabulated and discussed in a later section.

3. *The irradiation correction.*—Throughout this section results given refer to diameters, *not* semi-diameters; this is to facilitate comparison with Cullen's results. The correction applied for irradiation was $-0''{\cdot}55+0''{\cdot}30\sec z$, where z is the Sun's zenith distance. The correction was not computed for each observation; instead, a mean value of z for each month was used, and the same correction applied to each observation in that month, according to Table II.

TABLE II

Irradiation corrections

Month	Correction to be added to (O–C)	Month	Correction to be added to (O–C)
	″		″
Jan.	+0·45	July	−0·20
Feb.	+0·15	Aug.	−0·17
Mar.	−0·05	Sept.	−0·10
Apr.	−0·15	Oct.	+0·06
May	−0·19	Nov.	+0·31
June	−0·21	Dec.	+0·57

These values are taken from Cullen's paper. They were obtained from an analysis of the observations made by seven regular observers in the period 1915–1925. Some of the observations used are, of course, contained in the present investigation. The constant term, $+0''{\cdot}55$, was chosen so that the mean of all the observations considered was not altered by the application of the irradiation corrections.

The present work provided a good opportunity of confirming the values obtained by Cullen. The corrections given in Table II were first applied and corrections for personality obtained, in a manner to be described. The personality corrections were then applied, and all the observations were classified according to month. A least-squares solution, to fit the new diameter residuals for each month (horizontal and vertical combined) to a curve of the form $a+b\sec z$, showed that an additional correction of $+0''{\cdot}21\ +0''{\cdot}05\sec z$ was required. The constant term is of no importance; it arises mainly because the personality corrections in the present investigation have been referred to observer W as standard, whereas Cullen used the mean (O − C) of his seven observers as the standard. The coefficient of the second term indicates that the coefficient of

sec z in the complete correction should be $+0''\cdot35$. The probable error of this coefficient, however, is about $\pm0''\cdot06$ and it was therefore not considered worthwhile to apply additional corrections for irradiation, the effect of which would in any case be small in the present investigation.

Miss Giannuzzi, in a recent paper (**21**), has also investigated the irradiation term in the Greenwich observations. She collected all the observations made between 1851 and 1937 and arranged them according to month. The monthly means have not been analysed for a sec z term in her paper, but this can be done very easily and yields a coefficient of $+0''\cdot33$, a value intermediate between the two quoted above.

No significant differences in the irradiation terms of different observers could be detected; nor was there any noticeable difference between the horizontal and vertical diameters in this respect. It must be emphasized, however, that the data are not really sufficient for detailed consideration of these points.

After removal of the irradiation term, the probable error of a single observation is about $\pm0''\cdot87$ for a horizontal diameter and $\pm0''\cdot63$ for a vertical diameter. As is to be expected, these probable errors are smaller than the value (about $\pm1''$) for both diameters before correcting for irradiation.

4. *Personality corrections.*—The difference between the individual mean semi-diameters obtained by two observers in the same year was assumed to be due to personality differences and a weighted mean of the differences for each pair of observers was formed. Comparison of the weighted mean with the individual differences showed that the first one or two differences obtained with each new observer tended to show rather a large scatter, presumably due to inexperience. It was therefore decided to revise the personality solution by omitting the first two years' observations of each new observer and the first two years' observations of every observer after the introduction of the impersonal micrometer, i.e. no observations made prior to 1917 were kept.

TABLE III

Personality corrections to semi-diameters

Observer	Horizontal personality	Vertical personality
	"	"
W	0·00	0·00
RC	−0·24	+0·04
HA	−0·02	+0·25
HB	+0·11	+0·41
LS	+0·34	+0·16

The personality corrections given by the weighted means are not self-consistent, because of the effects of weighting. For example, the (horizontal) values $W-RC=+0''\cdot24$ and $W-HB=-0''\cdot03$ would suggest $RC-HB=-0''\cdot27$, whereas the actual value is $-0''\cdot38$. A compromise solution was therefore obtained by the method of least-squares. The results are shown in Table III, which gives the correction required to refer an observed horizontal or vertical semi-diameter to W as standard.

The personality corrections obtained by this procedure are independent of any changes in the Sun's diameter from year to year. It is, however, questionable

TABLE IV

Horizontal semi-diameters corrected for personality

Year	W	RC	HA	HB	LS	Combined mean
	"	"	"	"	"	"
1917·5	960·90	960·22	960·82	...	...	960·84
1918·5	1·08	...	0·72	...	...	0·94
1919·5	0·78	0·58	0·88	...	...	0·76
1920·5	0·92	0·40	0·64	...	...	0·66
1921·5	0·91	0·73	0·65	...	...	0·75
1922·5	0·64	0·96	0·58	..	...	0·74
1923·5	0·60	0·54	0·66	960·74	...	0·63
1924·5	1·07	0·72	0·96	0·78	960·72	0·84
1925·5	0·58	0·86	0·82	0·79	0·50	0·74
1926·5	0·48	0·82	1·04	0·68	1·21	0·88
1927·5	0·96	0·75	0·70	0·55	0·95	0·76
1928·5	0·74	0·94	0·59	1·08	0·60	0·80
1929·5	1·00	1·23	0·92	1·20	0·54	1·02
1930·5	0·76	1·04	1·19	0·96	0·48	0·91
1931·5	0·71	0·86	0·87	0·74	1·37	0·91
1932·5	0·91	0·81	0·89	1·09	1·22	0·97
1933·5	0·94	1·06	0·92	1·02	1·04	1·00
1934·5	0·82	1·05	1·06	0·80	0·96	0·96
1935·5	...	0·76	1·00	0·78	1·16	0·90
1936·5	...	1·00	0·70	0·90	0·88	0·86

TABLE V

Vertical semi-diameters corrected for personality

Year	W	RC	HA	HB	LS	Combined mean
	"	"	"	"	"	"
1917·5	960·86	960·59	960·75	...	...	960·82
1918·5	1·04	...	0·88	...	...	0·97
1919·5	1·06	1·08	0·96	...	...	1·02
1920·5	0·98	1·00	0·94	...	...	0·98
1921·5	1·29	0·93	0·95	...	...	1·04
1922·5	1·10	0·96	1·23	...	...	1·11
1923·5	1·26	0·79	1·04	961·04	...	1·04
1924·5	1·18	1·12	1·10	1·37	961·26	1·20
1925·5	0·86	0·95	0·96	1·14	0·82	0·96
1926·5	1·24	1·26	1·01	0·82	1·34	1·10
1927·5	1·11	1·24	1·12	0·92	1·38	1·16
1928·5	1·28	1·16	1·26	1·30	1·32	1·26
1929·5	1·32	1·70	1·52	1·50	0·55	1·39
1930·5	1·30	1·28	1·30	1·20	0·81	1·17
1931·5	1·16	1·28	1·27	1·32	1·48	1·29
1932·5	1·20	1·34	1·30	1·56	1·36	1·36
1933·5	0·98	1·25	1·46	1·30	1·45	1·30
1934·5	1·24	1·45	1·44	1·28	1·56	1·40
1935·5	...	1·33	1·38	1·26	1·60	1·38
1936·5	...	1·89	1·35	1·66	1·58	1·59

whether personality differences remain strictly constant from year to year, and whether the mean personality of all observers is constant. If the personalities of all observers are subject to changes of the same sign the combined means will obviously be affected. The apparent variations in the solar diameters therefore include the effects of possible real variations and changes in mean personality.

The results obtained by each observer, corrected for personality, for the horizontal and vertical semi-diameters are tabulated in Tables IV and V. The combined mean for each year has also been tabulated for the two co-ordinates. It must be emphasized that only constant corrections have been applied for personality; no attempt has been made to remove slopes or "waves" in differences between two observers. Changes in personality peculiar to one observer show up as a systematic drift of his results from the mean. For example, the measurements of horizontal semi-diameter obtained by RC show a tendency to increase over the entire period covered by his observations.

An indication of the magnitude of changes of personality to be expected can be obtained by dividing the data in these tables into groups. For example, we can compare the mean personality differences of the observers W, RC and HA for the years 1919·5 to 1926·5 with those for the years 1927·5 to 1934·5. The results are given in Table VI. It will be seen that there are long-term changes of two or three tenths of a second in personality differences, and the possibility of comparable changes in combined mean semi-diameters, due to personality changes, cannot be excluded.

TABLE VI

Personality differences in two periods of eight years

	Horizontal semi-diameters		Vertical semi-diameters	
	W–RC	W–HA	W–RC	W–HA
	″	″	″	″
1919·5 to 1926·5	−0·19	−0·05	+0·15	+0·35
1927·5 to 1934·5	−0·35	+0·01	−0·10	+0·12

5. *Discussion of results.*—The mean values for the horizontal and vertical semi-diameters have been meaned in pairs to give points corresponding to the beginning of each year. These points are plotted on a larger scale in Figs. 2 and 3; Fig. 4 is a plot of mean sunspot areas for comparison.

The variations in these values are rather greater than can be accounted for as random scatter of the observations; however, it will be shown that they could be explained as variations in personality and do not necessarily represent real variations in the size of the Sun.

Working from the probable errors of $\pm 0''{\cdot}87$ for a horizontal diameter and $\pm 0''{\cdot}63$ for a vertical diameter obtained above, and ignoring possible variations in personality, we should expect the probable error of one of the plotted points to be $\pm 0''{\cdot}05$ at most. The total ranges in semi-diameter are rather larger. The greatest difference in the horizontal semi-diameters is between the years 1923·0 and 1933·0, the values and probable errors being as follows:

$$1923{\cdot}0: \quad 960''{\cdot}68 \pm 0''{\cdot}05$$
$$1933{\cdot}0: \quad 960''{\cdot}98 \pm 0''{\cdot}03.$$

Thus the range is nearly four times the sum of the probable errors. For the vertical semi-diameters the extreme values are:

$$1918{\cdot}0: \quad 960''{\cdot}89 \pm 0''{\cdot}02$$
$$1936{\cdot}0: \quad 961''{\cdot}48 \pm 0''{\cdot}04$$

and the range is nearly ten times the sum of the probable errors.

It must be emphasized that the probable errors quoted have been deduced from the internal accordance of each observer's measures in any one year; they do not, therefore, include the effects of possible random and systematic errors in the personality corrections applied. The effect of uncertainties in the personality corrections can be studied by considering the internal agreement of the diameters obtained by *different* observers in the same year. For example, working from the scatter of the individual means for each year, we can estimate the standard deviation from a constant value (nearly enough the mean of all observations) to be expected in the yearly means for all observers combined, on

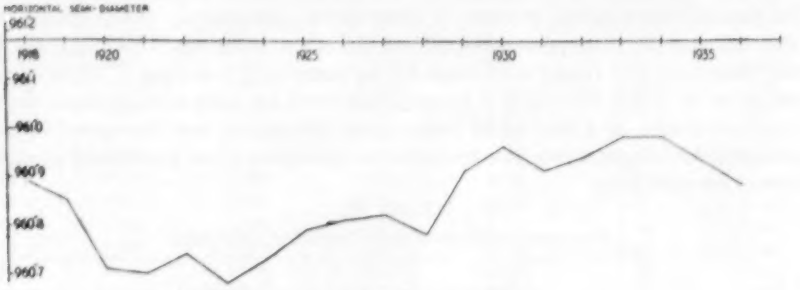

FIG. 2.—*Mean corrected horizontal semi-diameters.*

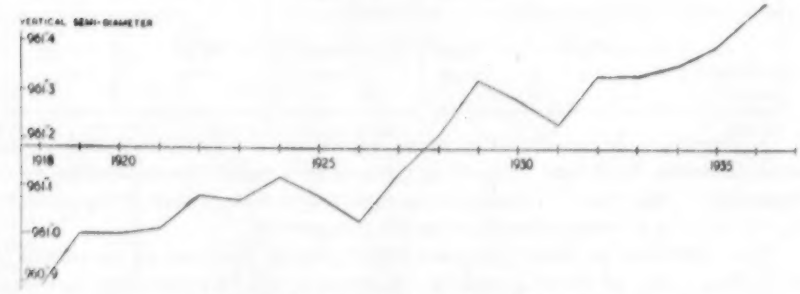

FIG. 3.—*Mean corrected vertical semi-diameters.*

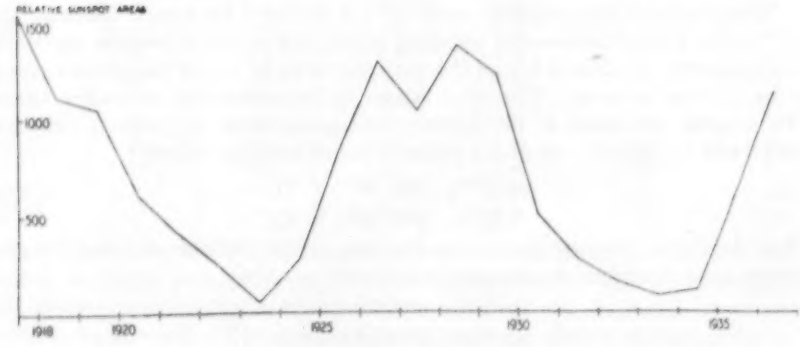

FIG. 4.—*Relative sunspot areas.*

the assumption that there are no real variations in the diameter of the Sun. The problem of weighting is awkward, since the probable error of an observer's mean for a year is only partly dependent on the number of observations obtained by him; any systematic error due to a departure of his personality correction for that year from its mean value over several years will not depend on the number of observations. Since the systematic errors seemed likely to be of more importance than the random errors, it was decided to give equal weight to each annual mean, independent of the number of observations.

The standard deviations calculated in this way from the discordances between annual means for individual observers were:

$0''\cdot26$ for the horizontal semi-diameters

$0''\cdot20$ for the vertical semi-diameters.

The actual standard deviations from a constant value of the combined annual means are:

$0''\cdot22$ for the horizontal semi-diameters

$0''\cdot38$ for the vertical semi-diameters.

These values show that, if anything, the combined yearly means for the horizontal semi-diameters are more nearly constant than would be expected. This conclusion is the opposite of Miss Giannuzzi's; she used the observations obtained by a larger number of observers without applying personality corrections, on the assumption that changes in the mean personality corrections would then be sufficiently small to be ignored. The present analysis suggests that this assumption may not be justified. It can be seen from Table IV that the scatter of the individual means, corrected for personality, about the combined mean is too large to inspire any confidence in the reality of the variations from year to year.

With the vertical semi-diameters the position seems to be quite different; the means seem to show larger variations than would be expected. The main contribution to the comparatively large calculated standard deviation comes from the progressive change in the means. An inspection of either Table V or Fig. 3 shows fairly clear evidence of a positive slope in the yearly means. This slope appears to be confirmed by most, if not all, observers. The slope is equivalent to an increase of about $0''\cdot03$ per year in the semi-diameter, i.e. about three times that found by Miss Giannuzzi in the horizontal semi-diameters, and of the opposite sense. There is no evidence to indicate whether the drift should be interpreted as a real change in the diameter of the Sun, as an instrumental or atmospheric effect, or as a drift in the mean personality.

There does not appear to be any marked drift in the uncorrected vertical semi-diameters meaned for all observers. Indeed, the uncorrected results tabulated in Table I for both co-ordinates behave rather differently in the period 1917 to 1937 from those in Tables IV and V for the same period. The uncorrected horizontal semi-diameters for the dates corresponding to the extremes of the corrected horizontal semi-diameters are:

1923·0: $960''\cdot89$

1933·0: $960''\cdot77$.

The change is of opposite sign to that in the corrected results. For the uncorrected vertical semi-diameters the results are:

1918·0: $960''\cdot97$

1936·0: $961''\cdot06$.

The change is of the same sign as that in the corrected results, but is much smaller.

The differing shapes of the uncorrected and corrected curves demonstrate the importance of personality corrections. It seems probable that at least some of the difference can be explained by the fact that two new observers with large personalities of the same sign in both co-ordinates started observing in 1923 and 1925 respectively. Their observations have an increasing effect on the uncorrected means from these dates onward.

An inspection of Figs. 2, 3 and 4 shows that there is no obvious connection between sunspot activity and the apparent variations in diameter. There is, in fact, no significant correlation between the two phenomena.

It must be concluded that the Greenwich observations considered here do not provide any clear evidence of the existence of real variation in the size of the Sun.

Royal Greenwich Observatory,
Herstmonceux Castle, Sussex :
1955 *June* 16.

References

(1) A. Auwers, *Astr. Nach.*, 3068, 367, 1891.
(2) L. Ambronn, *Gott. Abhand.*, N.F. **3**, No. 3, 1905.
(3) C. L. Poor, *Ap. J.*, **22**, 305, 1905.
(4) L. Ambronn, *Ap. J.*, **23**, 343, 1906.
(5) A. Secchi, *C.R. Acad. Sci. Paris*, **75**, 606 and 1581, 1872; *Ibid.*, **77**, 253 and 905, 1873.
(6) L. Gialanella, *Contr. Sci. Oss. Roma*, Nos. 107, 112, 1943.
(7) L. Gialanella, *Contr. Sci. Oss. Roma*, No. 109, 1943.
(8) C. L. Poor, *Ap. J.*, **22**, 103, 1905.
(9) M. Cimino, *Contr. Sci. Oss. Roma*, No. 122, 1945.
(10) M. Cimino, *Contr. Sci. Oss. Roma*, No. 128, 1946.
(11) T. Fortini, *Contr. Sci. Oss. Roma*, No. 150, 1949.
(12) T. Fortini, *Contr. Sci. Oss. Roma*, No. 153, 1949.
(13) L. Gialanella, *Contr. Sci. Oss. Roma*, No. 167, 1951.
(14) L. Gialanella, *Contr. Sci. Oss. Roma*, No. 171, 1952.
(15) M. Cimino, *Contr. Sci. Oss. Roma*, No. 193, 1953.
(16) M. Cimino, *Contr. Sci. Oss. Roma*, No. 196, 1953.
(17) M. A. Giannuzzi, *Mem. Soc. Astron. Ital.*, **XXIV**, No. 3, 1953.
(18) G. B. Airy, *M.N.*, **22**, 80, 1862.
(19) W. G. Thackeray, *M.N.*, **45**, 389, 1885.
(20) R. T. Cullen, *M.N.*, **86**, 344, 1926.
(21) M. A. Giannuzzi, *Rend. Sc. Lincei*, **XVIII**, 62, 1955.

ATOMIC OSCILLATOR STRENGTHS AND EXCITATION POTENTIALS

C. W. Allen and A. S. Asaad

(Received 1955 October 5*)

Summary

The ratio between calculated and observed oscillator strengths is discussed for atoms of the astrophysically important iron group (Ti to Ni). The ratio is found to vary systematically and very greatly with excitation potential, being high for small E.P. Reasons are advanced for believing that observed values may be preferred to calculated values. The data lead to the surprising result that there is a general increase of true oscillator strength (factor of 1000 or more) for observed lines as E.P. increases by 3 or 4 volts.

A knowledge of the oscillator strengths of spectral lines is essential for deriving the abundance and excitation conditions of atoms in astrophysical sources. Estimates can be made theoretically or by observation and in the simpler atoms these usually agree. This paper discusses the case of the more complex atoms of the iron group (Ti to Ni) which are of very great astrophysical significance.

The theoretical approach finds a very general expression in a paper by Bates and Damgaard (**1**), which provides rules and tables from which oscillator strengths can be calculated. The method was developed primarily for simple atoms and was shown to give reasonable results for systems containing one or two electrons outside closed shells. As far as we are aware no attempt has been made to examine whether the method can be applied to more complex atoms. There is no theoretical justification for doing this, but we had expected that the results of a rule-of-thumb application of the procedure might at least bear some useful relation to the true value.

For comparison with theoretical calculations one needs reliable measurements of oscillator strengths which should preferably be on an absolute scale. The measurements used for the present work are by King (**2, 3**) and Kopfermann and Wessel (**4**) for Fe; Hill and King (**5**) and Davis, Routly and King (**6**) for Cr; King (**7**) and Estabrook (**8**) for Ni; Huldt and Lagerqvist (**9**) for Mn; King (**2**) for Ti, and King, Parnes, Davis and Olsen (**10**) for Co. Differences of the order of a factor of three exist between sets of absolute measurements, so that satisfactory absolute accuracy cannot be considered established. However, the accuracy is quite sufficient to demonstrate the part played by the excitation potential as illustrated in Figs. 1 and 2.

In order to compare theory with observation we use the difference $\log \varpi f$ (theor) $-\log \varpi f$ (obs) where f is the oscillator strength and ϖ the statistical weight. The difference has been plotted against excitation potential (upper) in Fig. 1. The theoretical values have been computed from the Bates–Damgaard tables using the mean excitation potentials of the multiplet to derive the ϵ values.

* Received in original form 1955 August 19.

Tables by Moore (**11, 12**), Goldberg (**13**) and Allen (**14**) are used in the calculations. Observations are available on an absolute scale for Fe I, Cr I, Mn I and Ni I which are plotted in Fig. 1(*a*) (the King (**3**) absolute evaluation of Fe I is used). For Co I and Ti I values are relative only and the data taken from the tabulation (**2, 10**) are plotted in Fig. 1(*b*).

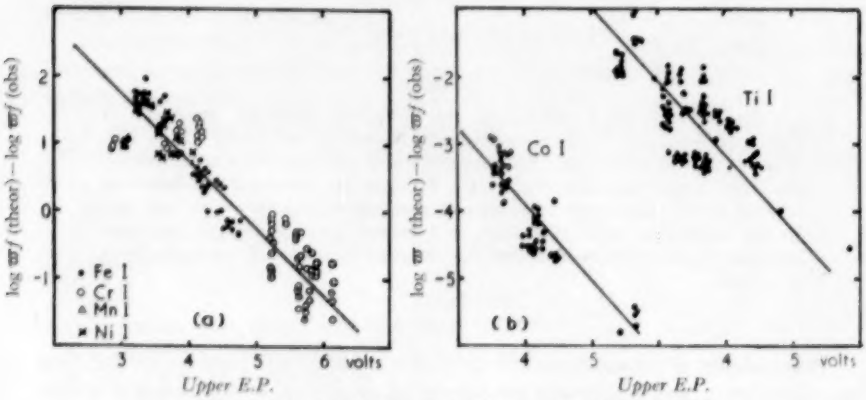

FIG. 1.—*Comparison of theoretical and observed oscillator strengths.*
(a) Observed ϖf absolute.
(b) Observed ϖf relative.

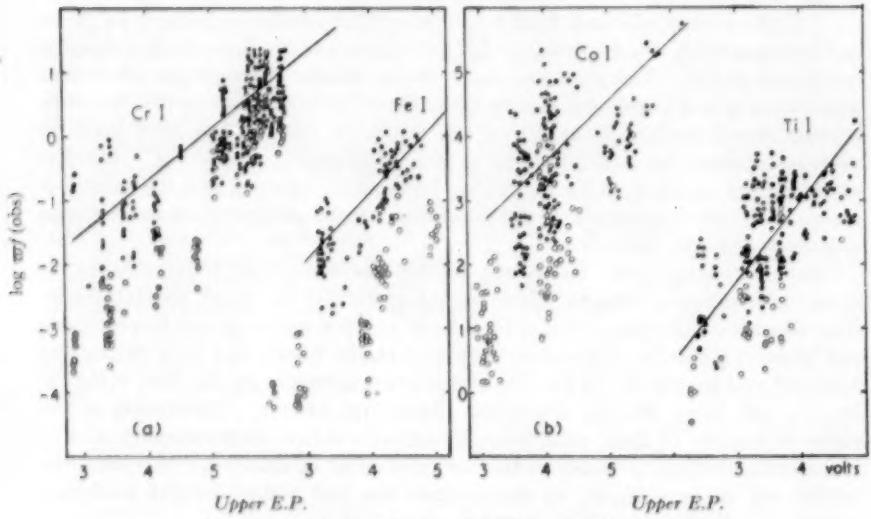

FIG. 2.—*Comparison of observed oscillator strength with E.P.*
● *Allowed in LS coupling.*
○ *Intercombination lines.*

The most surprising result evident from Fig. 1, is the approximate linear relation between log ϖf (theor)—log ϖf (obs) and E.P. The systematic change with E.P. is far greater than the scatter. It is seen that, relative to the observed values, the theoretical values are up to 50 times larger for small E.P. and down to 30 times smaller for large E.P. There is thus a total error of over 1000 in the

theoretical values as compared with the observed. The slope of the curve is so constant as to suggest that some temperature error has crept into the observations, but the correction is impossibly large. It would imply that the true temperature of the King furnace was nearly twice as great as estimated.

Since both ϖf (theor) and ϖf (obs) in Fig. 1(*a*) are intended to be absolute, the graph would indicate agreement by a horizontal curve at zero ordinate. We find that neither the high E.P. nor the low E.P. lines are in agreement but that agreement comes arbitrarily at a medium E.P. of 4·8 volts. There is no tendency for the curve to flatten out at this level.

Fig. 1(*a*) shows that the absolute evaluations of the four elements are in reasonable agreement with one another. Two of the elements, Fe I and Cr I, show the E.P. effect with approximately the same slope, while Mn I and Ni I do not have sufficient range to show this effect.

The E.P. effect can be demonstrated just as readily from relative measurements of ϖf. Fig. 1(*b*) shows that for Co I and Ti I the slope of the curves is much the same as in Fig. 1 (*a*). Within likely error the slope for all the curves is 1·0 (using 10-based logarithms and E.P. in volts). By comparing Figs. 1(*a*) and (*b*) and assuming the curves to coincide we obtain the following conversion factors by which the relative values should be multiplied to make them absolute:

$$\text{for Co I (2):} \quad 1{\cdot}7 \times 10^{-5};$$

$$\text{for Ti I (10):} \quad 8{\cdot}5 \times 10^{-6}.$$

That the E.P. effect is not caused solely by the application of the Bates–Damgaard procedure may be seen by considering the application of the *f*-sum rule. This rule is equivalent to the statement that the strongest lines associated with each level have oscillator strengths of the order unity. In Fig. 2 we plot simply log ϖf (obs) against E.P. In this case the scatter is much larger because of intrinsic differences in line intensities. Absolute values are in Fig. 2(*a*) and relative in Fig. 2(*b*). We see that there is a systematic tendency for ϖf (obs) to increase with E.P. with about the same slope as in Fig. 1. This means that log ϖf (*f*-sum theor) − log ϖf (obs) is much the same as log ϖf (Bates–Damgaard theor) − log ϖf (obs). No doubt a similar result would be obtained by using any existing method of calculating oscillator strengths for more complex atoms. It is worth noting from Fig. 2 that the intercombination lines show the effect as well as the lines allowed in LS coupling.

With such large discrepancies between theoretical and observed values one has to face the quandary of which to regard as right and which wrong. It is not likely that any compromise would be correct. Fortunately there are three convincing arguments in favour of the correctness of the observed values: (*a*) a furnace temperature error large enough to explain the result is unthinkable, (*b*) using theoretical values with some copper arc measurements now in progress would yield an impossible excitation temperature of 20 000 deg. K, and (*c*) independent measurements of lines by emission (**15**) as well as absorption all show the effect.

If we conclude that the observations are correct, we are led to the following rather surprising results:

(*a*) Oscillator strengths for lines of high E.P. may have values well above 10.

(*b*) Oscillator strengths of lines of low E.P. (the strongest permitted lines with LS coupling) have values of the order 0·01, which contrasts strangely with the well-established *D* lines of Na, Ca I 4227, and the *H* and *K* lines of Ca II.

(*c*) The existing theories give no *a priori* indication of absolute oscillator strength since the E.P. of 4·8 volts where the values appear to be correct is entirely fortuitous. We are therefore entirely dependent on observations for estimates of absolute oscillator strengths.

A partial explanation of the E.P. effect may be that, as the E.P. increases, more and more electrons contribute to s, the effective number of electrons. Also for the absorption oscillator strengths of high-level lines the negative emission components in the f-sum rule $\Sigma f_{abs} = s - \Sigma f_{em}$ may add progressively to give a high value. This however would not explain the surprising regularity and generality of the effect, nor the reason why the low-level lines should have such small oscillator strengths.

One of us (A. S. A.) expresses his gratitude to the Egyptian Government for sending him to London University to carry out research in spectroscopy.

University of London Observatory,
Mill Hill Park,
*London, N.W.*7 :
1955 *August* 17.

References

(1) D. R. Bates and A. Damgaard, *Phil. Trans.* A, **242,** 101, 1949.
(2) R. B. King and A. S. King, *Ap. J.*, **87,** 24, 1938.
(3) R. B. King, *Ap. J.*, **95,** 78, 1942.
(4) H. Kopfermann and G. Wessel, *Z. f. Phys.*, **130,** 100, 1951.
(5) A. J. Hill and R. B. King, *J.O.S.A.*, **41,** 315, 1951.
(6) M. H. Davis, P. M. Routly and R. B. King, *Proc. Conf. Stellar Atmospheres*, 1954, p. 48.
(7) R. B. King, *Ap. J.*, **108,** 87, 1948.
(8) F. B. Estabrook, *Ap. J.*, **113,** 684, 1951.
(9) L. H. Huldt and A. Lagerqvist, *J.O.S.A.*, **42,** 142, 1952.
(10) R. B. King, B. R. Parnes, M. H. Davis and K. H. Olsen, *J.O.S.A.*, **45,** 350, 1955.
(11) C. E. Moore, *Atomic Energy Levels*, Vols. I and II, 1952.
(12) C. E. Moore, *Multiplet Table of Ast. Interest*, Part I.
(13) L. Goldberg, *Ap. J.*, **82,** 1, 1935; **84,** 11, 1936.
(14) C. W. Allen *Astrophysical Quantities*, p. 55, 1955.
(15) J. Aarts, D. Harting and C. J. Bakker, *Physica*, XX, 1250, 1954.

NOTE CONCERNING "THE CONSTANTS OF THE VELOCITY ELLIPSOID FROM THE RADIAL VELOCITIES OF 820 STARS"

D. G. Ewart

(Communicated by the Director, University Observatory, Glasgow)

(Received 1955 June 3)

Summary

Erroneous values of the solar motion and of the constants of the velocity ellipsoid published in a previous paper are corrected. The revised results indicate no definite variation in the constants of the velocity ellipsoid for the faint stars, but the variation in the solar motion is confirmed.

---

1. In a previous paper (**1**), the derivation of the constants of the solar motion and of the velocity ellipsoid from the radial velocities of a sample group of faint stars—HD magnitudes 8·5–8·6, spectral types F to M—obtained at Lick Observatory by Moore and Paddock was described. It was recently brought to my notice by Dr T. R. Tannahill that the solution for "ALL" stars was incorrect, the figures given not being the means of the values for the three zones. On examination, it was found that it had been assumed that the equations could be solved for the whole sky by taking the mean galactic latitude as 0°, which procedure is fallacious.

A new solution was consequently required, and it was decided to re-check the previous solutions simultaneously. In so doing, two errors of sign were discovered in the solution for the solar motion. A fresh analysis was therefore performed, the details of which are given below.

2. No changes were made in the methods of analysis. For the solar motion, the normal equations were formed, and for the calculation of the areal corrections, their approximate solutions found to be:—

$$U = 21{\cdot}05 \text{ km/sec}, G = 41^\circ, g = +22^\circ \text{ with a } K\text{-term of } +1{\cdot}0 \text{ km/sec}.$$

The complete solutions of the normal equations—including the corrections—were found to be:—

$$U = 22{\cdot}31 \pm 1{\cdot}20 \text{ km/sec}, A = 280^\circ{\cdot}0 \pm 5^\circ{\cdot}8, D = +47^\circ{\cdot}9 \pm 2^\circ{\cdot}8,$$

$$G = 44^\circ{\cdot}3 \pm 3^\circ{\cdot}5, g = +20^\circ{\cdot}4 \pm 3^\circ{\cdot}1, \text{ and a } K\text{-term of } +1{\cdot}17 \pm 0{\cdot}79 \text{ km/sec}.$$

The weighted mean results of Moore and Paddock are $U = 22{\cdot}44$ km/sec, $A = 280^\circ$, $D = +44^\circ{\cdot}5$.

The constants of the velocity ellipsoid were again determined separately for the latitude zones 0°, 20° and 45°. For the whole sky solution, the iterative method of solution described by Smart and Chandrasekhar (**2**) was used, the initial values being the means of the zone results. The results, together with those of the previous solution and those of Smart's analysis (**3**) of the radial velocities of Schlesinger's *Catalogue of Bright Stars*, 1930 are given in Table I. It must be noted that the values for the whole sky from Smart's analysis are means of the three zones—weighted in the case of the longitude of the major axis. In

the table, the first line gives the revised values of the constants, the second line the "old" values and the third line Smart's values, except for the case of "ALL" stars, where the doubly erroneous "old" values are not listed.

TABLE I

Zone	No. of stars	$1/K$	$1/H$	K/H	G_0
0°	167	37·78	32·24	0·853	298°·1
		38·89	32·56	0·837	292 ·5
	(619)	(33·70)	(20·90)	(0·619)	(340 ·5)
20°	277	39·63 ± 1·78	31·73 ± 2·81	0·801 ± 0·159	327°·9 ± 17°·1
		41·45	26·11	0·630	324·4
	(981)	(30·10)	(26·40)	(0·879)	(332·2)
45°	296	53·63 ± 5·89	19·17 ± 7·48	0·357 ± 0·165	344°·6 ± 11°·1
		53·52	17·94	0·336	343 ·7
	(1068)	(37·20)	(22·10)	(0·594)	(338 ·8)
ALL	820*	40·98 ± 4·61	27·74 ± 2·32	0·677 ± 0·117	331°·4 ± 6°·4
	(2668)	(33·70)	(23·10)	(0·697)	(339 ·5 1 ·4)

* This solution includes the zones centred at $b = \pm 69°$ for which no separate solution was made.

3. As was noted in the previous paper, the only solution to which any weight can be attached is that for "ALL" stars. Again the value of the axis-ratio of the velocity ellipsoid agrees well with Smart's determination, but the velocity dispersions along the axes are greater for the faint stars. This is not unexpected, both because of the lesser amount of the material available for analysis and because of the greater probable errors of the solar motion. For the longitude of the major axis of the ellipsoid, the result is inconclusive because of the large probable error, as regards the vertex.

Summarizing the revised results, it appears that although there are no definite indications of variation in the ellipsoidal constants between the brighter and the fainter stars—excepting the increased dispersions along the axes—there is a variation in the solar motion, in velocity, and in the longitude of the apex.

University Observatory,
Glasgow, W.2:
1955 *May* 24.

References

(1) D. G. Ewart, *M.N.*, **113**, 553, 1953.
(2) W. M. Smart and S. Chandrasekhar, *M.N.*, **98**, 658, 1938.
(3) W. M. Smart, *M.N.*, **99**, 61, 1939.

MEAN DAILY AREAS AND HELIOGRAPHIC LATITUDES OF SUNSPOTS IN THE YEARS 1953 AND 1954

Royal Greenwich Observatory

(Communicated by the Astronomer Royal)

(Received 1955 September 27)

The following results are in continuation of those for the years 1951 and 1952 in *M.N.*, **114**, 606, 1954. They are derived from the measurement at Herstmonceux of photographs taken at the Royal Greenwich Observatory, the Royal Observatory, Cape of Good Hope, and at the Kodaikanal Observatory, India.

Table I gives the mean daily areas of umbrae, whole spots and faculae for each synodic rotation of the Sun included in the years 1953 and 1954. The

TABLE I

No. of rotation	Rotation commenced U.T. 1952–3–4	Days photographed	Mean daily areas: Projected* Umbrae	Whole spots	Faculae	Corrected for foreshortening† Umbrae	Whole spots	Faculae
1328	Dec. 15·18	28	125	685	475	86	486	554
1329	Jan. 11·52	27	48	251	472	30	161	552
1330	Feb. 7·86	27	1	5	231	0	2	272
1331	Mar. 7·19	28	28	159	357	20	120	427
1332	Apr. 3·50	27	93	578	262	66	406	315
1333	Apr. 30·76	27	37	237	254	32	215	312
1334	May 27·98	27	66	349	273	45	243	330
1335	June 24·18	27	26	132	290	18	101	347
1336	July 21·38	28	59	319	275	42	228	337
1337	Aug. 17·60	27	33	173	294	26	139	361
1338	Sept. 13·86	27	27	146	324	19	103	386
1339	Oct. 11·13	28	12	57	224	10	48	258
1340	Nov. 7·43	27	0	1	127	0	2	151
1341	Dec. 4·74	27	2	9	62	1	7	73
1342	Jan. 1·07	27	0	1	53	0	1	62
1343	Jan. 28·41	28	0	2	48	0	1	58
1344	Feb. 24·75	27	53	289	112	32	181	129
1345	Mar. 24·07	28	1	4	62	0	3	74
1346	Apr. 20·35	27	0	1	40	0	1	49
1347	May 17·58	27	0	3	20	0	2	24
1348	June 13·79	27	0	2	10	0	2	11
1349	July 10·98	27	7	39	111	6	34	130
1350	Aug. 7·20	28	13	61	105	9	42	134
1351	Sept. 3·44	27	0	2	134	0	2	160
1352	Sept. 30·71	27	5	21	328	3	18	373
1353	Oct. 28·00	27	12	75	269	10	64	316
1354	Nov. 24·31	28	18	94	246	16	84	280

* Expressed in millionths of the Sun's disk.

† Expressed in millionths of the Sun's hemisphere.

numbers of the rotations are in continuation of Carrington's series. The annual means for the two years are included in Table II, which summarizes similar figures for the years since the last sunspot minimum of 1944. As 1954 was also a minimum year Table II covers the whole of the most recent 11-year cycle.

TABLE II

Year	No. of days		Mean daily areas					
			Projected*			Corrected for foreshortening†		
	Photographed	Without spots	Umbrae	Whole spots	Faculae	Umbrae	Whole spots	Faculae
1944	366	157	30	160	284	23	126	344
1945	365	14	102	560	774	78	429	940
1946	365	0	389	2381	1794	291	1817	2188
1947	365	0	558	3559	2326	405	2637	2894
1948	366	0	419	2618	1849	314	1977	2331
1949	365	0	485	2873	2140	356	2129	2597
1950	365	3	274	1638	1421	203	1222	1754
1951	365	2	259	1552	1145	188	1136	1379
1952	366	24	96	548	594	70	404	711
1953	365	148	35	197	278	25	146	331
1954	365	237	9	49	117	6	35	138

* Expressed in millionths of the Sun's disk.
† Expressed in millionths of the Sun's hemisphere.

Table III gives for each rotation in the years 1953 and 1954 the mean daily area of the whole spots (corrected for foreshortening) and mean heliographic latitude of the spotted areas separately for the northern and southern hemispheres of the Sun. The mean heliographic latitude of the entire spotted area and the mean distance of all spots from the equator are also tabulated. Corresponding annual mean values of all these quantities for the years 1944 to 1954 are given in Table IV. The years of minimum, 1944 and 1954, are each given twice in Table IV: once for all spots occurring during each of the years and once with distinction between spots of the old cycle, appearing at low latitudes, and those, at high latitudes, of the new cycle.

Tables II and IV are in continuation of similar tables in *Monthly Notices:* for the years 1874 to 1888, **49**, 381, 1889: 1889 to 1902, **63**, 465, 1903: 1901 to 1914, **76**, 402, 1916: 1913 to 1924, **85**, 1007, 1925: 1923 to 1933, **94**, 870, 1934: and 1933 to 1945, **110**, 501, 1950.

The chief features of the record for the years 1953 and 1954 are as follows:—

(1) Throughout 1953 sunspot activity continued to decrease, reaching a minimum during the first half of 1954. The mean daily area of sunspots during 1953 was less than half that for 1952 and the mean daily area for 1954 was less than half that for 1953. The most prolonged periods of low sunspot activity occurred in January–February and April–June of 1954. The exact epoch of sunspot minimum may be put as 1954·3. High-latitude spots of the new cycle were first recorded in August 1953 but were not frequent until a year later.

(2) The largest spot group of 1953 crossed the Sun's central meridian on April 28·2. The mean latitude for the disk-passage was 10°·9 N. and the mean area 839 millionths of the hemisphere.

TABLE III

No. of rotation	Rotation commenced U.T.	Spots north of the equator: Mean daily area	Spots north of the equator: Mean heliographic latitude	Spots south of the equator: Mean daily area	Spots south of the equator: Mean Heliographic latitude	Mean latitude of entire spotted area	Mean distance from equator of all spots
	1952–3–4		°		°	°	°
1328	Dec. 15·18	263	9·85	223	9·79	+ 0·83	9·82
1329	Jan. 11·52	49	6·47	112	8·76	− 4·14	8·06
1330	Feb. 7·86	2	2·91	0·4	10·50	+ 0·51	4·27
1331	Mar. 7·19	93	3·26	27	13·62	− 0·53	5·59
1332	Apr. 3·50	394	7·94	12	8·31	+ 7·46	7·95
1333	Apr. 30·76	215	10·10	0·2	9·33	+10·08	10·10
1334	May 27·98	135	12·03	108	13·75	+ 0·54	12·80
1335	June 24·18	7	12·43	94	8·89	− 7·46	9·13
1336	July 21·38	207	12·48	21	5·00	+10·87	11·79
1337	Aug. 17·60	133	12·51	7	6·52	+11·62	12·23
1338	Sept. 13·86	69	9·70	34	9·30	+ 3·38	9·57
1339	Oct. 11·13	2	14·40	46	7·72	− 6·73	8·02
1340	Nov. 7·43	2	16·00	0·3	4·86	+13·08	14·44
1341	Dec. 4·74	3	0·31	4	9·00	− 5·40	5·63
1342	Jan. 1·07	0·4	8·92	0·4	16·70	− 2·73	12·45
1343	Jan. 28·41	1	31·31	0	...	+31·31	31·31
1344	Feb. 24·75	1	7·30	180	9·65	− 9·58	9·64
1345	Mar. 24·07	0·4	6·00	3	4·41	− 3·32	4·58
1346	Apr. 20·35	1	20·80	0	...	+20·80	20·80
1347	May 17·58	2	16·41	0	...	+16·41	16·41
1348	June 13·79	1	20·67	1	20·89	− 3·08	20·80
1349	July 10·98	34	22·17	0	...	+22·17	22·17
1350	Aug. 7·20	5	25·20	37	26·48	−20·64	26·34
1351	Sept. 3·44	1	24·38	2	24·50	− 9·18	24·46
1352	Sept. 30·71	13	29·40	5	31·78	+13·69	30·01
1353	Oct. 28·00	8	25·75	56	31·26	+23·89	30·55
1354	Nov. 24·31	84	33·08	0·3	25·88	+32·88	33·05

TABLE IV

Year	Days photographed	Spots north of the equator: Mean daily area	Spots north of the equator: Mean heliographic latitude	Spots south of the equator: Mean daily area	Spots south of the equator: Mean heliographic latitude	Mean latitude of entire spotted area	Mean distance from equator of all spots
			°		°	°	°
1944	366	42	19·00	83	22·81	−8·70	21·53
1944	366 Old Cycle	7	4·17	6	7·61	−1·14	5·72
	366 New Cycle	35	22·18	77	24·02	−9·63	23·45
1945	365	121	20·13	309	20·26	−8·92	20·22
1946	365	1127	20·74	690	18·79	+5·73	20·00
1947	365	992	16·58	1645	17·86	−4·91	17·38
1948	366	936	14·92	1041	13·53	−0·06	14·19
1949	365	1178	14·30	951	12·14	+2·49	13·33
1950	365	771	13·62	452	13·05	+3·77	13·41
1951	365	730	11·62	406	10·78	+3·62	11·32
1952	366	195	7·60	208	8·37	−0·64	8·00
1953	365	107	9·90	38	9·75	+4·72	9·86
1954	365	12	28·84	23	17·20	−1·55	21·16
1954	365 Old Cycle	1	9·25	12	8·24	−7·17	8·30
	365 New Cycle	11	30·27	11	27·60	+1·86	28·96

The C.M.P. of the largest spot of 1954 was March 17·1. Its latitude was 8°·2 S. and mean area 403 millionths. The largest new-cycle spot during 1954 occurred in latitude 33°·7 N. and had its C.M.P. on December 15·5; its mean area was 317 millionths.

(3) On 148 days in 1953 and 237 days in 1954 no sunspots could be seen on the Sun, while on 69 days in 1953 and 180 days in 1954 faculae were also absent. January 1954 and May 1954 each had only two days with spots present.

(4) The ratio of mean corrected areas of faculae/sunspots was 2·27 in 1953 and 3·9 in 1954. The ratio of mean corrected areas of umbra/whole spot was 0·171 in 1953 and 0·171 in 1954.

(5) In 1953 the northern hemisphere was more spotted than the southern, while in 1954, when new-cycle spots first predominated, the reverse was true. In 1954 the mean distance from the equator of all new-cycle spots (28°·96) was the highest similar figure in the Greenwich records, the previous highest being 27°·6 for the new-cycle spots in 1934. The old-cycle spots of 1953 and 1954 were, on the average, at approximately the same latitudes (8°–9°) as the spots of 1952.

The number and distribution, northern and southern hemispheres, of spot groups of

(*a*) two days' duration or longer,

(*b*) one day's duration

were as follows:—

	1953		1954	
	(*a*)	(*b*)	(*a*)	(*b*)
Northern spots	35	11	20	10
Southern spots	26	13	13	8
Total	61	24	33	18

(6) The following table gives the mean daily areas of sunspots and of faculae, corrected for foreshortening and expressed in millionths of the Sun's hemisphere, for each calendar month of the years 1953 and 1954.

	1953		1954	
Month	Spots	Faculae	Spots	Faculae
Jan.	289	577	1	54
Feb.	10	381	1	58
Mar.	70	420	157	130
Apr.	406	324	3	70
May	196	314	1	33
June	218	370	2	19
July	81	280	11	50
Aug.	269	351	58	188
Sept.	141	416	2	144
Oct.	47	299	16	379
Nov.	9	182	58	295
Dec.	6	64	106	223

Finally, short descriptive surveys of the sunspots of 1953 and 1954 have been given in *Monthly Notices*, **114**, 358, 1954 and **115**, 185, 1955, respectively.

Royal Greenwich Observatory,
Herstmonceux Castle, Sussex:
1955 *September* 16.

CONTENTS

PAGE

M. W. Feast, The spectrum of Nova Sagittarii 1954 (Haro–Herraro) 461

David S. Evans, An occultation of Antares observed at the Union Observatory ... 468

A. R. Hogg, Surface Photometry of the Magellanic Clouds 473

V. C. Reddish, The Period–luminosity relation in Population II 480

R. Hanbury Brown, H. P. Palmer and A. R. Thompson, Polarization measurements on three intense radio sources 487

B. E. J. Pagel, Centre-limb variations in the equivalent widths of some infra-red Fraunhofer lines 493

I. W. Busbridge, Finite atmospheres with isotropic scattering 521

H. H. Plaskett, The Oxford 35 m solar telescope 542

P. J. Message, The second-order theory of the figure of Jupiter 550

P. J. D. Gething, Greenwich observations of the horizontal and vertical diameters of the Sun 558

C. W. Allen and A. S. Asaad, Atomic oscillator strengths and excitation potentials 571

D. G. Ewart, Note concerning "The constants of the velocity ellipsoid from the radial velocities of 820 stars" 575

Royal Greenwich Observatory, Mean daily areas and heliographic latitudes of sunspots in the years 1953 and 1954 577

Printed in London by Taylor & Francis, Ltd., 1956 August